NASA Technical Memorandum 100166

The Tribological Behavior of Polyphenyl Ether and Polyphenyl Thioether Aromatic Lubricants

(NASA-TM-100166) THE TRIBOLOGICAL BEHAVIOR OF POLYPHENYL ETHER AND POLYPHENYL THIOETHER AROMATIC LUBRICANTS Ph.D. Thesis - Kyushu Univ., Japan (NASA) 231 p Avail: NTIS HC A11/MF A01 CSCL 11H G3/27
N87-26231
Unclas
0087711

William R. Jones, Jr.
Lewis Research Center
Cleveland, Ohio

July 1987

NASA

CONTENTS

Page

INTRODUCTION 1

NOMENCLATURE 2

MATERIALS 3

SURFACE TENSION 6

BACKGROUND 6

EFFECT OF SURFACE TENSION ON HEAT TRANSFER 6

ROLE OF SURFACE TENSION IN ELASTOHYDRODYNAMICS 9

EXPERIMENTAL 13

Apparatus 13

Procedure 15

Calculation of Surface Tension 17

Results 17

WETTABILITY 20

BACKGROUND 20

EXPERIMENTAL 23

Tilting Plate Apparatus 23

Tilting Plate Procedure 23

Sessile Drop Apparatus 25

Sessile Drop Procedure 25

Results 28

WETTABILITY ADDITIVES 32

BOUNDARY LUBRICATION 34

BACKGROUND 34

LUBRICATION REGIMES 37

BOUNDARY FILM FORMATION 39
    Physical Adsorption 39
    Chemisorption 39
    Chemical Reaction 39
PHYSICAL PROPERTIES OF BOUNDARY FILMS 43
    Melting Point 43
    Shear Strength 46
    Boundary Film Thickness 46
    Chain Length 52
EFFECT OF OPERATING VARIABLES ON FRICTION 52
    Load 52
    Speed 52
    Temperature 55
    Atmosphere 55
EFFECT OF OPERATING VARIABLES ON WEAR 55
    Load 55
    Speed 55
    Temperature 59
    Atmosphere 59
    Running-In 59
ADDITIVE BEHAVIOR OF BOUNDARY LUBRICATED SYSTEMS 59
BOUNDARY LUBRICATION STUDIES 62
VANE PUMP TESTS 62
    Apparatus 62
    Procedure 66
    Results and Discussion 67

Viscosity Effect 71

Fluid Degradation 72

Summary of Results 74

PIN-ON-DISK STUDIES - 5P-4E 74

Apparatus 75

Atmosphere Monitoring and Control 77

Procedure 77

Disk Temperature Calibration 78

Results and Discussion 79

Effect of Atmosphere on Wear and Friction of Unlubricated Steel 79

Effect of Atmosphere on Base Fluid Wear 79

Effect of Wettability Additive (TCAA) on Rider Wear . . . 82

Dip Cell Experiments 87

Effect of Wettability Additive (TCAA) on Friction 87

Summary of Results 88

PIN-ON-DISK STUDIES - THIOETHER FORMULATIONS 88

Experimental Lubricants 89

Formulated Type II Ester 89

Thioether Formulations (Phosphorus Ester Additives) . . 89

Thioether Formulations (Organic Acid Additives) 89

Wear Results 91

Formulated Type II Ester 91

Thioether Base Fluid 91

Thioether Formulations (Phosphorus Ester Additives). . . 95

Thioether Formulations (Organic Acid Additives). 95

Coefficient of Friction 100

Discussion 100

Effect of Moisture on Additive Performance 101

Summary of Results 102

PIN-ON-DISK STUDIES - EFFECT OF OXYGEN CONCENTRATION 102

Apparatus 103

Procedure 103

Results 103

Thioether Wear 103

5P-4E Wear 106

Comparison of Wear for Thioether and 5P-4E 106

Coefficient of Friction 110

Discussion 110

Summary of Results 116

PIN -ON-DISK STUDIES (AROMATIC SILICON AND TIN COMPOUNDS) . . 116

Background 116

Friction and Wear Results 117

Summary of Results 120

FERROGRAPHY 120

BACKGROUND 120

APPARATUS AND PROCEDURE 123

Cleaning Procedure 123

Analytical Ferrograph 123

Ferroscope 126

Test Atmospheres 126

- RESULTS 5P-4E 126
    - Wear 128
    - Ferrograph 128
    - Effect of Temperature 129
    - Effect of Oxygen and Moisture 129
    - Carbonaceous Debris 134
    - Adhesive Wear Debris 139
    - Cutting Wear Debris 139
    - Spherical Debris 141
    - Summary of Ferrography Results 143
- THIOETHER RESULTS 143

THERMAL STABILITY 145

- BACKGROUND 145
    - Mechanism 145
    - Arrhenius Rate Law 146
    - Tensimeter 147
    - Useful Lives 150
    - Generalizations 150
    - Bond Dissociation Energy 153
- AROMATIC TIN AND SILICON COMPOUNDS 156
    - Results and Discussion 156
    - Summary of Results 161

OXIDATION STABILITY 161

BACKGROUND 161

Mechanisms 163

Rate Equations 164

Oxidizability 164

Chain Initiation 166

Chain Propagation 168

Chain Termination 171

Inhibition of Autoxidation 171

Metal Catalysis in Oxidation 173

Homogeneous and Heterogeneous Catalysis 174

Chain Branching 174

EXPERIMENTAL METHODS 175

Oxygen Diffusion 175

Microtests 177

Stirred Flow Reactor 179

Microoxidation Corrosion Apparatus 180

CHEMILUMINESCENCE 183

Emission as Function of Time 184

Apparatus 186

Microoxidation Apparatus 186

Chemiluminescence Apparatus 186

Bath and Light-tight Enclosure 189

Procedure 189

Results 191

Comparison with Micro-oxidation Corrosion Data 198

MECHANISM OF OXIDATION 200
  Initiation 200
  Propagation 202
  Termination 204
OXIDATION INHIBITORS 205
FORMATION OF HIGH MOLECULAR WEIGHT PRODUCTS 206
MODELS 208
GOLDBLATT RADICAL ANION THEORY 208
KAJDAS NEGATIVE-ION CONCEPT 209
CONCLUDING REMARKS 211
REFERENCES 213

ABSTRACT

The tribological behavior of several polyphenyl ethers and polyphenyl thioethers is reported. Tribological areas covered include: surface tension and wettability measurements, boundary lubrication, ferrography, thermal and oxidative stability and chemiluminescence.

THE TRIBOLOGICAL BEHAVIOR OF POLYPHENYL ETHER AND POLYPHENYL THIOETHER AROMATIC LUBRICANTS

William R. Jones, Jr.

National Aeronautics and Space Administration
Lewis Research Center
Cleveland, Ohio U.S.A.

INTRODUCTION

Aromatic compounds (materials containing benzene rings) have been studied for over 150 yr. Their high resistance to thermal and oxidative degradation was noted early on by many researchers. With the advent of modern chemistry in the early 1900's, it is now known that this stability is associated with its particular form of chemical bonding. The bonding system of benzene, which is made up of six overlapping p orbitals on carbon, gives rise to 6 π molecular orbitals. This monocyclic π system has special stability associated with filled orbital shells. Such systems are said to be aromatic and to possess aromatic stability. Originally, the term aromatic was coined because most of the benzene ring compounds had strong odors. Now the term has more general meaning (ref. 1).

Therefore, it is not surprising that when the need for lubricants of high stability was being predicted in the 1950's that research was focused on aromatic compounds. However, most aromatic species containing multiple benzene rings did not possess the proper physical properties (i.e., most were high melting solids). It soon became obvious that in order to have a fluid with a reasonable liquid range that the phenyl groups would have to be linked by oxygen or some other element in order to impart some chain flexibility.

The first members of the polyphenyl ether class were synthesized by Ullman in 1906 (ref. 2). Staudinger and Staiger (ref. 3) prepared ethers containing three to six benzene rings in 1934 and measured their viscosities. Work was done in Russia in 1945 by Akchurin (ref. 4) on para-linked ethers. In 1949 Kotera prepared the five ring compound; (p-bis(p-phenoxyphenoxyphenyl)) ether (ref. 5).

In the 1950's a number of contracts were let by the U.S. Air Force in order to develop new high temperature hydraulic fluids. Much work was done on preparation and properties of a variety of polyphenyl ether compounds by Monsanto Chemical Company and Shell Development Company (ref. 6).

There is another class of aromatic fluids quite similar to the polyphenyl ethers. These fluids, originally deemed C-ethers, were developed by Monsanto Chemical Company in the 1960's (ref. 7). They consisted of a mixture of polyphenyl and thiophenyl ethers.

Finally, other classes of high temperature fluids - the aromatic tin and aromatic silicon compounds (ref. 8) have also been reported.

The objective of this thesis is to compile and document the tribological research that has been carried out on all of these aromatic lubricant classes.

NOMENCLATURE

The polyphenyl and thioether fluids are named around the group present in the center of the main ether chain (ref. 9). A compound containing an even number of benzene rings will have an oxygen atom (ether linkage) at the center and would be named as an ether. An example follows:

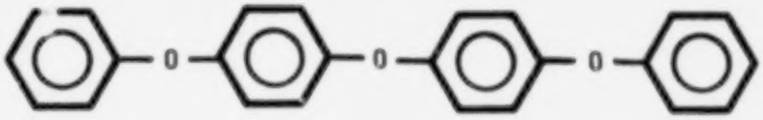

Bis (p-phenoxyphenyl) ether

A compound containing an odd number of benzene rings will have a benzene ring at the center and thus will be named as a benzene compound.

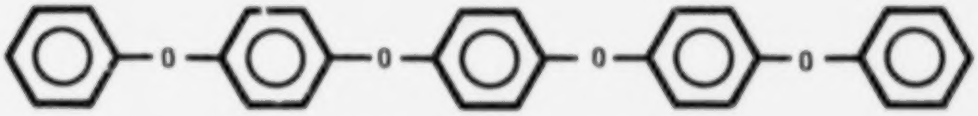

p-Bis (p-phenoxyphenoxy) benzene

When the ether linkages are not all the same or other substituents are present on the rings, the nomenclature becomes too cumbersome. In those cases, a type of chemical shorthand is used as shown in the following example:

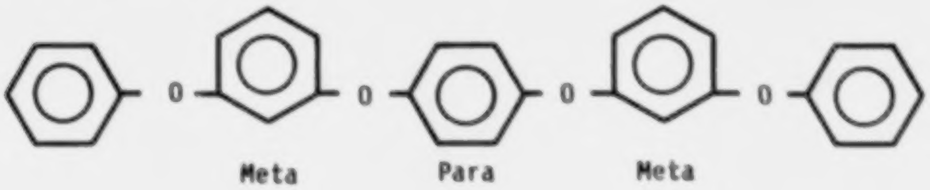

This compound whose proper name is p-bis (m-phenoxyphenoxy) benzene is abbreviated as mpm-5P-4E. The P refers to the number of phenyl or benzene rings and the E to the number of oxygen or ether linkages.

In practice, a commercial preparation of these materials will contain a variety of different individual compounds. One reason for this is that synthesis will often produce a mixture of compounds. However, it is also important from a liquid range perspective. This is because a mixture will possess a much lower pour point than the melting point of individual compounds. An example of a mixture of isomers is shown below:

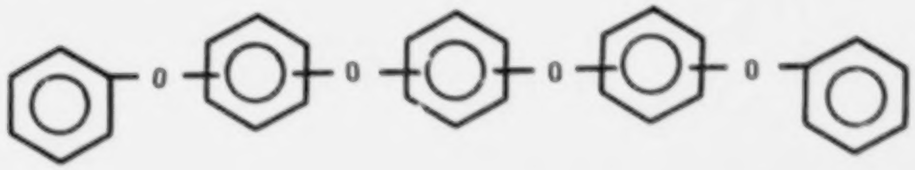

This mixture would be named mix-bis (mix-phenoxyphenoxy) benzene.

The thioether components are named more conventionally as are the aromatic tin and silicon compounds.

MATERIALS

The materials studied in this thesis represent a variety of different classes of aromatic compounds. They are the polyphenyl ethers, polyphenyl thioethers (C-ethers), and a series of aromatic tin and silicon compounds. Their structures appear in figure 1 and their properties are summarized in table 1.

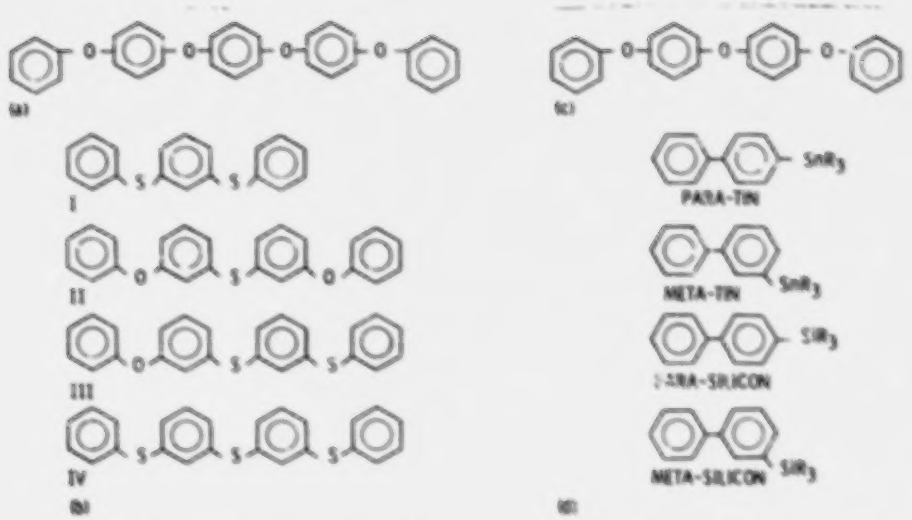

(a) Mix-bis (mix-phenoxyphenoxy) benzene (5P-4E).

(b) The thioether mixture consisting of 1, 3-bis (phenylthio) benzene (I), 1, 1'-thiobis (3-phenoxybenzene) (II), 1-phenoxy-3-((3-(phenylthio)phenyl)thio)benzene (III) and 1, 1'-thiobis (3-(phenylthio) benzene) (IV).

(c) Mix-bis (p-phenoxyphenyl) ether (4P-3E).

(d) General chemical structures of organotin and organosilicon compounds. Alkyl group is represented by R.

Figure 1. - Structures of the lubricants used in the experiments.

TABLE 1. - SUMMARY OF EXPERIMENTAL FLUID PROPERTIES

Fluid properties	Five-ring polyphenyl ether mix-5P-4E	Four-ring polyphenyl ether mix-4P-3E	Thioether (C-ether)	n-Butyl stannyl biphenyl	n-Butyl-silyl biphenyl
Kinematic viscosity, cS					
0 °C			13 000		
38 °C	360	63	25	10	23
99 °C	13	6.0	4.1	2.4	3.6
Pour point, °C	5	-12	-29		
Flash point, °C	288	260	230		
Fire point, °C	350	282	285		
Density at 38 °C, kg/m^3(g/ml)	1.19×10^3 (1.19)	1.17×10^3 (1.17)	1.18×10^3 (1.18)		

Other properties, such as surface tension and surface wettability, which are quite important in determining the tribological characteristics of these lubricants, are covered in detail in the following section.

SURFACE TENSION

BACKGROUND

Surface tension is one of the fundamental fluid properties. The unit of surface tension, 10^{-5} N/cm (1 dyn/cm), is equivalent to 10^{-7} J/cm^2 (1 erg/cm^2). Therefore, surface tension is a direct measure of surface interfacial energy. The surface energy of a fluid relative to adjacent phases influences the transport and distribution of fluid. Thus, surface tension is found to be an important parameter in the behavior of seals, oil spreading rates, foam stability, capillarity, fluid flow through porous solids, two-phase flow, mist lubrication, wettability of low-energy solids, two-phase heat transfer, and lubricant starvation (refs. 10 and 11). In practice, these operations often take place over a range of temperatures. It is important, therefore, to know the surface tension of the fluids used and how it varies with temperature.

Numerous methods for the measurement of liquid surface tension are available. These include the sessile drop, capillary pull, capillary rise, drop weight, surface rupture, and maximum bubble pressure (refs. 11 to 13). The role of surface tension in heat transfer (cooling) and in elastohydrodynamics (EHD) is discussed in the next two sections.

EFFECT OF SURFACE TENSION ON HEAT TRANSFER

Turbine engines of advanced high Mach number aircraft will be required to operate at ever increasing temperatures. Therefore, lubricating systems will be subjected to higher heat inputs, and the cooling capacity of the lubricant will become increasingly important.

lubricant properties (thermal conductivity, specific heat, specific gravity, and viscosity) and lubricant flow rate are important in determining heat-transfer (cooling) rates. Surface tension, by its effect on spreadability, may also influence the cooling capacity.

Poor wettability has been recognized as a factor in reducing heat transfer involving phase changes for many years (ref. 14). In boiling water experiments, increases in heat-transfer coefficients have been reported upon the addition of wetting additives.

Two-phase heat transfer which occurs in nucleate boiling is probably also present in the lubricating system of a turbine engine. However, in lubrication, temperatures would be too low to produce significant vapor formation by lubricant boiling. Bubble formation could be caused by dissolution and coalescence of entrained or dissolved gases or cavitation under the combined effects of heating and agitation occurring in the bearings, seals and gear components.

Figure 2 illustrates the effect of bubble shape on differences in liquid surface wettability. Clearly, the totally wetted condition of figure 2(a) would be more conducive to efficient heat transfer than the nonwetting condition of figure 2(b). The completely wetted surface would have a much greater percentage of area covered by liquid than the surface in the nonwetting condition. Heat transfer through the vapor phase would be only a fraction of that obtained through the liquid. In actual practice, the intermediate condition of partial wetting (fig. 2(c)) would probably occur. Nevertheless, the previous argument would still be valid. Lubricant surface tension should affect not only bubble formation and size but also the rate of liquid return to the void by bubble collapse or detachment.

Surface tension can also be an important factor in determining the wettability characteristics of a lubricant. In autophobic liquids or in systems with organic contamination, low-energy surface films are formed. Fluids having surface tensions greater than the surface energy of the low-energy films will not spread on these layers (ref. 15). Examples of surface contamination which produced

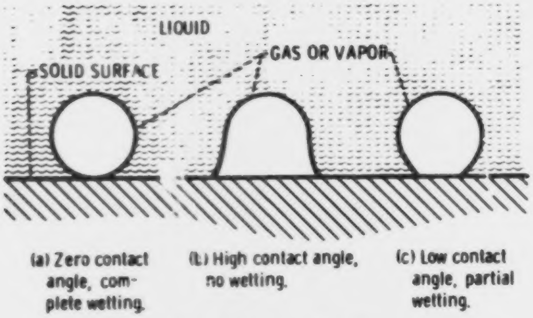
LIQUID
SOLID SURFACE
GAS OR VAPOR
(a) Zero contact angle, complete wetting.
(b) High contact angle, no wetting.
(c) Low contact angle, partial wetting.

Figure 2. - Effect of surface wettability on bubble shape.

nonwetting situations in ball bearings which led to premature failure are reported by Freeman, Allen, and Singer (ref. 16).

In addition, temperature gradients can cause evaporation of lower molecular weight lubricant components producing another important spreading phenomena known as the Marangoni effect. Here mass transfer results from surface tension gradients between the different molecular weight components. The Marangoni phenomenon and its effect on lubrication has been discussed in detail by Hirano (ref. 10).

ROLE OF SURFACE TENSION IN ELASTOHYDRODYNAMICS

The life of highly loaded bearings is related to the ability of an elastohydrodynamic (EHD) film to separate the bearing surfaces sufficiently so that asperity contact can be reduced or eliminated. A fundamental feature of EHD that has been well established from theory and experiment (ref. 17) is that film thickness is determined by the EHD pressure generated in the convergent inlet region. If there is an insufficient supply of lubricant in the inlet region, the EHD pressure generation will be inhibited; and the resulting film thickness will be diminished.

The amount of lubricant in the inlet region is determined by the location of the inlet lubricant boundary as shown in figure 3. The inlet distance S ahead of the contact region is the distance over which the EHD pressure can build up. By definition

$$S = x_b - a \tag{1}$$

where x_b is the distance from the lubricant boundary to the center of the Hertzian region and a is the calculated Hertzian radius of dry contact. For point contacts (ref. 17) the required inlet distance to obtain a flooded condition S_f is approximated by

$$S_f = \frac{3.52\ Rh_o^{2/3}}{a^{1/3}} \tag{2}$$

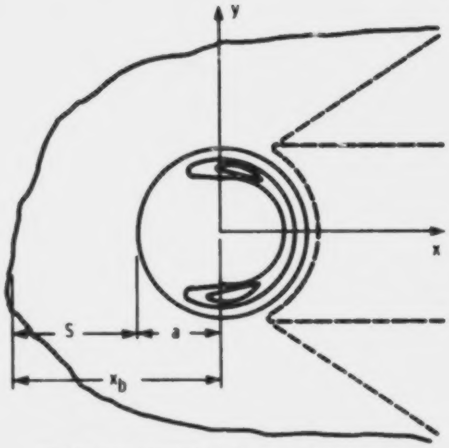

(a) Plan view showing requirements for starvation.

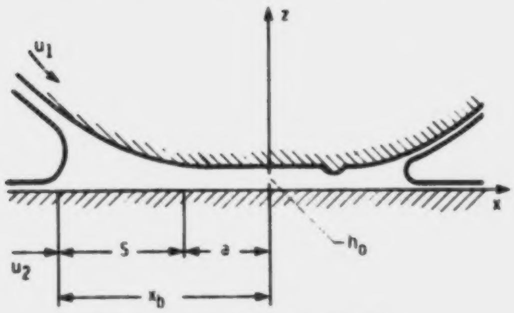

(b) Cross-sectional view along centerline.

Figure 3. - Contact geometry.

Thus, as bearing speed increases (i.e., h_o becomes larger), a greater inlet distance S_f is required to obtain a flooded condition.

The inlet distance is a function of several variables, including the quantity of available lubricant, contact geometry, speed of bearing surfaces, lubricant viscosity, and surface tension. The role of surface tension can be illustrated by considering two lubricated surfaces (e.g., a ball loaded on a flat) in static contact as shown in figure 4. Figure 4(a) shows the shape of the lubricant-air interface for a hypothetical case of a zero-surface-tension fluid. A real fluid with a finite surface tension will cause a pressure differential across an interface wherever the surface is curved. The pressure differential Δp is given by

$$\Delta p = \frac{\gamma_{LV}}{r_b} \tag{3}$$

where γ_{LV} is the surface tension, and r_b is the effective radius of curvature at the lubricant boundary. To establish equilibrium, the interface will tend to approach an infinite radius of curvature, and thus form a fluid meniscus around surfaces of close proximity (see fig. 4(b)). In this way surface tension should aid the filling of an EHD inlet region. Under dynamic conditions the shape of the fluid meniscus will be affected by the distribution of lubricant on the bearing surfaces and by the pressure and flow fields around the contact region. The effectiveness of surface tension to recapture and maintain lubricant in the inlet region will, according to equation (3), depend on the curvature of the lubricant boundary and the surface tension of the lubricant.

Therefore, from the previous discussions, it is obvious that lubricant surface tension is an important tribological fluid property. The next sections describe a technique to measure lubricant surface tension as a function of temperature. The maximum bubble pressure technique was chosen because of the following advantages:

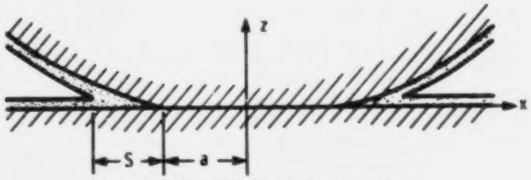

(a) Lubricant with zero surface tension.

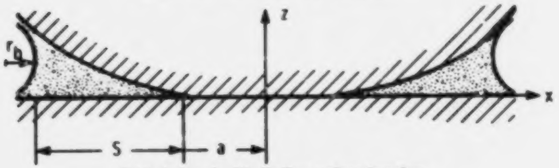

(b) Lubricant with finite surface tension.

Figure 4. - Contact geometry under static conditions.

(1) The bubble need not be observed under the liquid surface.

(2) All fluid is submerged in a constant-temperature bath, and thus temperature control is facilitated.

(3) The formation of fresh surfaces reduces the possibility of impurities collecting at the surface.

(4) The method is readily adapted for measurements over a broad temperature range.

(5) The bubble apparatus containing a given pair of capillary tubes can be calibrated with a standard fluid (e.g., water or benzene), so that it is not necessary to determine the exact tube radii.

Perhaps the most important advantage of the bubble-pressure technique lies in the fact that the method can often be assumed to be independent of the solid-liquid contact angle. Most other methods are quite dependent on the contact angle. The angle must be either assumed zero or measured, which is usually quite difficult.

EXPERIMENTAL

Apparatus

The bubble-pressure apparatus (fig. 5) consists of two parts. The lower part is a heat-resistant glass tube which acts as a reservoir for the test fluid. The upper part contains two capillary tubes and one open tube. It is sealed to the lower part by a ground-glass joint. The two capillary tubes are of the same length but different diameters, and both may be opened or closed with stopcocks. The capillary diameters are approximately 1 and 0.02 mm. The open tube is connected to a 2000 cm^3 flask which acts as a pressure damping device. The flask is connected to a vacuum line and a differential strain-gage pressure transducer. This transducer measures the differential pressure between the test chamber and the ambient room pressure. The bubble apparatus is placed in a constant-temperature bath containing glycerol as the heat-transfer fluid. Temperature control in the bath is specified to be ±0.01 °C from 40 to 200 °C.

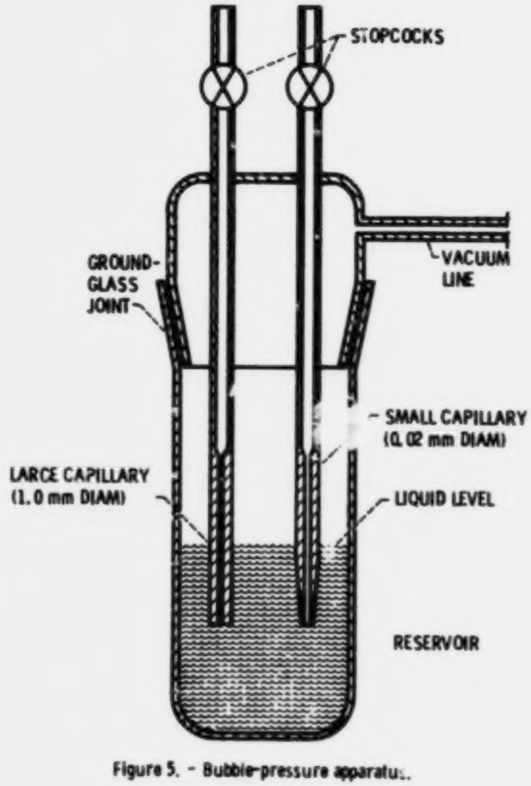

Figure 5. - Bubble-pressure apparatus.

However, because of the high viscosity of the glycerol, temperature control is poorer from 40 to 80 °C.

Procedure

The bubble apparatus is cleaned in hot chromic acid solution and rinsed with tap water and then with distilled water. Approximately 100 cm^3 of test fluid ($1 \times 10^{-4} m^3$) are placed in the reservoir. The test fluid itself acts as a lubricant for the ground-glass joint. The apparatus is placed in the bath, and the desired temperature is set. Then 10 to 15 min are allowed for temperature equilibrium to be established.

The large capillary tube is opened, and a slight vacuum is pulled in the test chamber. The pressure differential across the chamber causes air to be drawn through the capillary and results in the formation of a stream of bubbles. The pressure is regulated so that one or two bubbles a second are formed. The differential pressure rises to a maximum as the bubble is being formed and drops sharply as the bubble breaks away from the capillary tip and travels to the surface. Then the pressure differential increases again and the process is repeated. These pressure changes are recorded on an x,y-recorder. A schematic of a typical recorder trace appears in figure 6.

After several pressure spikes have been recorded for the large capillary, the small tube is opened and the large tube is closed. The procedure is repeated. The smaller capillary, of course, requires a greater pressure difference for bubble formation. The manner of bubble formation is also different. The pressure difference rises to a maximum, and then a stream of bubbles appears. This process decreases the pressure difference, and bubble formation stops. The pressure difference increases again, and the process is repeated. A recorder trace for this behavior also appears in in figure 6.

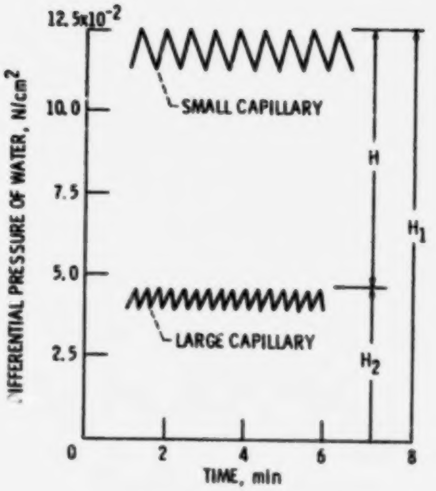

Figure 6. - Typical differential pressure curves for large and small capillary tubes.

Calculation of Surface Tension

The surface tension is calculated by using the equation developed by Sudgen (ref. 12)

$$\gamma_{LV} = AP\varphi \tag{4}$$

where A is the apparatus constant, P is the pressure difference between the two capillaries ($H_1 - H_2$, from fig. 6) in N/cm^2, and φ is a correction factor, which is given by the following equation:

$$\varphi = 1 + \frac{0.69\ r_2 gD}{P} \tag{5}$$

D is the liquid density (g/cm^3), g, the acceleration due to gravity (981 cm/s^2), and r_2, the large capillary radius (mm). The apparatus constant is determined by using distilled water as the calibrating fluid. Organic contamination was removed by distillation from a permanganate solution. The constant A for the apparatus was determined by this method to be 3.32×10^{-3} cm. To check the accuracy of this constant, the surface tension as a function of temperature was determined for two other pure compounds, benzene and bromobenzene. Both were of reagent grade purity. The benzene and bromobenzene surface tensions were compared to literature values, and a maximum error of 1.9 percent and an average error of less than 1.0 percent were obtained.

Results

Surface tension as a function of temperature for 5P-4E, measured by the maximum bubble pressure technique, appears in figure 7. A maximum value of 46 dyn/cm was obtained at 23 °C. The surface tension then decreases linearly with increasing temperature which occurs with most organic liquids. A temperature coefficient of surface tension ($d\gamma/dT$) of 0.088 dyn/cm °C was obtained. γ_{LV} at 23 °C and $d\gamma/dT$ for a series of other liquid lubricants, including 4P-3E and the thioether, appear in table 2 for comparison.

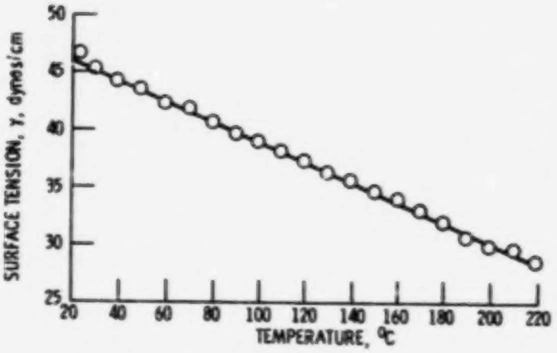

Figure 7. - Surface tension as a function of temperature for a five ring polyphenyl ether (5P-4E) using the maximum bubble pressure technique.

TABLE 2. - SURFACE TENSION AT 23 °C AND TEMPERATURE COEFFICIENT OF SURFACE TENSION FOR SEVERAL LIQUID LUBRICANTS

Test lubricant	Temperature coefficient of surface tension, $-d\gamma/dt$, N/(cm)(°C)	Surface tension at 23 °C	
		N/cm	dyn/cm
Five-ring polyphenyl ether (5P-4E)	0.088×10^{-5}	46.0×10^{-5}	46.0
Four-ring polyphenyl ether (4P-3E)	.088	44.8	44.8
Thioether	.088	44.8	44.8
Synthetic paraffinic oil	.064	30.3	30.3
Superrefined naphthenic mineral oil	.064	30.3	30.3
Superrefined paraffinic mineral oil	.077	29.8	29.8
Fluorosilicone	.063	25.0	25.0
Fluorinated polyether	.053	17.3	17.3

As can be seen, the two polyphenyl ethers and the thioether have very similar surface tensions and temperature coefficients. They are also much higher than the other classes of liquid lubricants. This may have important ramifications in regard to surface wettability which is discussed in the next section.

WETTABILITY

BACKGROUND

When a liquid forms a finite contact angle on a surface ($\theta \neq 0$), we say the liquid is nonspreading. If the contact angle is zero, the liquid wets the surface completely and spreads freely over the surface at a rate depending on viscosity and surface roughness.

At room temperature, the surface-free energies of organic liquids and lubricants are less than 100 erg/cm^2. Metals and ceramics have surface-free energies ranging from 500 to 5000 erg/cm^2. Theoretically, one would then expect all organic liquids to spread freely on any high energy solid. This is because the spreading would result in a large decrease in the free energy of the system.

If one considers low energy solids such as polymers, the situation could, and does, exist where the surface energy (surface tension) of a fluid is greater than that of the surface. For that situation, the fluid would not spread and a drop having a finite contact angle would occur. An analogous situation could occur if low energy contaminant films are present on the high energy solid surface (ref. 18).

Considering the five ring polyphenyl ether (5P-4E) and M-50 steel (a typical bearing steel) one would predict that this fluid type should spread freely on a clean M-50 surface. However, it has been well documented (ref. 19) that this does not always occur. Another class of chemically similar fluids, thioethers, have exhibited similar wetting problems (ref. 20). This nonspreading phenomenon occurred in spite of procedures to remove polar impurities which might have produced oleophobic films.

Many years ago, Fox et al. (ref. 15) reported similar nonwetting properties for certain pure organic fluids such as 1-octanol, trichlorodiphenyl, and tri-o-cresyl phosphate. It was hypothesized that these fluids were nonspreading because the molecules adsorbed on the solid surface formed a film whose critical surface energy was less than the surface tension of the fluid itself. The term "autophobic liquids" was coined to describe this behavior.

Since two of the fluids mentioned above were aromatic and thus were chemically somewhat similar to the aromatic polyphenyl ether (5P-4E), it seemed plausible that 5P-4E may also be autophobic.

To check this possibility, two things are needed: surface tension as a function of temperature and the critical surface energy of spreading, γ_c. The surface tension for 5P-4E has been measured and appears in figure 7 for temperatures from 23 to 220 °C.

The critical surface energy of spreading, γ_c, of an adsorbed monolayer is more difficult to measure. The classical technique to measure γ_c for low energy polymer surfaces is to plot the cosine of the contact angle ($\cos \theta$) for a homologous series of organic liquids as a function of their surface tension (γ_{LV}). Empirically, a rectilinear relationship was established. The γ_c was defined by the intercept of the horizontal line $\cos \theta = 1$ with the extrapolated straight line plot of $\cos \theta$ versus γ_{LV}. A typical plot for the wettability of polytetrafluoroethylene (PTFE) by a series of n-alkanes appears in figure 8 (ref. 18).

This yields a γ_c for PTFE of approximately 18.5 dyn/cm at 20 °C. Essentially, this means that, at 20 °C, a n-alkane having a surface tension >18.5 dyn/cm will not spread on a PTFE surface. On the other hand, a n-alkane with a surface tension <18.5 dyn/cm will spread spontaneously.

To determine the γ_c of an adsorbed surface film, a modification of this technique can be used. If one were to use a series of organic liquids of varying surface tensions, the possibility exists for chemical or physical interaction with the adsorbed surface film. This could alter the wetting properties of the surface.

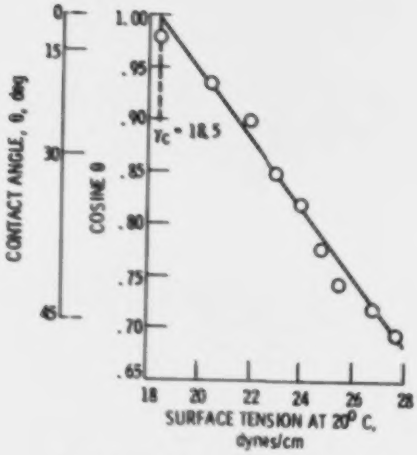

Figure 8. - Wettability of polytetrafluoroethylene by n-alkanes (from ref. 18).

Another way to determine γ_c for the surface film would be to measure contact angle as a function of temperature. As temperature varies, the surface tension varies and an analogous plot of $\cos\theta$ versus γ_{LV} could be plotted for one fluid. Therefore, contact angles as a function of temperature were measured for 5P-4E on M-50 steel.

EXPERIMENTAL

Tilting Plate Apparatus

Two different techniques were used to measure contact angle as a function of temperature (1) a tilting plate apparatus, and (2) a sessile drop apparatus.

The tilting plate apparatus shown schematically in figure 9 consists of a stainless steel fluid reservoir (~0.5 l) and a small M-50 steel plate (4.1 by 1.3 by 0.24 cm) which can dip into the liquid in the reservoir at various angles. The plate is attached to a lever arm which is rotated at slow speed by a motor. The reservoir and plate are contained in a chamber for atmosphere control. Contact angles are measured with a goniometer through a side window. The fluid is heated by a variable resistance heater located in the base of the reservoir. Temperature is monitored by a thermometer immersed in the fluid.

Tilting Plate Procedure

The fluid reservoir and M-50 steel plate were thoroughly cleaned by scrubbing with a paste of levigated alumina and water, rinsed with tap water and finally distilled water and allowed to air dry. The plate was then positioned in the chamber. Approximately 0.5 l of 5P-4E was thoroughly degassed by heating to 150 °C under a vacuum. The degassed fluid was transferred to the reservoir after the chamber had been purged for 30 min with dry nitrogen. A continuous nitrogen purge was maintained during the test. The reservoir heater was set

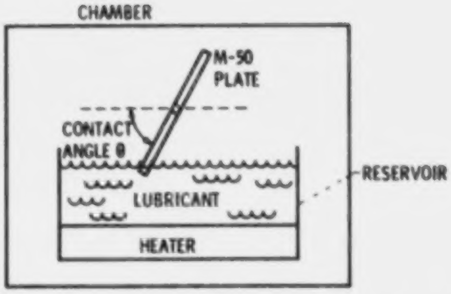

Figure 9. - Schematic diagram of tilting plate contact angle device.

for the proper fluid temperature. After temperature stabilization, the plate was tilted so that the fluid recedes off the plate and a curved meniscus formed. The plate is continuously rotated at slow speed (~1 rpm) until the meniscus becomes straight as it contacts the plate. At this point, the angle of the plate is measured with a goniometer. Then the temperature is increased (normally 25 °C), allowed to stabilize, and the procedure repeated. Only advancing angles were measured.

Sessile Drop Apparatus

A sessile drop apparatus was also used to measure contact angles. This apparatus is shown in figure 10. It consists of a low power microscope for horizontal observation of a fluid drop. A drop is placed on the test specimen which is in turn placed on a heated platen. A light source allows for back illumination of the drop. A cover allows for atmosphere control. Specimen temperature is sensed by a contact thermocouple and maintained by a temperature controller. Contact angles are measured by a goniometer eyepiece.

Sessile Drop Procedure

For tests with this apparatus, the M-50 steel plate was cleaned as previously described. It was then placed on the platen and the cover closed. A nitrogen flow is maintained over the specimen. Several drops of degassed 5P-4E were placed on the specimen through a port in the top of the cover. This was accomplished by dipping a flamed platinum wire in the degassed lubricant and touching the plate. Drop size varied but typically was in the range of 0.5 to 1.5 µl.

The light source and microscope stage were then adjusted to produce a sharp silhouette of the drop. Then a goniometer eyepiece was used to measure the contact angle as illustrated in figure 11. The temperature was then increased by 5 °C and the measurement repeated.

ORIGINAL PAGE IS
OF POOR QUALITY

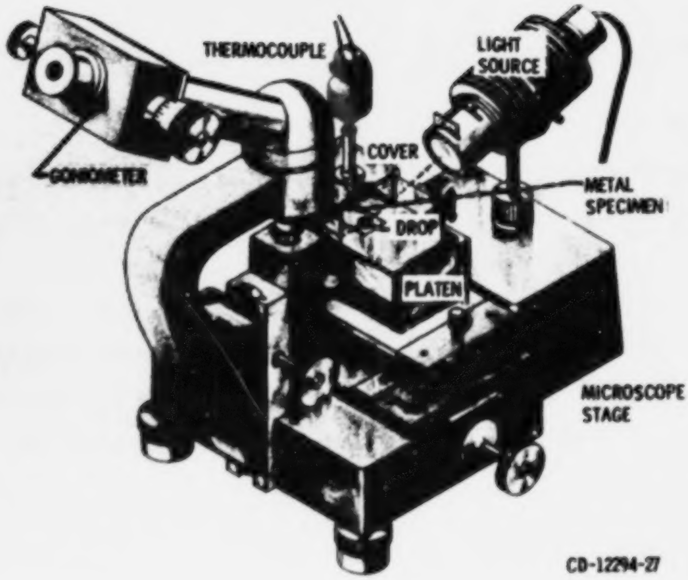

CD-12294-27

Figure 10. - Sessile drop contact angle apparatus.

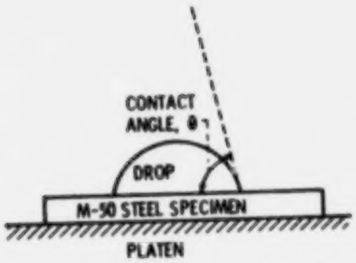

Figure 11. - Representation of contact angle measurement from sessile drop apparatus.

Results

Contact angles for various temperatures for 5P-4E using both test devices appear in table 3. Values range from a high contact angle of 50° at 70 and 90 °C for the plate apparatus to a low contact value of 5° at 180 °C for the sessile drop technique. Values for the plate apparatus are consistently higher than from the sessile drop measurements. There is no apparent reason for these differences, other than that two completely different techniques were used. Reproducibility of contact angles at any particular condition was about ±2°. Error in angle measurement using a goniometer is considered to be ±1°. These variations are similar to those reported in the literature (ref. 18).

The contact angle data from table 3 has been plotted in the standard $\cos\theta$ versus γ_{LV} format. The data for the tilting plate apparatus appears in figure 12 and for the sessile drop apparatus in figure 13. A least squares technique was used to determine the best straight line for each set of data. Extrapolated to $\cos\theta = 1$, γ_c was determined to be 30.1 dyn/cm for the tilting plate technique and 31.3 dyn/cm for the sessile drop technique. This is good agreement considering that two completely different techniques were used.

One problem using this procedure is that γ_c can also change with temperature. Surface film density will decrease with increasing temperature. However, this effect is not great and γ_c will increase only slightly as temperature rises (ref. 18).

A second consideration is the possibility of lubricant and metal oxidation and lubricant degradation at high temperatures. The contact angle measurements were all performed in a nitrogen atmosphere to preclude any oxidation problems. Surface tension measurements were made in air. However, it is not felt that an air atmosphere presented any problems for these tests. 5P-4E is oxidatively stable at the highest temperature (220 °C) reached in the surface tension measurements.

TABLE 3. - CONTACT ANGLES FOR A FIVE-RING POLYPHENYL ETHER (5P-4E) ON M-50 STEEL AT VARIOUS TEMPERATURES IN A DRY NITROGEN ATMOSPHERE

Temperature, °C	Contact angle, deg	
	Tilting plate apparatus	Sessile drop apparatus
25	-----	30,32,34
50	-----	27,27,29
70	47,50	--------
75	-----	24,24,27
80	40	--------
90	50	--------
100	40,42	22,23,24
110	37,38	--------
115	41	--------
120	33,36	--------
125	-----	19,20,22
130	29,33	--------
140	31,36	--------
145	37	--------
150	29,34	15,16,17
155	34	--------
160	27,28	--------
165	31	--------
170	22,27	--------
175	24	7,9,11
180	18,20	5,5,11
185	20	--------
190	22	--------

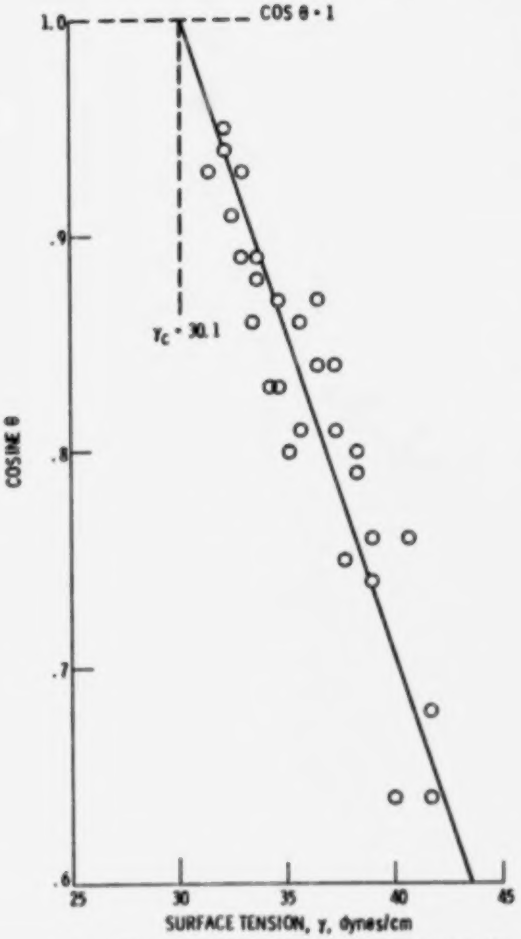

Figure 12. - Cosine of the contact angle of 5P-4E on M-50 steel as a function of surface tension - tilting plate apparatus (dry nitrogen atmosphere).

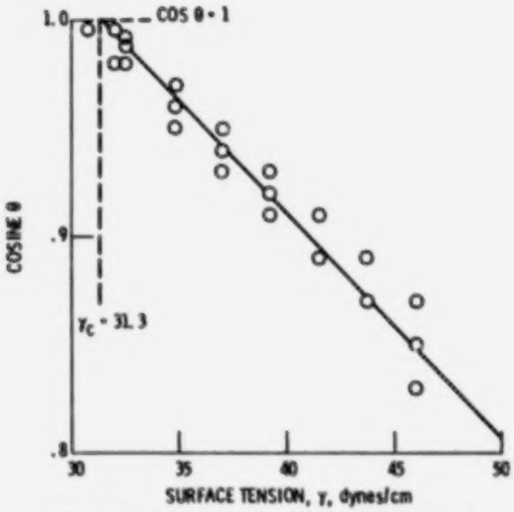

Figure 13. - Cosine of the contact angle of 5P-4E on M-50 steel as a function of surface tension - sessile drop apparatus (dry nitrogen atmosphere).

These values indicate that 5P-4E is autophobic (i.e., it will not spread on its own surface film on M-50 steel until its surface tension falls below about 30 to 31 dyn/cm). This surface tension corresponds to a fluid temperature of approximately 190 to 200 °C.

Therefore, 5P-4E is inherently nonspreading on steel surfaces over most of its practical temperature range. This fact may contribute to some of the wear problems associated with this fluid, which will be described later. It seems likely that the thioethers are also autophobic. Chemically, the thioethers are very similar to the polyphenyl ethers since they are mixtures of thiophenyl ethers. Thus, the wetting problems associated with this fluid may be explained by a similar phenomenon. Preliminary contact angle measurements of thioethers on steel support this supposition.

WETTABILITY ADDITIVES

Because wettability problems had been encountered with the polyphenyl ether class of lubricants, an obvious approach would be to utilize additives to promote better wetting. If one could lower the surface tension (γ_{LV}) below the critical surface energy for wetting (γ_c), then spontaneous spreading should occur.

A number of investigators have shown that additives can lower the surface tension of nonaqueous solutions. McBain and Perry (ref. 21) showed that lauryl-sulfonic acids lowered γ_{LV} for a series of hydrocarbons. Many silicones and fluorochemicals have been found to depress γ_{LV} of organic liquids (ref. 22).

Three different additives were chosen to study their effect on wettability (γ_{LV} depression) and on boundary lubrication behavior of 5P-4E. These materials were: trichloroacetic acid, (TCAA) (0.1 wt %), a dimethylsilicone (DMS) (1 wt %) and stearyl siloxane (SS) (1 wt %).

The maximum bubble pressure apparatus described previously was used to determine γ_{LV} as a function of temperature for each of the solutions. The results of these measurements are shown in figure 14.

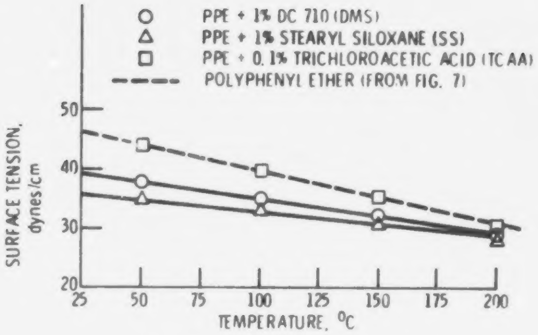

Figure 14. - Surface tension as a function of temperature for a polyphenyl ether (5P-4E) and three wettability additives.

These results indicated that TCAA had no effect on γ_{LV} while DMS and SS both depressed γ_{LV} with SS having the greater effect. For example at 50 °C, SS depressed γ_{LV} by ~20 percent and DMS by ~13 percent. As temperature increased the effect was less pronounced (about 5 percent for both additives at 200 °C).

Contact angle measurements with the sessile drop apparatus yielded conflicting results. The TCAA solution (no γ_{LV} depression) showed a small improvement in wettability as the solution spread at 20 °C lower than the base fluid. The DMS solution spread at about a 40 °C lower temperature. However, the SS solution behaved similarly to the base fluid, essentially showing no effect. The reason for this anomaly is not known. Wear results on some of these solutions are reported in the next section concerning boundary lubrication.

BOUNDARY LUBRICATION

BACKGROUND

The purpose of lubrication is to separate surfaces in relative motion by a material which has a low resistance to shear so that the surfaces do not sustain major damage. This low resistance material can be a variety of different species (e.g., adsorbed gases, chemical reaction films, liquids, solid lubricants, etc.).

Depending on the type of intervening film and its thickness, a number of lubrication regimes can be identified. A classical way of depicting some of these regimes is by use of the well known Stribeck curve (fig. 15). Stribeck (ref. 23) performed comprehensive experiments on journal bearings around 1900. He measured the coefficient of friction as a function of load, speed, and temperature. However, it was difficult to condense this data into usable form. Some years later, Hersey (ref. 24) performed similar experiments and devised a plotting format based on a dimensionless parameter. The Stribeck curve, or more appropriately, the

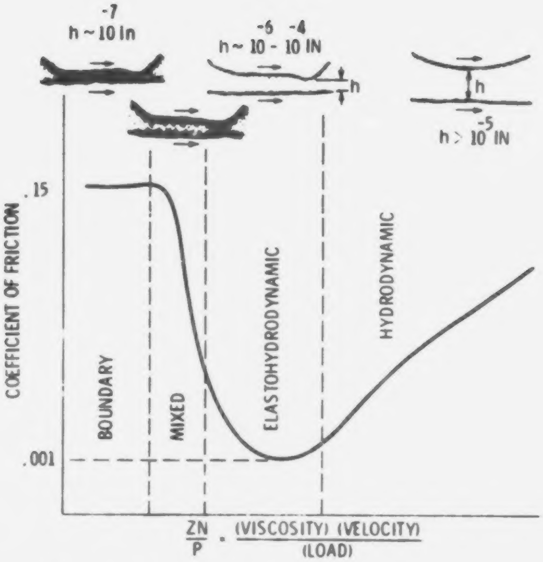

Figure 15. - Coefficient of friction as a function of speed-velocity-load parameter (Stribeck-Hersey curve) (ref. 23).

Stribeck-Hersey curve takes the form of the coefficient of friction as a function of the viscosity (Z), velocity (N), and load (P) parameter, ZN/P.

At high values of ZN/P which occur at high speeds, low loads, and at high viscosities, the surfaces are completely separated by a thick (>0.25 μm) ($>10^{-5}$ in.) lubricant film. This is the area of hydrodynamic lubrication where friction is determined by the rheology of the lubricant. For nonconformal concentrated contacts where loads are high enough to cause elastic deformation of the surfaces and pressure-viscosity effects on the lubricant, another fluid film regime, elastohydrodynamic lubrication (EHD) can be identified. In this regime film thicknesses (h) may range from (0.025 to 2.5 μm) (10^{-6} to 10^{-4} in.).

As film thickness becomes progressively thinner, surface interactions start taking place. This regime of increasing friction in which there is a combination of asperity interactions and fluid film effects is referred to as the mixed lubrication regime.

Finally, at low values of the ZN/P parameter, one enters the realm of boundary lubrication. This regime is characterized by the following:

1. It is a highly complex regime involving metallurgy, surface topography, physical and chemical adsorption, corrosion, catalysis, and reaction kinetics.

2. The most important aspect of this regime is the formation of protective surface films to minimize wear and surface damage.

3. The formation of these films is governed by the chemistry of both the film former as well as the surface and other environmental factors.

4. The effectiveness of these films in minimizing wear is determined by their physical properties which include: shear strength, thickness, surface adhesion, film cohesion, chain length, melting point or decomposition temperature, and solubility.

It is obvious that a concise definition of boundary lubrication is not possible. For the purposes of this thesis, the following general definition will be used. Boundary lubrication is lubrication by a liquid under conditions where there is appreciable solid-solid interactions. Friction and wear are determined predominantly by interactions between the solid surfaces and between the surfaces and the liquid. The viscous properties of the liquid play little or no part in this process.

Lubrication Regimes

Besides the Stribeck-Hersey curve an idealized plot of wear rate as a function of relative load can also delineate the various lubrication regimes as well as some wear transitions (fig. 16) (ref. 25).

Region OA. - This region encompasses the regimes of hydrodynamic and elastohydrodynamic lubrication (EHD), the latter as point A is approached. Since there are no surface interactions in this region except for startup or shutdown, little or no wear occurs. This is excluding rolling element fatigue which can occur without surface interactions.

Region AX. - Region AX is the mixed lubrication regime where surface interactions begin to occur at A and become more prevalent as point X is approached. Wear is low because there are still fluid film effects.

Region XY. - This is the region of boundary lubrication. The degree of metal to metal contact and the wear rate increase as the load increases. Wear is mild and tends to be corrosive to the left of B and adhesive to the right of B. The location of B is quite variable and depends on the corrosivity of the lubricant formulation. For a noncorrosive lubricant, adhesive wear can occur at X. On the other hand, a corrosive additive can extend the boundary regime to Z' before boundary film failure occurs.

Region YZ. - This is the regime of severe wear where scuffing and scoring occur. Machinery cannot operate successfully in this region and, therefore, the location of this transition point is quite important. At point Z, there is total surface failure and seizure occurs.

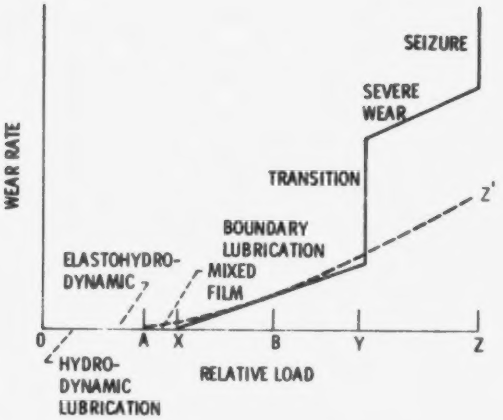

Figure 16. - Wear rate as a function of relative load depicting the various regimes of lubrication (ref. 25).

Boundary Film Formation

The most important aspect of boundary lubrication is the formation of surface films (from additives or the lubricant itself) which will protect the contacting surfaces. Basically, there are three mechanisms of boundary film formation: physical adsorption, chemisorption and chemical reaction (ref. 26).

Physical adsorption. - Physical adsorption involves intermolecular forces analogous to those involved in condensation of vapors to liquids. Physical adsorption is usually rapid, reversible, and nonspecific. Energies involved in physical adsorption are in the range of heats of condensation. Physical adsorption may be monomolecular or multilayer. There is no electron transfer in this process. An idealized example of the physical adsorption of hexadecanol on an unreactive metal is shown in figure 17. Because of the weak bonding energies involved, physically absorbed species are not very effective boundary lubricants.

Chemisorption. - Chemisorption of a species on a surface is usually specific, may be rapid or slow and is not always reversible. Energies involved in chemisorption are large enough to imply that a chemical bond has formed (i.e., electron transfer has taken place). Chemisorption is a monomolecular process. It also may require an activation energy as opposed to physical adsorption which requires none. A species may be physically adsorbed at low temperatures and chemisorbed at higher temperatures. In addition, physical adsorption may occur on top of a chemisorbed film. An example of the chemisorption of stearic acid on an iron oxide surface to form iron stearate is illustrated in figure 18.

Chemical reaction. - Although chemisorption involves a chemical reaction, this section mainly deals with inorganic reaction products on surfaces. This process is also specific, may be rapid or slow (depending on temperature, reactivity and other conditions), and is irreversible. Films can be unlimited in thickness. An idealized example of a reacted film of iron sulfide on an iron surface is shown in figure 19.

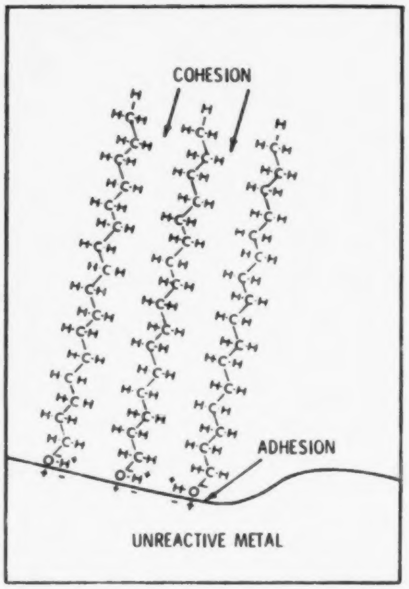

Figure 17. - Physical adsorption hexadecanol (ref. 27).

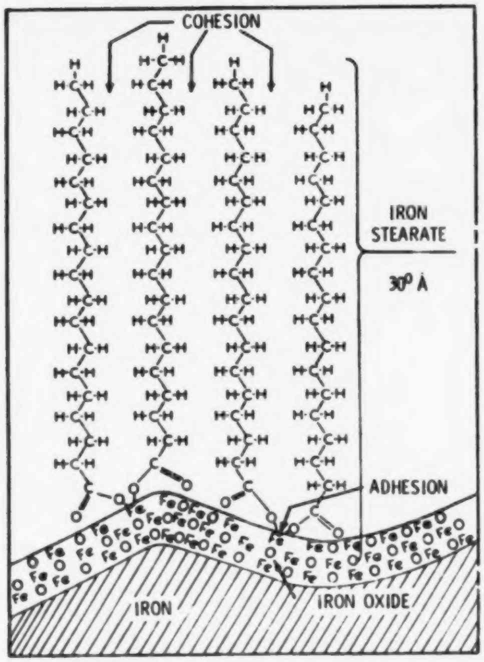

Figure 18. - Chemisorption of stearic acid on an iron surface to form iron stearate (ref. 27).

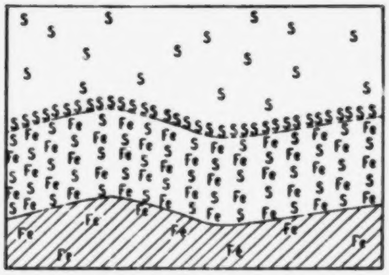

Figure 19. - Inorganic film formed by reaction of sulfur with iron to form iron sulfide (ref. 27).

Another chemical reaction of import to boundary lubrication is "friction polymer" formation. In 1958, Hermance and Egan (ref. 28) reported on the occurrence of organic deposits on electrical relay contacts and coined the term "friction polymer." Since that time many investigators have observed the presence of this material in lubricated contacts. Although little is known about its mode of formation or its chemical structure, it can, in some cases, act as a boundary lubricant.

Physical Properties of Boundary Films

The physical properties of boundary films that are important in determining their effectiveness in protecting surfaces include: melting or decomposition temperature, shear strength, thickness, surface adhesion, cohesion and solubility in the bulk lubricant.

Melting point. - The melting point of boundary films is probably the most common property which correlates with film failure. The literature is replete with such examples. Russell, et al., (ref. 29) reported friction transitions for copper lubricated with pure hydrocarbons. Friction data for two hydrocarbons (mesitylene and dotriacontane) appear in figure 20 as a function of temperature. Obviously, the films of these nonpolar materials, which are not chemically bound to the copper surface, provide little protection in the liquid state.

In contrast, chemisorption of fatty acids on reactive metals yields failure temperatures based on the softening point of the soap rather than the melting point of the parent fatty acid. Examples of transition temperatures for several fatty acids appear in figure 21 (ref. 30).

Chemically reacted inorganic surface films such as oxides and sulfides do not have failure transitions that correlate with their melting points. These materials often have very high melting points (>1000 °C) and other factors (such as decomposition or physical removal) may limit their effectiveness at temperatures well below their melting point.

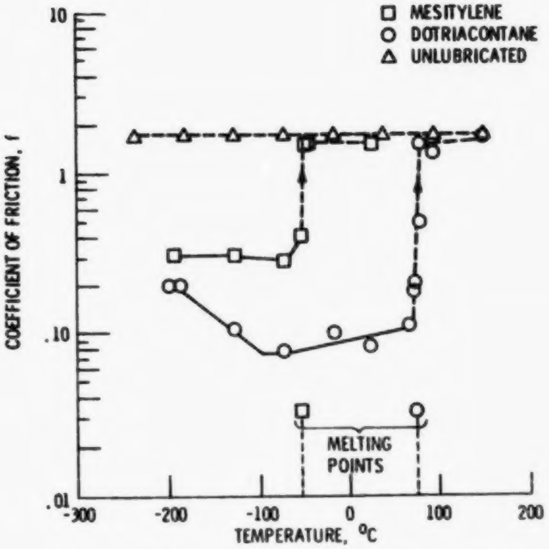

Figure 20. - Friction versus temperature for copper lubricated with hydrocarbons in dry helium (ref. 29).

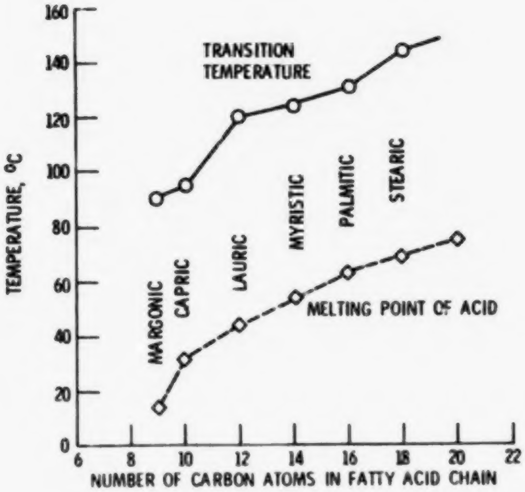

Figure 21. - Frictional transition temperatures for several fatty acids on steel as a function of chain length (ref. 30).

Shear Strength. - The shear strength of a boundary lubricating film should be directly reflected in the friction coefficient. In general, this is true with low shear strength soaps yielding low friction while high shear strength salts yield high friction (ref. 27). This relationship is illustrated in figure 22. Shear strength is also affected by both pressure and temperature. For example, shear stress as a function of load (pressure) for stearic acid is shown in figure 23 (ref. 31).

Boundary Film Thickness. - Boundary film thicknesses can vary from a few angstroms (absorbed gas) to thousands of angstroms (chemical reaction film). The effect of thickness on friction has been discussed in detail by Kragelskii (ref. 32). In general, as the thickness of a boundary film increases, the coefficient of friction decreases (fig. 24(a)). However, continued increases in thickness may result in an increase in friction (fig. 24(b)). This figure has the general shape of the familiar Stribeck-Hersey curve (fig. 15). Another point of interest: shear strength of all boundary films decreases as their thickness increases, which may be related to the above.

For physically absorbed or chemisorbed films, surface protection is usually enhanced by increasing film thickness (ref. 30). The frictional transition temperature of multilayers also increases with increasing number of layers.

For thick chemically reacted films there is an optimum thickness for minimum wear which depends on conditions. The relationship between wear and lubricant (or additive) reactivity is shown in figure 25. Here, if reactivity is not great enough to produce a thick enough film, adhesive wear occurs. On the other hand, if the material is too reactive, very thick films are formed and corrosive wear ensues. Lubricant or additive reactivity is also a function of temperature and concentration (fig. 26) (ref. 33).

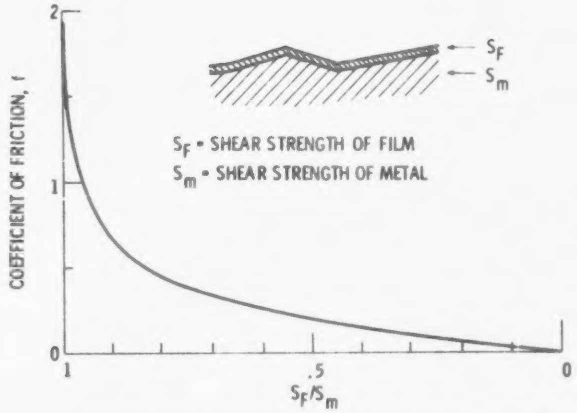

Figure 22. - Friction as a function of the ratio of shear strengths of film and metal (ref. 27).

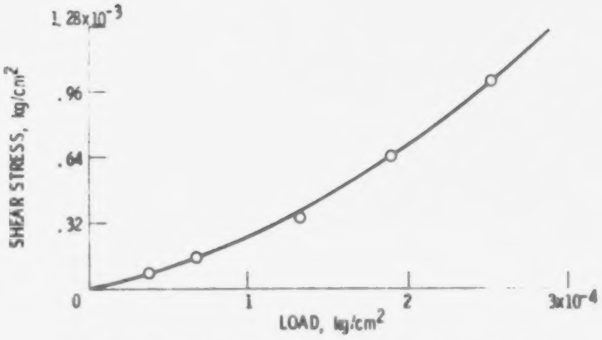

Figure 23. - Shear stress as a function of load for a thin layer of solid stearic acid (ref. 31).

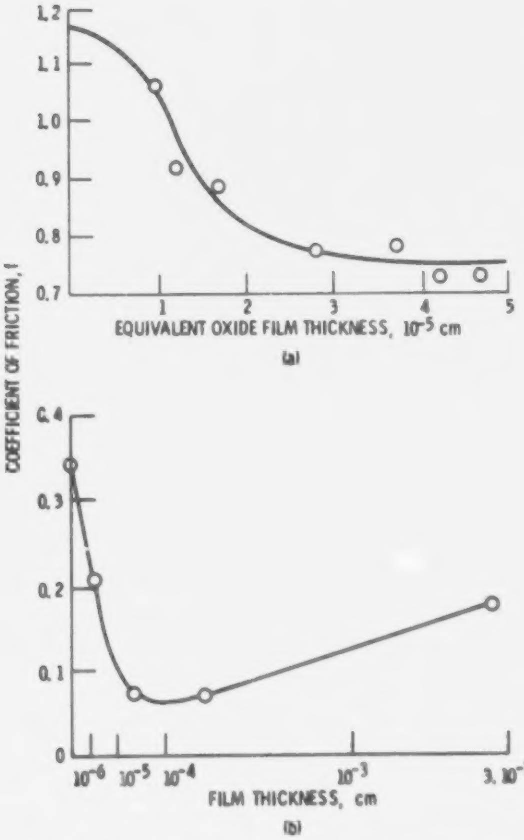

Figure 24. -- Relationship between friction and thickness of surface films: (a) coefficient of friction against oxide film thickness on copper; (b) coefficient of friction against thickness of indium film (ref. 32).

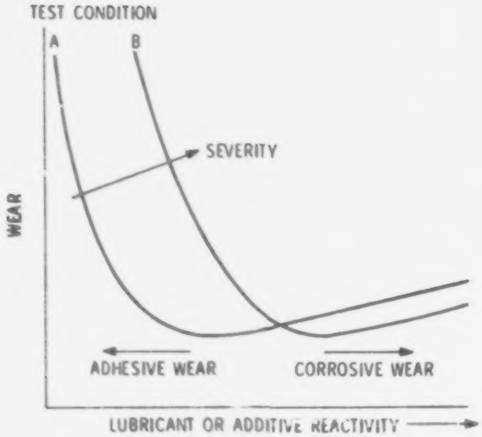

Figure 25. - Relationship between wear and lubricant reactivity (ref. 33).

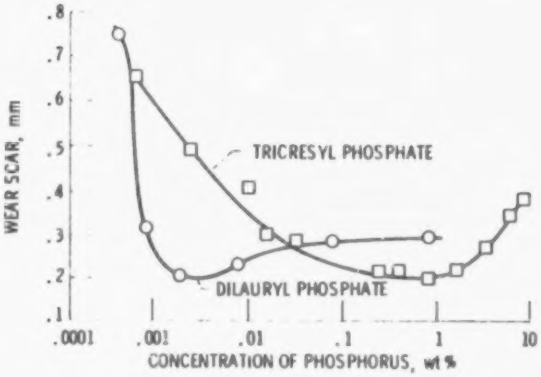

Figure 26. - Wear versus additive concentration from four-ball tests (ref. 33).

Chain Length

Another interesting phenomenon which affects the properties of boundary films is the chain matching effect. Simply stated, when the carbon chain length of a straight chain additive (such as a fatty acid) coincides with that of the solvent or base oil, scuffing resistance is enhanced. This is clearly shown in four-ball tests where the maximum critical load occurs with a C_{16} fatty acid in n-hexadecane base fluid ($C_{16}H_{34}$) (ref. 34).

Effect of Operating Variables on Friction

Load. - As mentioned in the earlier discussion on the Stribeck-Hersey curve (fig. 15), in the boundary lubrication regime, the coefficient of friction is essentially constant with increasing load. This is a statement of Amonton's law which says that the coefficient of friction is independent of load. This law is amazingly well obeyed for most systems if there is no boundary film failure. This is illustrated in figure 27 (ref. 35) for copper surfaces lubricated with two fatty acids. At loads (>50 g) the coefficient of friction is essentially constant. The increasing friction at decreasing loads is probably related to molecular orientation effects and the fact that film penetration does not occur.

Speed. - In general, in the absence of viscosity effects, friction changes little with speed over a sliding speed range of 0.005 to 1.0 cm/sec (ref. 36). Where viscosity effects do come into play, two types of behavior are observed. These are illustrated in figure 28 (ref. 37). Here, relatively nonpolar materials such as mineral oils show a decrease in friction with increasing speed while polar fatty acids show the opposite trend. In addition, the mineral oil behavior is usually associated with stick-slip phenomena. This is of practical importance since a good boundary lubricant does not lead to stick-slip behavior.

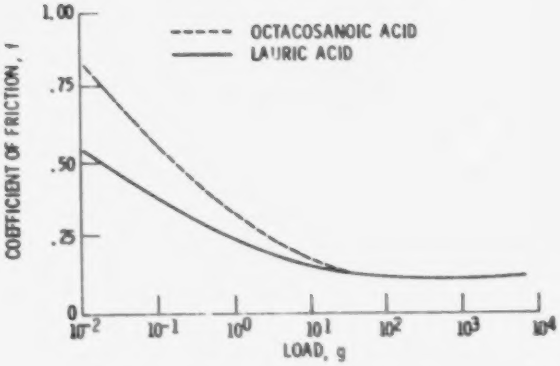

Figure 27. - Friction versus load for copper lubricated with fatty acids (ref. 35).

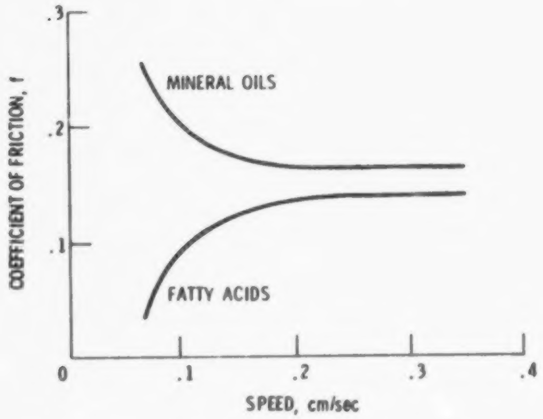

Figure 28. - Friction versus speed (ref. 37).

At high speeds, viscous effects will be present and increases in friction are normally observed (fig. 29) (ref. 38). This portion of the friction curve is analagous to the rising portion of the Stribeck-Hersey curve (fig. 15) as one approaches hydrodynamic lubrication.

Temperature. - It is impossible to generalize about the effect of temperature on boundary friction. So much depends on the other conditions and the type of materials present. Temperature can cause disruption, desorption, or decomposition of boundary films. It can also provide activation energy for chemisorption or chemical reactions. The frictional transition temperatures of figure 21 show the effect of temperature on the melting of the chemisorbed fatty acids.

Atmosphere. - The presence of oxygen and water vapor in the atmosphere can greatly affect the chemical processes that occur in the boundary layer. These processes can, in turn, affect the friction coefficient. The importance of atmospheric and adsorbed oxygen is illustrated in figure 30 (ref. 39). Here, the "EP" activity of tricresylphosphate (TCP) is totally absent in a dry nitrogen atmosphere. In contrast, normal "EP" activity is present in dry air.

Effect of Operating Variables on Wear

Load. - It is generally agreed that wear increases with increasing load but no simple relationship seems to exist. This refers to the situation where no transition to severe wear has occurred. At this point, a discontinuity on wear versus load occurs which is illustrated in figure 16. Figure 31 illustrates the increase in wear scar radius with increasing load (ref. 36).

Speed. - For practical purposes, wear rate in the boundary lubrication regime is essentially independent of speed. Obviously, this does not hold if one moves into the EHD regime with increasing speed. This also assumes no boundary film failure due to contact temperature rise. An example of wear rate as a function of sliding

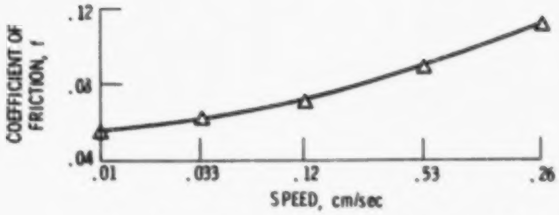

Figure 29. - Friction versus speed for steel/bronze lubricated with oleic acid (ref. 38).

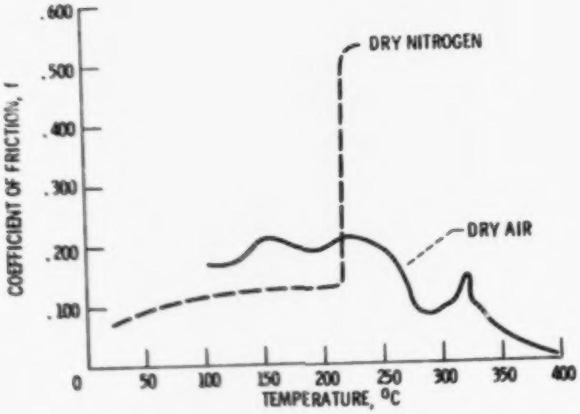

Figure 30. - Friction versus temperature for pure tricresyl phosphate on M-50 steel. (Ref. 39).

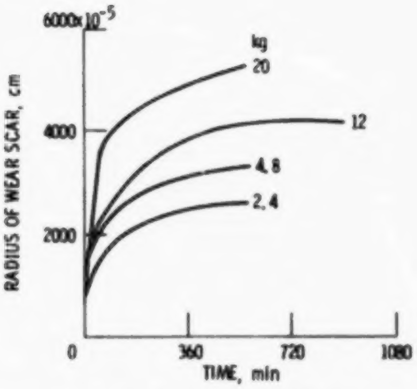

Figure 31. - Radius of wear scar as a function of time for several loads. (Ref. 36).

speed appears in figure 32 (ref. 40). These data indicate that fluid film effects are negligible only at 25 and 50 rpm and a 1 kg load.

Temperature. - As was the case for friction, there is no way to generalize the effect of temperature on wear. The same statements that pertain to friction also pertain to wear.

Atmosphere. - The effects of atmospheric oxygen and moisture on wear has been studied by many investigators. Oxygen has been shown to be an important ingredient in boundary lubrication experiments involving load carrying additives (refs. 36 and 41).

Running In. - It has long been known that the running-in of machine elements under certain conditions improves scuffing resistance. This phenomenon is probably related to increased surface hardness caused by work hardening as well as decreased surface roughness. This has been clearly shown by Yamamoto in disc machine studies (ref. 42).

Additive Behavior of Boundary Lubricated Systems

In discussing figure 16, it was stated that the boundary lubrication regime could be extended to higher loads by proper formulation of the lubricant with additives. A discussion of the variety of boundary additives is outside the scope of this thesis. However, the general behavior of the two common types of boundary additives, namely, antiwear and "EP", is illustrated in figure 33 (ref. 43). In figure 33 wear rate (K) is plotted as a function of load (F). There is a wear transition when boundary film failure occurs. The presence of an antiwear additive reduces wear (ΔK) but may have little or no effect on the wear transition load. On the other hand, an "EP" additive yields an increase in the load carrying capacity (ΔF) with little or no effect on the wear rate below the original base oil wear transition.

The most common antiwear additives are those which contain the element phosphorus. Typical examples include the metal dialkyldithiophosphates, organic phosphates and phosphites. "EP" additives include compounds containing sulfur and chlorine.

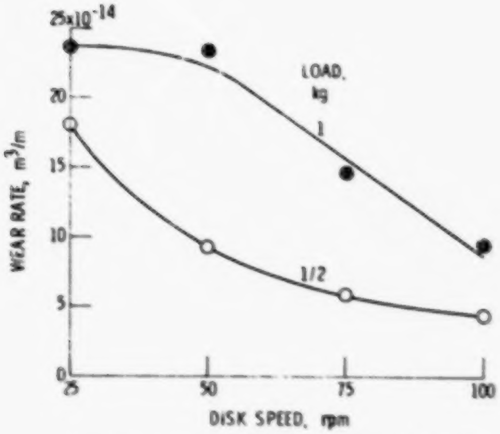

Figure 32. - Effect of disk speed on rider wear rate at two loads with ester-base lubricant. Atmosphere, dry air; disk temperature, 20° C; pure iron rider on M-50 (ref. 40).

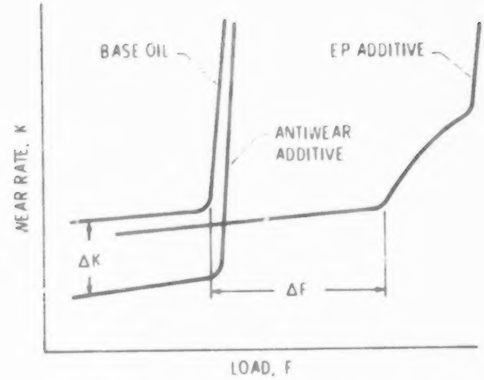

Figure 33. - Wear behavior of boundary-lubrication systems (ref. 43).

BOUNDARY LUBRICATION STUDIES

VANE PUMP TESTS

Early work concerning the boundary lubricating ability of polyphenyl and thioethers utilized a high temperature vane pump loop. Piston and vane pumps have been used by many investigators (refs. 44 and 45) for fluid evaluations. The vane pump has the advantages of simple construction, ease of maintenance, and high tolerance for fluid contamination. In addition, the vane-on-cam-ring sliding contact provides a sensitive technique for wear measurement.

At the time of these experiments, the use of inerted lubrication systems was being considered as an option to extend the high temperature capabilities of liquid lubricants. It was obvious that by excluding oxygen from the system, one could minimize or eliminate oxidative degradation. However, very little was known about boundary lubricating performance under these conditions. Therefore, the objectives of this portion of the study were:

(1) To determine the lubricating ability of some superrefined mineral oils and polyphenyl ethers by measurement of vane wear in a vane pump under inerted conditions,

(2) To determine qualitatively the resistance of the fluids to combined thermal and shear degradation,

(3) To determine the effect of operating viscosity on vane wear for the two fluid classes in this study.

Apparatus

The test apparatus (fig. 34) consists of a closed loop containing a vane pump, fluid reservoir, fluid heater, heat exchanger, filters, flow meter, and associated plumbing. All apparatus is made of 304 or 316 stainless steel except the pump assembly which is made of CVM M-50 tool steel.

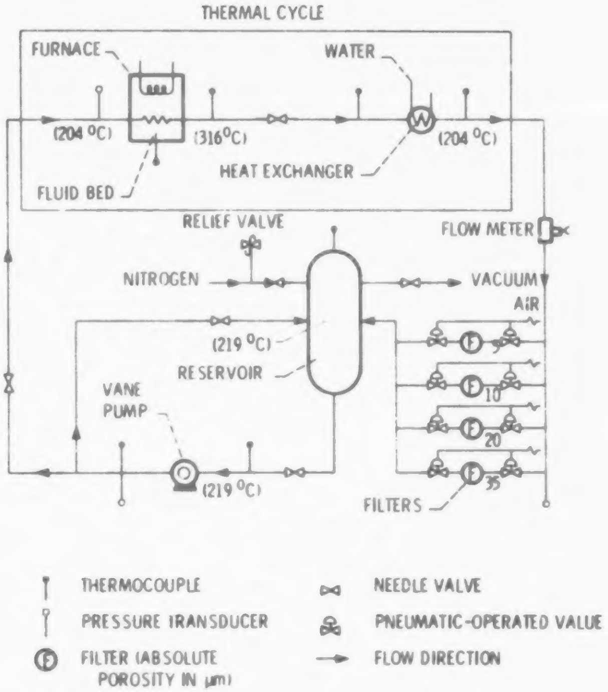

Figure 34. - High temperature fluid loop system.

Inspection and parts replacement are facilitated by the simple vane pump design (fig. 35). The cam ring, rotor, vanes, and one of the pressure plates are seen in an exploded view of the pump assembly (fig. 35). The inside diameter of the cam ring is 5.72 cm. Static "O" ring seals are Viton (fluorocarbon) with a continuous operating limit of 232 °C. The dynamic shaft seal consists of a bellows type carbon face seal in sliding contact with M-50 tool steel wear ring. A variable speed (500 to 5000 rpm) electric motor drives the pump through a coupling.

The fluid reservoir is made of stainless steel pipe and contains an immersion heater to maintain bulk fluid temperature at 219 °C. Reservoir design allows in situ deaeration by vacuum pumping and heating. An inert cover gas (nitrogen) at 2×10^3 N/m^2 (3 psig) is maintained in the reservoir.

During a test the fluid is further heated in a 13 kW industrial furnace. The furnace chamber is made of heavy wall stainless steel pipe. A 10 m coil of .635 cm stainless steel tubing is immersed in a bed of fluidized sand. The sand is the heat transfer medium and nitrogen the fluidizing agent. The oil enters the coil at about 204 °C and is heated to 316 °C during a residence time in the furnace of about 9 sec.

The heat exchanger consists of a coil of stainless steel tubing enclosed in a stainless steel shell. Water provides shell side cooling.

The filter system consists of four sintered stainless steel filters with mean pore sizes of 5, 10, 20, and 35 μm, respectively. The filters are mounted between air operated valves which are controlled by a pressure switch. Flow is directed through the filters in order of increasing pore diameter. Switching to the next coarser filter takes place when the inlet pressure to the preceding filter exceeds 3.4×10^4 N/m^2 (50 psig).

Instrumentation consists of thermocouples, pressure transducers, and a turbine flow meter. Fluid temperature is maintained constant at the furnace outlet and in the reservoir. Automatic shutdown is

ORIGINAL PAGE IS
OF POOR QUALITY

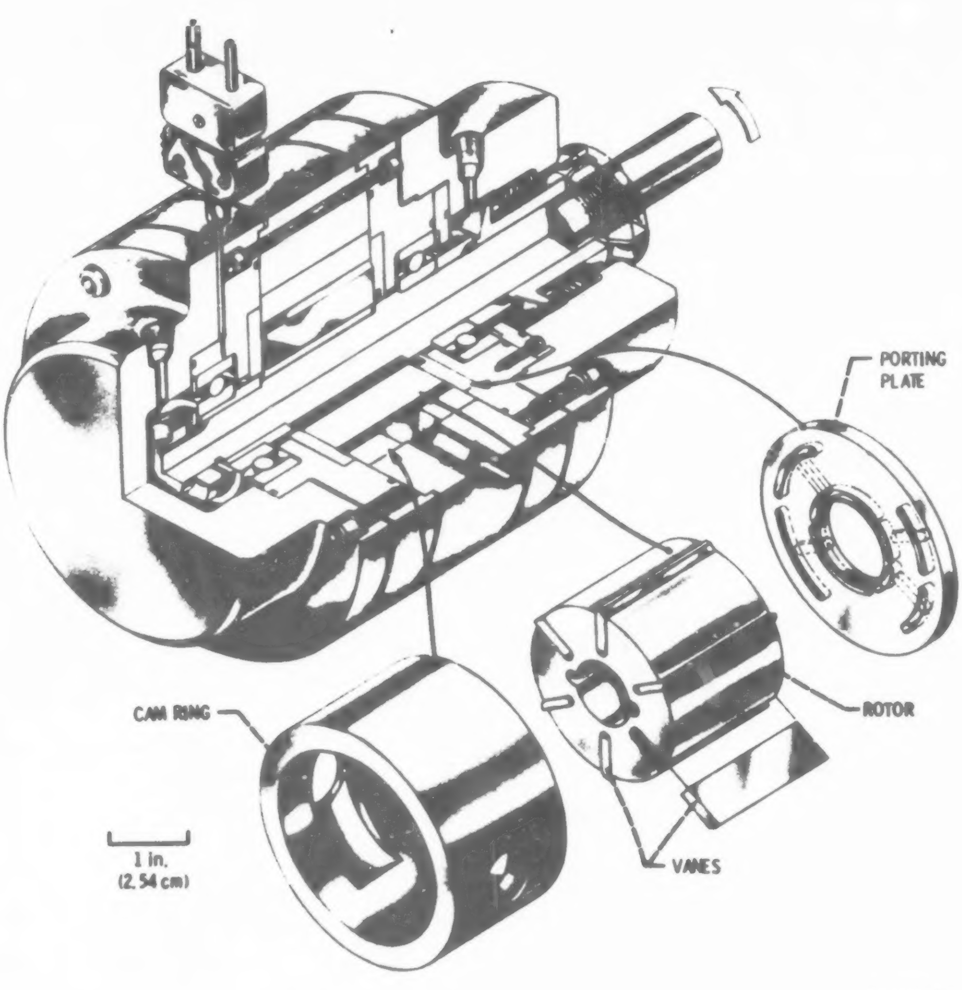

Figure 35. - Vane pump.

incorporated in the system in case of a malfunction. An automatic fire extinguishing system is also included.

Procedure

All lines are thoroughly cleaned, assembled, and purged with nitrogen. Six liters of the experimental fluid are degassed in situ after which the reservoir is backfilled with nitrogen. Vanes are weighted on an analytical balance which is accurate to 0.1 mg. The pump is then assembled and leak tested. A new set of vanes is used for each test.

After loop assembly, the experimental fluid is heated to 121 °C in the reservoir. The pump is started at low speed and the fluid is cycled through the bypass back into the reservoir until bulk fluid temperature reaches 219 °C. The fluid is then diverted through the rest of the system and pressure, temperature, flow rate, and speed conditions are set.

Normally, experiments are terminated at 50 and 150 hr for pump disassembly, inspection, vane wear measurement and fluid sample analysis. Experimental conditions, unless otherwise noted, were as follows:

(1) (1.72×10^6 N/m^2) 250 psig pump outlet pressure
(2) 316 °C fluid furnace outlet temperature
(3) 219 °C bulk fluid and pump-inlet temperature
(4) 3.16×10^{-5} m^3/sec (0.5 gpm) flow rate
(5) 1600 rpm pump speed (1.73×10^4 m/hr surface velocity)
(6) 150 hr test duration (50 hr inspection)
(7) Inert cover gas (nitrogen)
(8) Fluids were vacuum degassed for 24 hr at 121 °C
(9) Pump and vane material was CVM M-50 tool steel

Results and Discussion

Experiments were conducted with a number of high temperature hydraulic fluid and lubricant candidates. These fluids, their additives, and some viscosity data appear in table 4.

On the basis of vane wear measurements at 50 hr, the fluids can be divided into two groups. The first group includes the 77 cSt superrefined naphthenic mineral oil and two superrefined naphthenic-paraffinic mineral oil blends. The high wear group includes the 15 cSt superrefined paraffinic mineral oil, the four ring (4P-3E) and the five ring (5P-4E) polyphenyl ether, and the thioether. Vane wear for both groups appear in figures 36 and 37.

In figure 36, vane wear using the naphthenic oil was only 3 mg/vane for a 150 hr experiment. Vane wear for the two mineral oil blends (fig. 37) was similar to the naphthenic oil wear at 50 hr. However, both blend experiments were terminated at about 100 hr because of equipment malfunctions not related to the fluids.

All of the experiments with the fluids in the high wear class were terminated at 100 hr or less because of fluid-related pump malfunctions (bearing failures, low volumetric efficiency because of high vane wear, or complete loss of pump pressure due to coking deposits).

As shown in figure 36, immediate high wear (25 mg/vane after 12 hr) was obtained with 4P-3E. At test termination of 100 hr (because of low pump pressure), vane wear was 80 mg/vane. The 5P-4E polyphenyl ether experiment was terminated at 74 hr (because of low and erratic pump pressure). Vane wear data for the 5P-4E fluid falls on the wear curve for the 4P-3E (fig. 37).

A thioether experiment was terminated at 32 hr because of loss of pump pressure. Inspection revealed jammed vanes due to deposits on the vanes and rotor. After cleaning the rotor slots, repeated attempts to restart the pump were unsuccessful. The 32 hr thioether vane wear (fig. 37) was also similar to the 4P-3E results. In fact, wear for all three polyphenyl ether type fluids could be represented by a single curve of vane wear as a function of sliding distance.

TABLE 4. - EXPERIMENTAL FLUIDS

Base stock	Additives	Temperature, °C		
		38	99	219
		Kinematic viscosity, cS		
Superrefined naphthenic mineral oil	Antiwear, oxidation inhibitor	77	8.1	1.50
	Antiwear, oxidation inhibitor, 2.25 wt % paraffinic resin	84	8.7	1.59
Superrefined paraffinic mineral oil	Antiwear, oxidation inhibitor	15	3.2	0.92
	Antiwear, oxidation inhibitor, 5 wt % paraffinic resin	20	4.0	1.05
Superrefined naphthenic (73 wt %) paraffinic (27 wt %) blend	Antiwear, oxidation inhibitor	45	6.1	1.30
Superrefined naphthenic (29 wt %) paraffinic (71 wt %) blend	Antiwear, oxidation inhibitor	22	4.2	1.02
Four-ring polyphenyl ether (4P-3E)	None	66	6.2	1.24
Five ring polyphenyl ether (5P-4E)	None	357	13	1.88
Thioether	Proprietary additive package	25	4.1	1.05

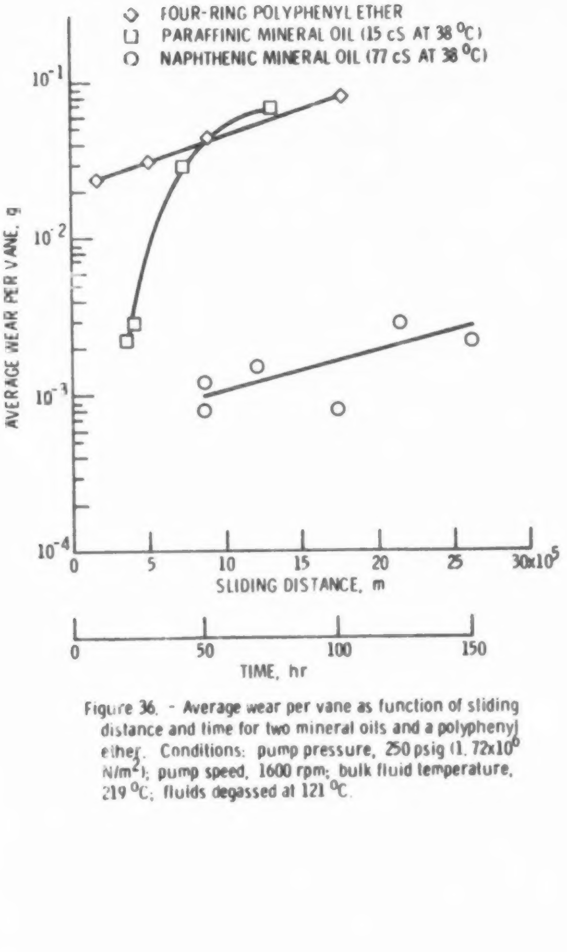

Figure 36. - Average wear per vane as function of sliding distance and time for two mineral oils and a polyphenyl ether. Conditions: pump pressure, 250 psig (1.72×10^6 N/m^2); pump speed, 1600 rpm; bulk fluid temperature, 219 °C; fluids degassed at 121 °C.

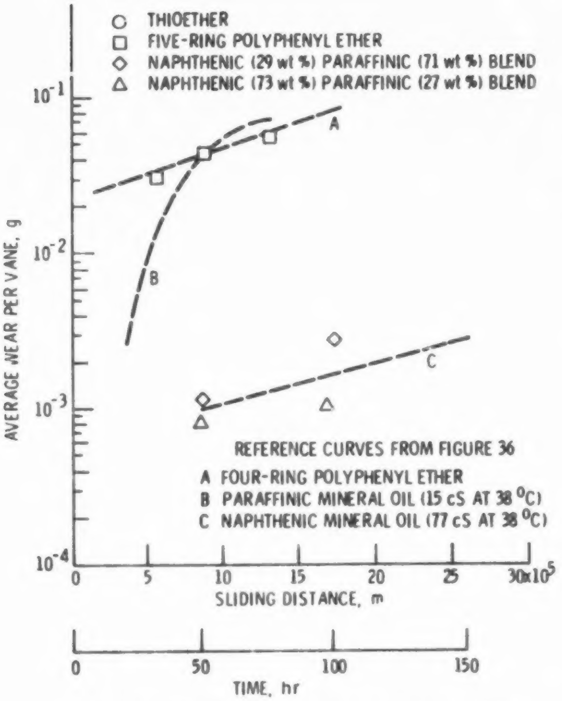

Figure 37. - Average wear per vane as function of sliding distance and time for a number of fluids. Conditions: pump pressure, 250 psig (1.72×10^6 N/m^2); pump speed, 1600 rpm; bulk fluid temperature, 219 °C; fluids degassed at 121 °C.

The paraffinic mineral oil, a hydrocarbon, seems to be out of place in the high wear group whose remaining members are synthetic polyphenyl ethers. The paraffinic oil describes a different wear against time curve than the polyphenyl ethers (fig. 36). The paraffinic oil has a much more gradual increase in wear compared to the immediate high wear of the polyphenyl ethers. However, at test termination of 74 hr (bearing failure), the paraffinic oil vane wear of 67 mg/vane has reached the 4P-3E wear level. It appears that the high wear obtained with the paraffinic oil is due to its low viscosity at 219 °C of (0.92 cSt) and not to any inferiority in chemical type when compared to the higher viscosity naphthenic mineral oil. This is discussed further in the next section.

Viscosity Effect

Bulk fluid viscosity at the test temperature of 219 °C had little effect on vane wear for the three polyphenyl ethers. Increasing the 219 °C viscosity from 1.05 to 1.88 cSt reduced vane wear rate less than 9 percent. However, the mineral oils have a sharp transition from high to low wear in the viscosity range of 0.92 cSt (paraffinic oil) to 1.02 cSt (71 wt % paraffinic - 29 wt % napthenic blend). Wear rate of the paraffinic oil is almost 40 times that for the 71 wt % paraffinic blend. It is unlikely that the slight chemical difference between these two fluids could be responsible for the large difference in wear rates. It appears that under the experimental conditions of this program, a 219 °C viscosity of about 1 cSt is necessary for a mineral oil to lubricate the vane pump effectively.

Vane pumps operate in a mixed film or partial hydrodynamic regime. Both hydrodynamic and boundary lubrication are important. For fluids of a particular chemical type, vane wear plotted against viscosity appears as a step function. As viscosity decreases and the hydrodynamic component diminishes, vane wear increases slowly until a sharp transition to high wear occurs. This transition corresponds to a shift from predominantly hydrodynamic to predominantly boundary lubrication. This is apparently the situation with the low viscosity paraffinic oil for which high vane wear occurred relative to the other mineral oils.

Fluid Degradation

Since oxygen was excluded in these tests, the fluids are degraded by a combination of thermal and shear stresses. The thermal conditions are well defined but because of the complex flow in the pump, the shear rate was not determined. Fluid degradation was determined by measuring changes in 38 and 99 °C kinematic viscosities, changes in neutralization number, and the filter clogging characteristics. All fluids showed little change in viscosity. Neutralization numbers for all fluids were relatively unchanged.

Table 5 contains filter clogging data for most of the fluids. As can be seen, the three polyphenyl ether fluids produced large quantities of insolubles as witnessed by the rapid rate of filter clogging. In fact, in order to continue the experiments with the polyphenyl ethers (4P-3E and 5P-4E), the filters had to be completely bypassed after the 35 μm filter was clogged. The naphthenic oil was still operating on the 5 μm filter at test termination. With the larger pore size filters in the system, a greater number of wear particles, as well as insolubles from thermal degradation, would remain in the oil, pass through the pump, and possibly accelerate the wear process. Therefore, vane wear in these fluids was probably higher than it would have been if the oils had been capable of filtration through a 5 μm filter. Nevertheless, it is reasonable to assume that the relative wear rates in the various fluids would still prevail. This is reasonable because the initial wear rates and thermal degradation was higher in these oils which caused the rapid filter clogging in the first place.

TABLE 5. - FILTER CLOGGING CHARACTERISTICS FOR VARIOUS FLUIDS

Fluid	Filter mean pore size, μm			
	5	10	20	35
	Time required for filter inlet pressure to exceed (3.4×10^5 N/m^2)			
Superrefined naphthenic mineral oil	>150	---	---	---
Superrefined paraffinic mineral oil	6	18	22	>28
Superrefined naphthenic (29 wt %) paraffinic (71 wt % mineral oil blend	25	50	>25	---
Four ring polyphenyl ether (4P-3E)	0.5	10.5	17	25
Five ring polyphenyl ether (5P-4E)	.5	10	24	30
Thioether	.2	2.5	>29	---

Summary of Results

A vane pump loop was used to determine the lubricating ability as well as thermal and shear degradation for a number of high temperature fluid candidates. Fluid temperature was cycled from 219 °C at the pump inlet to 316 °C in the fluid heater and back to 219 °C in the reservoir. An inert cover gas (nitrogen) was maintained in the reservoir. The pump and vanes were made of CVM M-50 tool steel. The major results were:

(1) Fluid chemical type and viscosity greatly influenced vane wear. Lowest vane wear was obtained with a 77 cSt superrefined naphthenic mineral oil. Higher vane wear was obtained with a 15 cSt superrefined paraffinic mineral oil. Two intermediate viscosity blends of these fluids yielded low vane wear. High wear was obtained with a four-ring and a five-ring polyphenyl ether and a thioether.

(2) The mineral oils and mineral oil blends showed no significant fluid degradation (thermal and shear). The three polyphenyl ether type fluids produced large quantities of insolubles but viscosities and neutralization numbers were essentially unchanged.

(3) High wear was obtained with the polyphenyl ethers over the entire viscosity range studied (1.05 to 1.88 cSt at 219 °C). Low vane wear was obtained with the mineral oils in the range (1.02 to 1.50 cSt) at 219 °C. With the mineral oils, a sharp transition to high wear occurred in the lower viscosity range of (0.92 to 1.02 cSt) at 219 °C.

PIN-ON-DISK STUDIES - 5P-4E

Because of the anomalous results obtained in the vane pump tests, more definitive boundary lubrication tests were obviously in order. In searching the literature, it was reported by Appeldoorn and Tao (ref. 46) that boundary lubrication with aromatic compounds was greatly influenced by atmospheric oxygen and moisture. Buckley et al. (ref. 47) showed that rider wear for a polyphenyl ether in a nitrogen atmosphere increased an order of magnitude after fluid degassing.

Four-ball tests (ref. 19) in nitrogen had yielded maximum wear at 200 °C. In the aforementioned vane pump studies in dry nitrogen, polyphenyl ethers exhibited high wear at 219 °C. Following those experiments, it was observed that the polyphenyl ethers exhibited poor wettability on the test specimens.

As previously described in the section on surface tension and wettability, a poor wetting condition could cause fluid starvation in the contact zone and prevent effective lubrication. Additives that can improve the wettability of a lubricant (i.e., decrease its contact angle) may improve its boundary lubrication characteristics. It is also possible that in a high speed bearing, where the cooling effect of the lubricant becomes important, an improvement in wettability may be beneficial by increasing local heat transfer rates.

Therefore, the objective of this portion of the study was to determine the effect of humidity and a wettability additive (trichloroacetic acid) (TCAA) on the boundary lubrication of steel in air and nitrogen atmospheres with 5P-4E.

Experimental conditions with the pin-on-disk apparatus included a 1-kg load (initial Hertz stress 1×10^9 N/m^2), 17-m/min surface velocity (100-rpm disk speed), 150 to 350 °C disk temperature range, a 1 hr test duration, and test atmospheres of wet and dry air and wet and dry nitrogen. Test specimens were made of consumable electrode vacuum melted (CVM) M-50 steel.

Apparatus

The friction and wear test apparatus is shown in figure 38. The test specimens were contained inside a stainless steel chamber. The atmosphere was controlled with respect to oxygen and moisture content.

ORIGINAL PAGE IS
OF POOR QUALITY

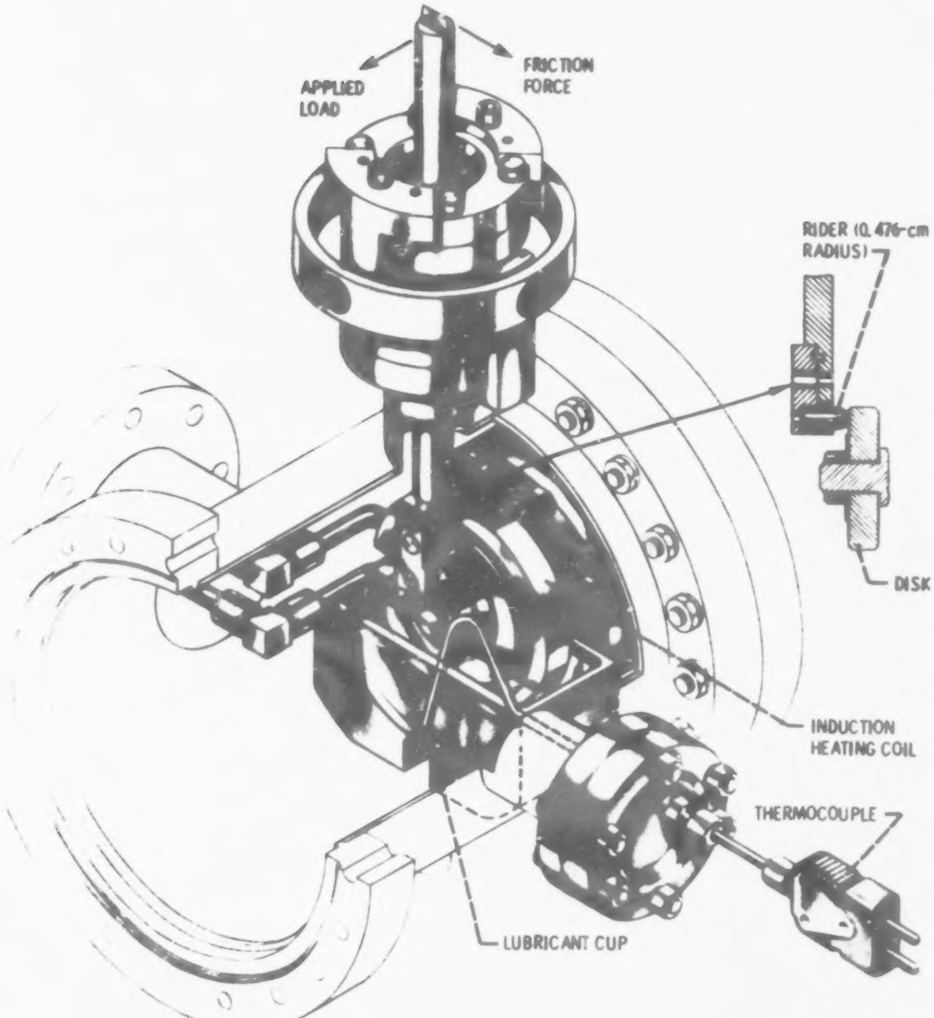

CD-10688-15

Figure 38. - Friction and wear apparatus.

A 6.3 cm-diameter disk was placed in sliding contact with a 0.476-cm-radius hemispherically tipped rider. A surface velocity of 17 m/min (100 rpm) was maintained. A normal load of 1 kg was applied with a deadweight. Riders and disks were made of CVM M-50 tool steel, disk hardness was Rockwell C 62 to 64 and rider hardness was 56 to 58.

The disk was partially submerged in a pyrex cup containing the test lubricant. The disks were heated by induction. Bulk lubricant temperature was recorded with a thermocouple. Disk temperature was monitored with an infrared pyrometer. Frictional force was measured with a strain gage and was recorded on a strip chart recorder.

Atmosphere Monitoring and Control

The four atmospheres used were (1) wet air, (2) wet nitrogen both at a relative humidity of 50±5 percent at 25 °C, (3) dry air (<100 ppm H_2O), and (4) dry nitrogen (<20 ppm H_2O).

The relative humidity was monitored by a direct reading hygrometer accurate to ±1.5 percent. The low water concentrations were monitored by a moisture analyzer with an accuracy of ±10 parts per million.

Dry nitrogen was obtained directly from compressed gas cylinders. Dry air was obtained by drying and filtering service air. Wet air and nitrogen were obtained by bubbling the dry gases through a water reservoir. The relative humidity was controlled manually at 50±5 percent.

Procedure

Disks and riders were made of CVM M-50 tool steel. They were ground and lapped to a surface finish of 4 to 8 μin. rms (10×10^{-8} to 20×10^{-8} m). Specimens were scrubbed with a paste of levigated alumina and water, rinsed with tap water and distilled water, then placed in a desiccator.

Lubricants were degassed at 150 °C under a vacuum. Dissolved oxygen concentration was measured with a polarographic probe and found to be less than 5 parts per million. Dissolved water content was not measured.

The specimens were assembled and 70 mL ($7\text{x}10^{-5}$ m^3) of lubricant were placed in the lubricant cup. The test chamber (3.7 l volume or $3.7\text{x}10^{-3}$ m^3) was purged with the test atmosphere for 10 min. at a flow rate in excess of 50 l/hr ($5\text{x}10^{-2}$ m^3/hr). The disk was heated by induction to test temperature while rotating and the rider loaded against the disk. Test atmosphere flow rate was reduced to 35 l/hr ($3.5\text{x}10^{-2}$ m^3/hr) and a 1-psig ($6.9\text{x}10^3$-N/m^2) pressure was maintained in the chamber. The lubricant was heated only by heat transfer from the disk and benefited by the cooling effect of the water circulating through the induction heating coil. Therefore, the bulk lubricant temperature (measured with a thermocouple) stabilized 100 to 150 °C below disk temperature.

Frictional force and bulk lubricant temperature were continuously recorded. Disk temperature was continuously monitored. Tests were terminated at 1 hr, and rider wear scar diameter was recorded.

Disk Temperature Calibration

Disk temperatures were monitored with an infrared pyrometer. Instrument accuracy (at constant emissivity) was ±1 °C with a reproducibility of 0.25 percent of the temperature.

Disk emissivity was about 0.15 initially and increased to 0.2 to 0.3 during a test. This change introduced a large error (>17 percent) in temperature measurement. Therefore, a 2.5-cm-diameter spacer with a black oxide coating ($e \simeq 0.55$) was placed between nut and disk. The pyrometer was then used to monitor the spacer temperature which was a function of disk temperature. Both temperatures were measured with thermocouples under static conditions and a calibration curve was obtained. A variation in spacer emissivity from 0.5 to 0.6 resulted in an error of less than 2 percent. Dynamic tests with and without test lubricant using a disk with a black oxide coating yielded results within 2.5 percent of the static calibration. Disk temperature was manually controlled to ±5 °C.

Results and Discussion

The wettability additive was trichloroacetic acid (TCAA) and was present in a concentration of 0.05 percent by weight. Disk temperature range was 150 to 350 °C. The lower temperature was arbitrarily chosen and the upper limit was dictated by lubricant volatility.

In order to facilitate discussion of rider wear, the wear data have been divided into three arbitrary levels. These levels are (1) low wear which corresponds to a wear rate of less than 10^{-12} m^3/hr (wear scar diameter (WSD), 0.5 mm), (2) intermediate wear (wear rate between 10^{-12} and 10^{-11} m^3/hr), and (3) high wear (wear rate greater than 10^{-11} m^3/hr; WSD, 1.0 mm).

Effect of Atmosphere on Wear and Friction of Unlubricated Steel

Rider wear and friction coefficient for the unlubricated situation in all four atmospheres appear in figure 39. High wear (10^{-11} to 10^{-10} m^3/hr) occurred in wet and dry nitrogen. Very high wear (10^{-10} to 10^{-9} m^3/hr) occurred in wet and dry air. The friction coefficient in all four atmospheres varied from 0.6 to 0.8 at 150 °C and from 0.4 to 0.6 at 360 °C.

Effect of Atmosphere on Base Fluid Wear

Dry air compared to dry nitrogen. - Rider wear for the base fluid in dry nitrogen and dry air appears in figures 40(a) and (b) respectively. Higher wear occurred in dry nitrogen from 150 to 250 °C and lower wear from 250 to 350 °C compared to the dry air situation. The polyphenyl ether is a poor lubricant in dry nitrogen from 150 to 200 °C. This agrees with the high wear obtained with this fluid in dry nitrogen in the previously discussed vane pump

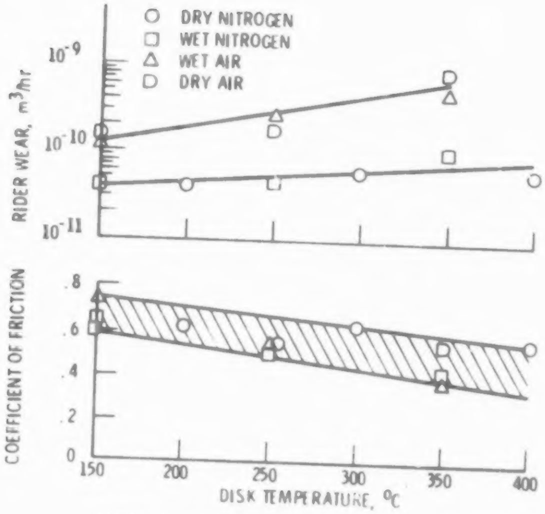

Figure 39 - Coefficient of friction and rider wear as a function of disk temperature for unlubricated M-50 steel in dry and wet nitrogen and in dry and wet air. Conditions: 1-kilogram load, 100-rpm disk speed, 17-meter-per-minute surface velocity, and 1-hour test duration.

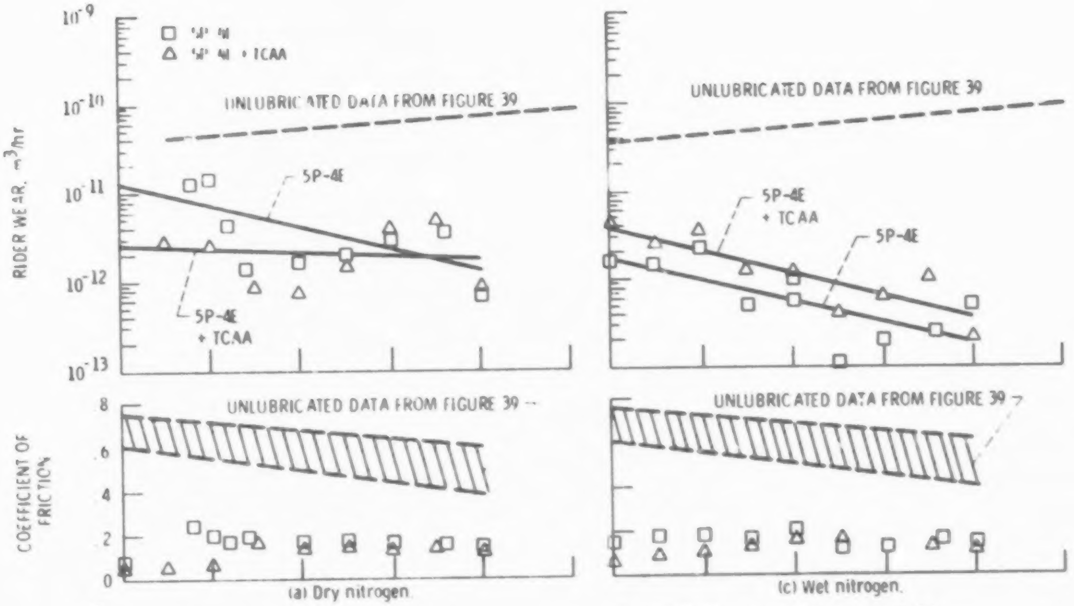

(a) Dry nitrogen.

(c) Wet nitrogen.

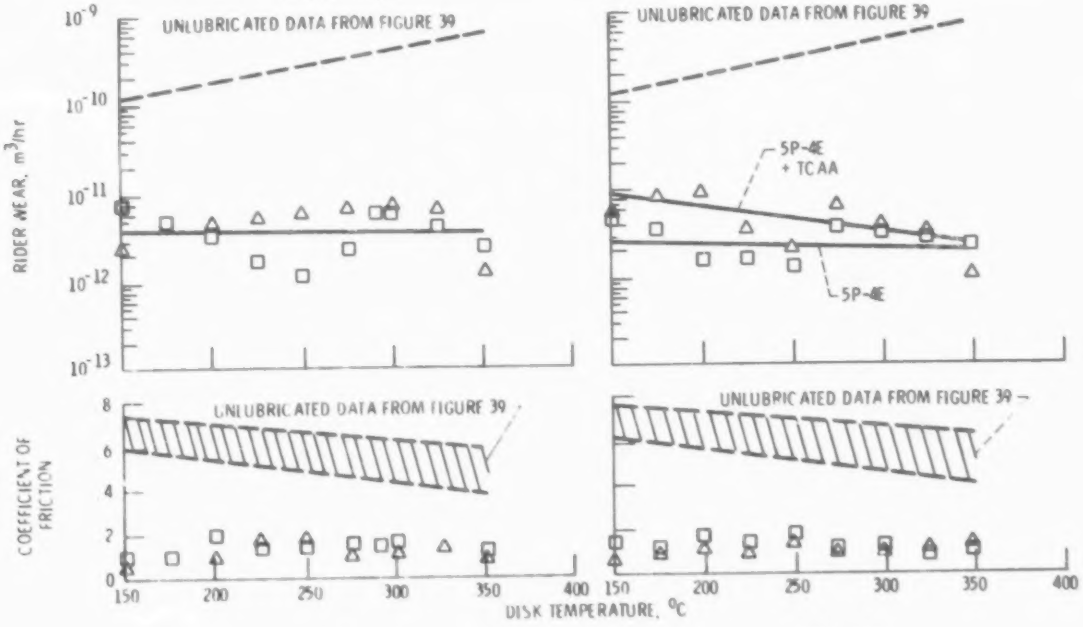

(b) Dry air.

(d) Wet air.

Figure 40. Coefficient of friction and rider wear as a function of disk temperature for polyphenyl ether (5P-4E) with and without trichloroacetic acid (TCAA). Conditions: 1-kilogram load, 100-rpm disk speed; 17-meter-per-minute surface velocity; and 1-hour test duration.

studies and in four-ball tests (ref. 19). This also agrees with the suggestion of Appeldoorn and Tao indicating that aromatics are poor boundary lubricants in dry nonoxidizing conditions (ref. 46).

Effect of moisture. - Rider wear for the base fluid in wet nitrogen and wet air appears in figures 40 (c) and (d), respectively. Substantially lower wear occurred in wet nitrogen compared to dry nitrogen. Slightly lower wear occurred in wet air compared to dry air. These results agree with the lower temperature results of reference 19. Moisture apparently reduces wear of sliding parts lubricated with aromatic fluids. Figure 41 summarizes wear data in the four atmospheres at temperatures of 150 to 250, and 350 °C.

Effect of Wettability Additive (TCAA) on Rider Wear

Dry nitrogen. - Rider wear for the polyphenyl ether with additive in dry nitrogen appears in figure 40 (a). The wettability additive (TCAA) reduced wear over most of the temperature range. The greatest wear reductions occurred in the 150 to 200 °C range.

Dry air. - Rider wear for the fluid with additive in dry air appears in figure 40 (b). Essentially no difference in wear occurred for the fluid with and without additive in dry air.

Wet nitrogen. - Rider wear for the fluid with additive in wet nitrogen appears in figure 40 (c). A small increase in wear occurred with the additive fluid in wet nitrogen. Figure 42 summarizes wear data for the fluid with and without additive in wet and dry nitrogen at disk temperautres of 150, 175, 200, and 225 °C.

Wet air . - Rider wear for the fluid with additive in wet air appears in figure 40 (d). Small increases in wear occurred over most of the temperature range. Figure 43 summarizes wear data for the fluid with additive in four atmospheres at temperatures of 150, 250, and 350 °C.

In general, TCAA was most effective in reducing wear in dry nitrogen from 150 to 200 °C. It had little or no effect on wear in dry air and wet nitrogen and appeared to be detrimental in wet air. Table 6 summarizes wear data for all conditions.

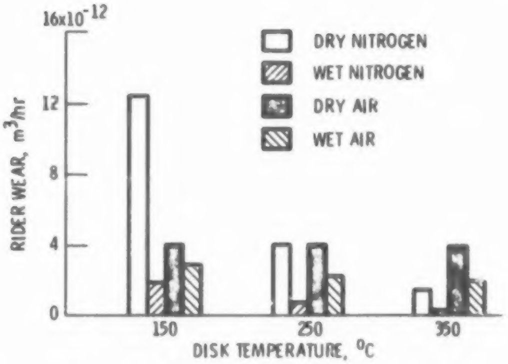

Figure 41. - Rider wear for polyphenyl ether (5P-4E) in wet and dry nitrogen and in wet and dry air at disk temperatures of 150, 250, and 350 °C.

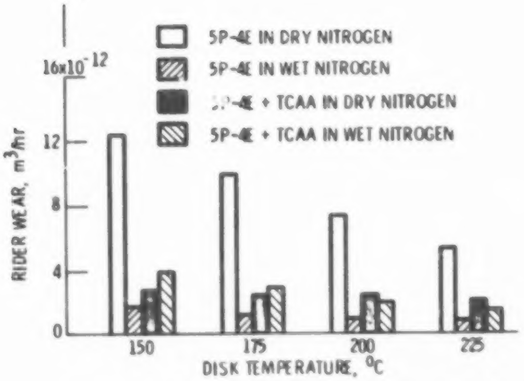

Figure 42. - Rider wear for polyphenyl ether (5P-4E) with and without trichloroacetic acid (TCAA) in wet and dry nitrogen at four disk temperatures.

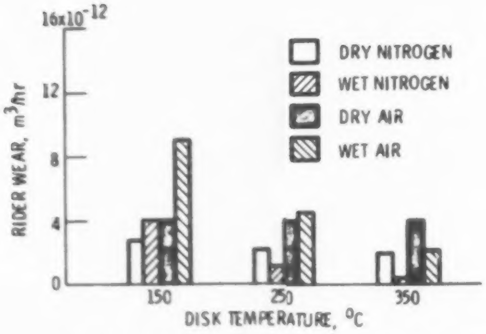

Figure 43. - Rider wear for polyphenyl ether (5P-4E) with trichloroacetic acid in wet and dry nitrogen and wet and dry air at disk temperatures of 150, 250, and 350 °C.

TABLE 6. - SUMMARY OF WEAR RESULTS

High wear	Intermediate wear	Low wear
$>10^{-11}$ m^3/hr	Between 10^{-12} and 10^{-11} m^3/hr	$>10^{-12}$ m^3/hr
In dry nitrogen from 150 to 175 °C without additive	In wet and dry air 150 to 350 °C with and without additive	In wet nitrogen 260 to 350 °C with additive
	In dry nitrogen 150 to 350 °C with additive	In wet nitrogen 200 to 350 °C without additive
	In dry nitrogen 175 to 350 °C without additive	
	In wet nitrogen 150 to 200 °C without additive	
	In wet nitrogen 150 to 260 °C with additive	

Dip Cell Experiments

Another simple experiment was used to determine the wettability of the base fluid (5P-4E) and 5P-4E plus the wettability additive (TCAA). This procedure, using a dip cell, was similar to that employed by Bigelow, Pickett, and Zisman (ref. 48).

A flask containing 100 mL (1×10^{-4} m^3) of the lubricant was heated slowly (5 °C/min). An M-50 tool steel specimen (4.1 by 1.3 by 0.24 cm) which was cleaned in the same manner as the disk and rider specimens was placed in the fluid. Starting at 150 °C the specimen was raised out of the fluid at 5 °C intervals to a maximum of 250 °C. The manner in which the fluid drained off the specimen was observed. The atmosphere above the fluid was controlled with respect to oxygen and moisture.

A poor wetting condition was observed for 5P-4E in dry nitrogen from 150 °C to approximately 195 °C in agreement with previous experiments. Partial wetting occurred from 195 to 200 °C. From 200 to 250 °C complete wetting occurred. The polyphenyl ether with TCAA exhibited complete wetting in dry nitrogen from 150 to 250 °C. Reproducibility in this experiment was about ±5 °C.

Effect of Wettability Additive (TCAA) on Friction

The coefficient of friction for the polyphenyl ether with and without TCAA in dry and wet nitrogen, and dry and wet air appears in figures 40(a) to (d), respectively.

A friction coefficient of less than 0.25 was observed for the polyphenyl ether with and without TCAA in all four atmospheres from 150 to 350 °C. From 150 to 200 °C, the additive generally decreased the friction coefficient from 25 to 50 percent. Little effect was observed above 200 °C.

Summary of Results

A pin-on-disk sliding friction apparatus was used to determine the effect of humidity and a wettability additive (trichloroacetic acid) on boundary lubrication of steel with a five-ring polyphenyl ether. The test atmospheres were (1) wet air (RH 50 %), (2) wet nitrogen (RH 50 %), (3) dry air (<100 ppm H_2O), and (4) dry nitrogen (<20 ppm H_2O). Other conditions included a 1-kilogram load, 17-m/min surface velocity, and a disk temperature range of 150 to 350 °C. Test specimens were made of CVM M-50 steel. The major results were as follows:

(1) Poor wettability was observed for the polyphenyl ether in dry nitrogen from 150 to 200 °C and high wear also occurred in this temperature range.

(2) Trichloroacetic acid improved the wetting characteristics of the polyphenyl ether in dry nitrogen. The additive decreased wear of the polyphenyl ether in dry nitrogen, increased wear in wet air, and had no or little effect on wear in wet nitrogen and dry air.

(3) A relative humidity of 50 percent decreased wear in nitrogen and had little effect on wear in air.

PIN-ON-DISK STUDIES - THIOETHER FORMULATIONS

It is obvious from the earlier data that the thioethers are in need of additives to improve their boundary lubricating characteristics. Therefore, the objectives of this portion of this investigation were (1) to determine the boundary lubricating characteristics of six thioether formulations (containing organic acid and phosphorus ester additives) in dry (<100 ppm H_2O) and moist air (relative humidity 50 percent at 25 °C) and temperatures from 25 to 300 °C, and (2) to compare these results to those obtained with a fully formulated Type II ester (MIL-L-23699) and the unformulated thioether base fluid.

Experimental conditions include a 1-kg load (initial Hz stress, 1×10^9 N/m^2), a 17-m/min surface speed, (100 rpm), and a test duration of 25 min. Test specimens were made of consumable electrode vacuum melted (CVM) M-50 steel.

Experimental Lubricants

The experimental fluids used in these experiments were a formulated Type II ester, a thioether base fluid, and six thioether formulated fluids. Table 7 contains the additive contents of the test fluids.

Formulated Type II Ester. - A fully formulated Type II ester was chosen as a reference fluid for these experiments. This lubricant is commercially available and meets General Electric D50TF1, Pratt and Whitney PWA521B, and MIL-L-23699 lubricant specifications.

Thioether Formulations. Phosphorus Ester Additives -

Formulation I. The first thioether formulation studied was the base fluid plus 0.10 WT percent bis (2-chloropropyl)-2-propene phosphonate. This additive should improve the boundary lubricating characteristics of the base fluid.

Formulation II. The second formulation studied was the base fluid plus 0.10 wt % di-isopropyl hydrogen phosphite. This is another additive to improve boundary friction and wear. This formulation has been previously studied in reference 49. It performed satisfactorily in short-term (3 hr) bearing tests at a bearing temperature of 316 °C in air and nitrogen. However, it required higher oil flow rates to stabilize the bearing temperature than did ester and synthetic paraffinic hydrocarbon lubricants.

Formulation III. The third formulation studied is identical to formulation II, except that 0.05 wt % trichloroacetic acid (TCAA) has been added to improve fluid wettability. This particular formulation has also been studied previously (ref. 50). This fluid provided marginally adequate boundary lubrication in small scale bearing screening tests at 316 °C for 100 hr in nitrogen. TCAA wettability and wear results in 5P-4E were discussed previously.

Thioether Formulations. Organic Acid Additives. -

Formulation IV. Formulation IV was the base fluid plus <0.10 wt % of a boundary additive (oxalic acid potassium salt).

C-2

TABLE 7.- ADDITIVE CONTENTS OF TEST FLUIDS

Formulated Type II Ester	Antifoam, anticorrosion, aromatic amine antioxidant, combined antioxidant and load carrying agent
Thioether base fluid	Antifoam (dimethyl silicone)
Formulation I	Antifoam, bis(2-chloropropyl)-2-propene phosphonate (0.10 wt %)
Formulation II	Antifoam, di-isopropyl hydrogen phosphite (0.10 wt %)
Formulation III	Antifoam, di-isopropyl hydrogen phosphite(0.10 wt %) trichloroacetic acid (0.05 wt %)
Formulation IV	Antifoam, oxalic acid potassium salt (<0.10 wt %)
Formulation V	Antifoam, perfluoro-glutaric acid (0.10 wt %)
Formulation VI	Antifoam, phenylphosphinic acid (0.08 wt %)

Formulation V. Formulation V was the base fluid plus 0.10 wt % of a boundary additive (perfluoroglutaric acid).

Formulation VI. Formulation VI was the base fluid plus 0.08 wt % of a boundary additive (phenylphosphinic acid).

Wear Results

Formulated Type II Ester. - This fluid was chosen as a reference fluid because it appeared to be a typical example of the polyol ester group of MIL-L-23699 lubricants. Wear results for this fluid appear in figure 44. No significant differences in wear were observed between the dry and moist air results. Therefore, a single wear-temperature curve appears in figure 44.

The wear rate is essentially constant at 1.4×10^{-13} m^3/min over the entire temperature range. The level of wear and the appearance of various wear scars indicate only marginally adequate lubrication was obtained with this ester under these conditions.

Thioether Base Fluid. - Wear results for this base fluid appear in figure 45. At 25 °C in dry air, the wear rate was about 7×10^{-14} m^3/min. The wear rate decreased to a minimum of approximately 4×10^{-14} m^3/min at 100 °C and then gradually increased to 10^{-13} m^3/min at 300 °C. In moist air, a similar wear-temperature curve is observed but with lower wear rates over the entire temperature range. The effect of moisture in reducing wear was more pronounced at the lower temperatures.

A comparison between the friction and wear results for the Type II ester and the thioether base fluid appears in figure 46. In both dry and moist air, the thioether base fluid yielded lower wear than the Type II ester over the entire temperature range. The maximum difference in wear occurred at about 100 °C. At 100 °C, the ester exhibited a wear rate approximately seven times greater in moist air and four times greater in dry air than the wear rate observed for the thioether base fluid.

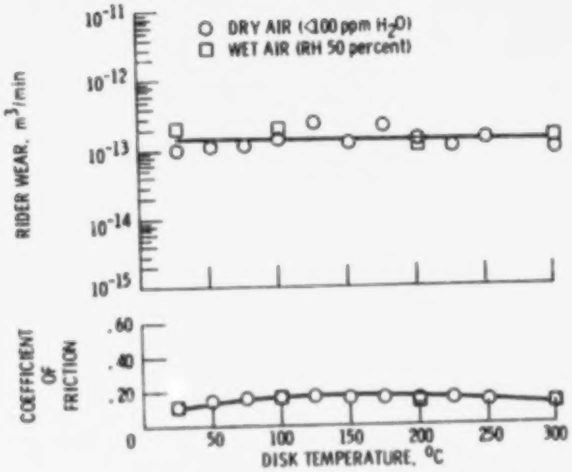

Figure 44. - Coefficient of friction and rider wear as a function of temperature for a Type II ester.

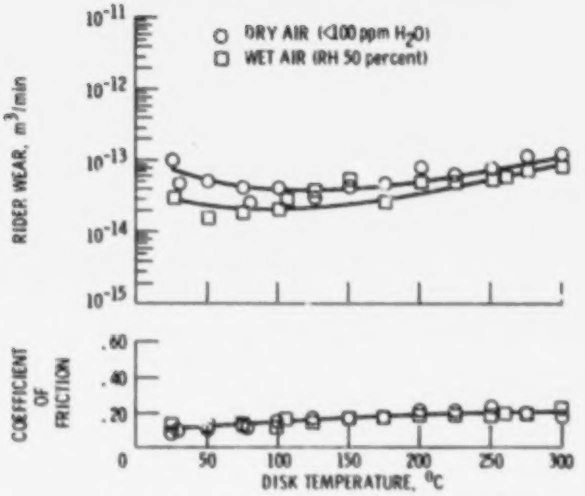

Figure 45. - Coefficient of friction and rider wear as a function of temperature for a thioether base fluid.

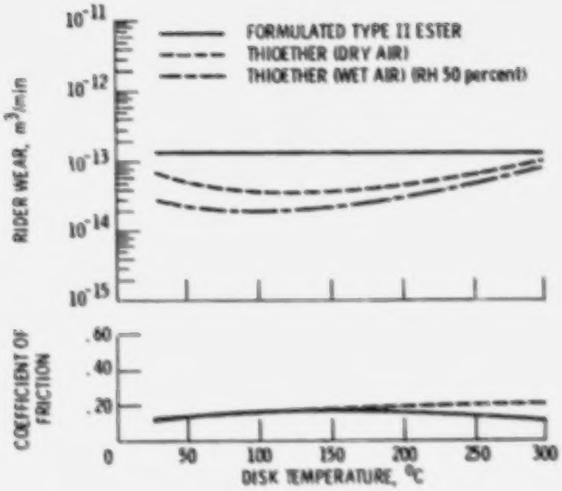

Figure 46. - Comparison of friction and wear results for a a formulated type II ester and a thioether base fluid.

Thioether formulations (phosphorus ester additives). - Wear results for formulations I, II, and III appear in figure 47. No significant differences in wear were observed between the dry and moist air results for formulations I and II. Therefore, only a single wear-temperature curve appears in figures 47(a) and (b). Formulation III, however, yielded lower wear rates in moist air than in dry air from 100 to 300 °C.

A qualitative comparison of the wear results for these three formulations and the base fluid appears in figure 48. The dry air results of figure 48(a) indicate essentially no difference in wear rate for the three formulations and the base fluid from 25 to 100 °C. From 100 to 300 °C formulations I, II, and III yielded lower wear rates than the base fluid.

In moist air (fig. 48(b)), these three formulations again yielded lower wear rates above approximately 150 °C. However, the 25 to 150 °C, the wear rate of the thioether base fluid was lower than the wear rates of the three formulations. The increasing effectiveness of the additives with increasing temperature is most likely related to their greater reactivity at the higher temperatures.

Thioether formulations (organic acid additives). - Wear results for formulations IV, V, and VI, containing organic acid additives, appear in figure 49. The wear rate for the Type II ester also appears in figure 49 for reference.

Moisture in the test atmosphere did not greatly affect the wear results for formulations IV and VI. However, formulation V yielded lower wear than the ester over essentially the entire temperature range. Formulation VI yielded lower wear than the ester from 25 to 150 °C and about the same wear from 150 to 300 °C.

Comparisons between the wear rates for the three formulations and the thioether base fluid appear in figure 50. In both dry (fig. 50(a)) and moist air (fig. 50(b)) formulations IV and VI yielded higher wear than the base fluid over almost the entire temperature range. Formulation V exhibited a somewhat more complex behavior yielding lower wear than the base fluid under most conditions but higher wear under others.

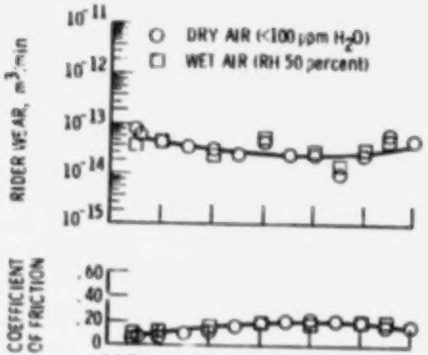

(a) Formulation I (Bis (2-chloropropyl)-2-propene phosphonate).

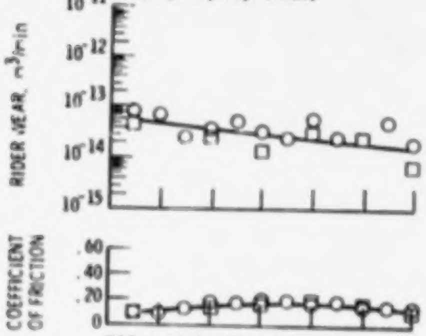

(b) Formulation II. (Di-isopropyl hydrogen phosphite).

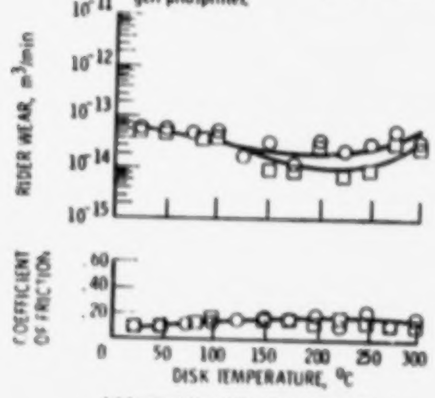

(c) Formulation III. (Di-isopropyl hydrogen phosphite + trichloroacetic acid).

Figure 47 - Coefficient of friction and rider wear as a function of temperature for three thinether formulations.

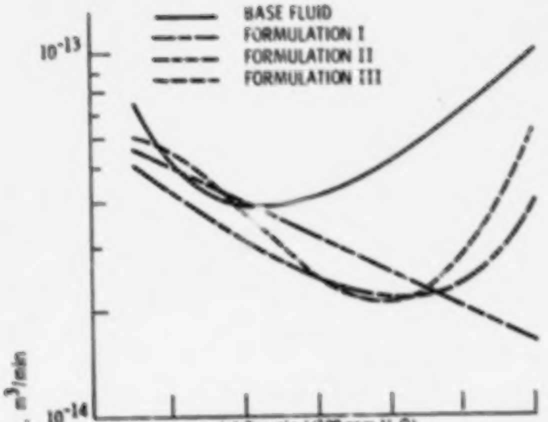

(a) Dry air (<100 ppm H_2O).

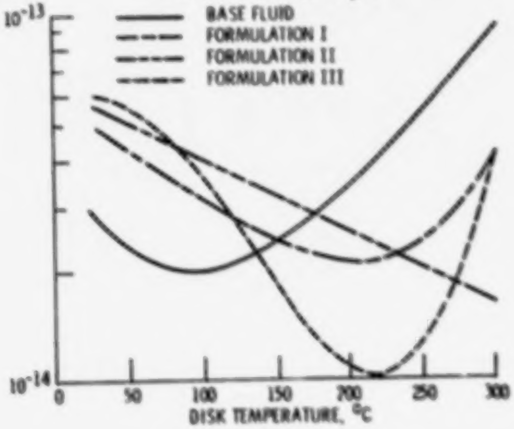

(b) Wet air (RH 50 percent).

Figure 48. - Rider wear as a function of temperature for a thioether base fluid and thioether formulations I, II, and III.

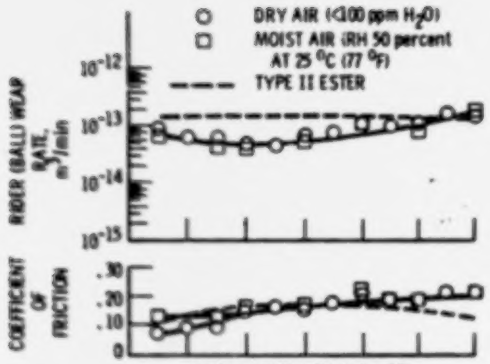

(a) Formulation IV (polyacid).

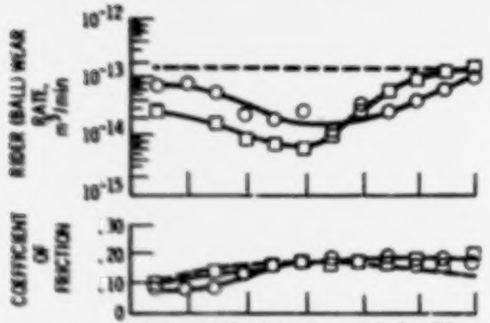

(b) Formulation V (perfluoroglutaric acid).

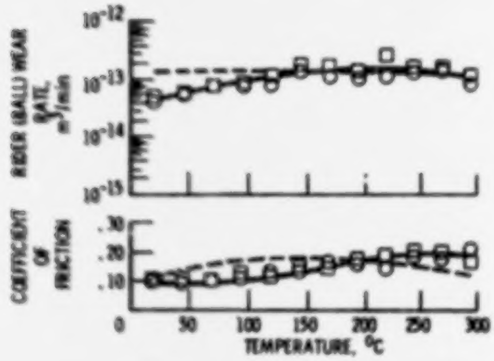

(c) Formulation VI (phenylphosphinic acid).

Figure 48. - Coefficient of friction and rider wear as a function of temperature for three thioether formulations.

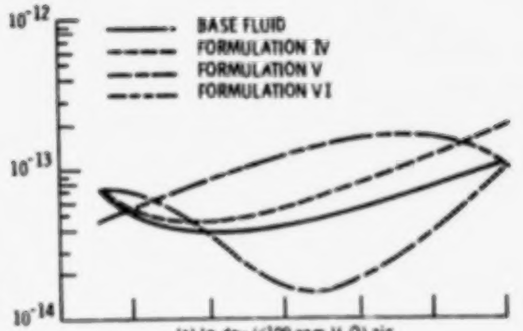

(a) In dry (<100 ppm H_2O) air.

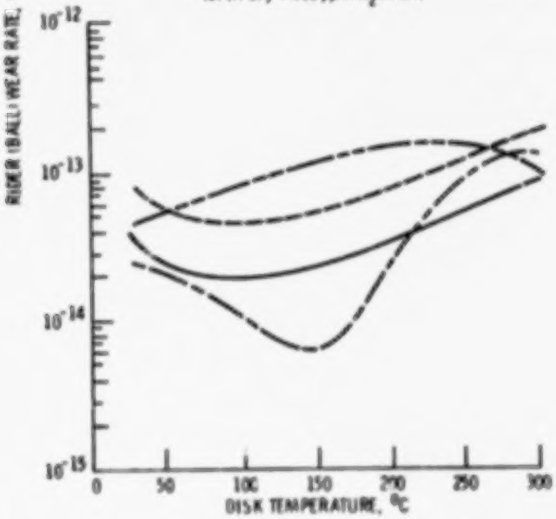

(b) In moist (RH 50 percent at 25 °C) air.

Figure 50. - Rider wear as a function of temperature for a thioether base fluid and thioether formulations IV, V, and VI.

Coefficient of Friction

Figure 46 contains a comparison between the friction coefficients for the Type II ester and the thioether base fluid. Figure 47 shows the friction-temperature curves for formulations I, II, and III. The friction-temperature curves for formulations IV, V, and VI appear in figure 49. As shown in these figures, all formulations and the base fluid exhibited slightly higher friction coefficients than the Type II ester from 150 to 300 °C and either similar or lower values from 25 to 150 °C. In general, above 200 C, the six formulations yielded slightly lower friction coefficients than the base fluid.

Discussion

Basically, the conditions of these experiments were so designed that the results should reflect antiwear rather than "EP" characteristics of the formulations. However, since the difference between these two regimes may be due to the temperature level existing in the contact, no doubt some "EP" activity may occur at the higher disk temperatures.

One of the common approaches to rationalize the performance of additives has been to measure their chemical reactivity toward iron or steel. Barcroft (ref. 51) and more recently Sakurai, et al. (ref. 52) have used the hot wire technique for such correlations.

Referring back to the background section on Boundary Lubrication, figure 25 shows a generalized curve of wear as a function of chemical reactivity. It can be seen that an optimum reactivity exists for minimum wear for a particular set of conditions. It should also be noted that this optimum value can shift if the severity of the test conditions are altered. For a particular additive system, a similar curve should result if wear were plotted as a function of temperature or additive concentration.

Unfortunately, no independent measurements have been made of the reactivities of the additives used in this study. It is interesting to note that most of the formulations exhibited the generalized wear-temperature behavior, as shown in figure 25. The fact that the thioether base fluid yields a similar curve would indicate that the lubricant molecule contains a reactive component, in this case, sulfur.

Two formulations (IV and VI) yielded higher wear than the unformulated base fluid. The formulation exhibiting the best overall wear performance was formulation V which contained perfluoroglutaric acid. Formulation III (di-isopropyl hydrogen phosphite and trichloroacetic acid) also gave good overall results.

Di-isopropyl hydrogen phosphite has been reported (ref. 53) to give very good antiwear activity in ester base fluids. It has also been reported that phosphites are better antiwear additives than phosphates (ref. 54) and that acid phosphites are more reactive than neutral phosphorus compounds (ref. 55).

The electron inductive effect of the halogens on the α carbons in perfluoroglutaric acid and trichloroacetic acid (with a pKa of 0.08) approaches the strength of the inorganic acids. Nevertheless, neither of these additives appeared to be unduly corrosive in these experiments.

Effect of Moisture on Additive Performance

It has been reported (ref. 41) that dissolved water may be deleterious with some additives by preventing proper adherence of the additive reaction products. Others have (ref. 56) reported that dissolved water is beneficial in promoting boundary film formation. In general, there was no great moisture effect for most of the formulations. Only the formulations containing the two strong carboxylic acids yielded different behavior in moist as compared to dry air. Formulation III containing trichloroacetic acid yielded lower wear in moist air above 150 °C.

Moisture appeared to be beneficial below 185 °C and detrimental above for formulation V (perfluoroglutaric acid). The thioether base fluid exhibited slightly lower wear rates in moist air. This follows the general lubricating behavior of aromatics as reported by

Appeldoorn and Tao (ref. 46). This parallels the behavior of 5P-4E as previously described in figure 42.

In conclusion, it has been shown that the thioethers are susceptible to additive treatment. However, it must be stated that the test conditions of this study are only a part of the spectrum of conditions that a lubricant or hydraulic fluid would be subjected to in service. Different results may be obtained under higher speeds, higher loads, and different metallurgies.

Summary of Results

The major results were the following:

(1) The six thioether formulations and the thioether base fluid yielded lower wear than the Type II ester under most test conditions.

(2) In dry air, all formulations (except IV and VI) yielded either similar or lower wear than the base fluid over the entire temperature range.

(3) In moist air, all formulations (except IV, V, and VI) yielded lower wear than the base fluid from 150 to 300 °C, but higher wear from 25 to 150 °C.

(4) Formulations IV and V yielded higher wear than the base fluid under all conditions. While formulation V exhibited lower wear than the base fluid under most conditions, it exhibited higher wear under others.

PIN-ON-DISK STUDIES - EFFECT OF OXYGEN CONCENTRATION

Because previous work had shown a strong effect of atmospheric oxygen on the wear behavior of aromatic fluids, it was decided to study this in more detail.

Therefore, the objectives of this portion of this thesis were (1) to determine the effect of various oxygen concentrations, varying from 20 percent, (air) to 0.001 percent (nitrogen) on the boundary lubricating characteristics of an unformulated thioether from 25 to

300 °C and (2) to compare these results with a five-ring polyphenyl ether (5P-4E) in air and nitrogen.

Experiments were conducted with a ball-on-disk sliding-friction apparatus. Test conditions included a load of 1 kg (initial Hertz stress of 10^9 N/m^2), a sliding speed of 17 m/min (100 rpm), and a test duration of 25 min. Test specimens were made of CVM (consumable electrode vacuum melted) M-50 steel.

Apparatus

The apparatus is identical to the one previously described (fig. 38) except that a 0.476-cm-radius ball was used instead of the hemispherically tipped pin. Figure 51 illustrates this change.

Procedure

The procedure previously described was utilized except for the following: The thioether was degassed at approximately 150 °C under a vacuum (2 torr) for 1 hr. Measurements by means of the Karl Fischer technique indicate that this procedure reduces dissolved water content in thioethers to less than 20 parts per million.

Several atmospheres, with oxygen concentrations from 20 percent (air) to 0.001 percent (nitrogen), were used. The intermediate oxygen concentrations studied were 10, 5, 1, 0.1, and 0.01 percent. These intermediate oxygen levels were obtained by mixing air and nitrogen streams. The moisture content of all atmospheres was less than 50 parts per million.

Oxygen concentration in the test atmosphere was monitored by an oxygen analyzer with an accuracy of approximately ±10 percent of the true value. Moisture content was monitored by a moisture analyzer with an accuracy of ±10 parts per million.

Results

Thioether wear. - Average rider (ball) wear rate as a function of disk temperature for a number of oxygen concentrations is presented in figure 52. The results for the 20-percent-oxygen (air) atmosphere are from figure 45.

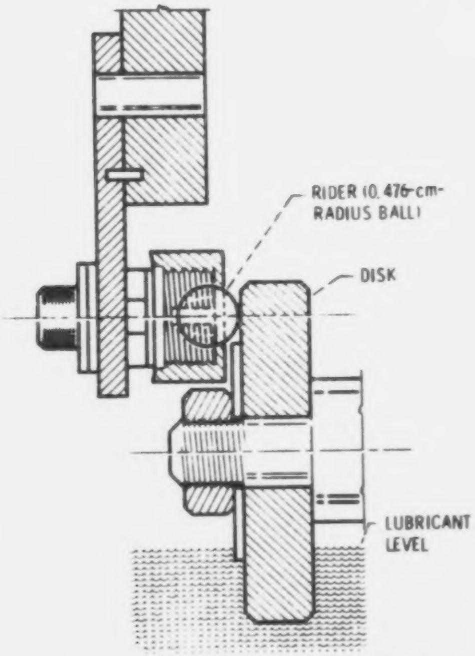

Figure 51. - Ball on disk specimen configuration.

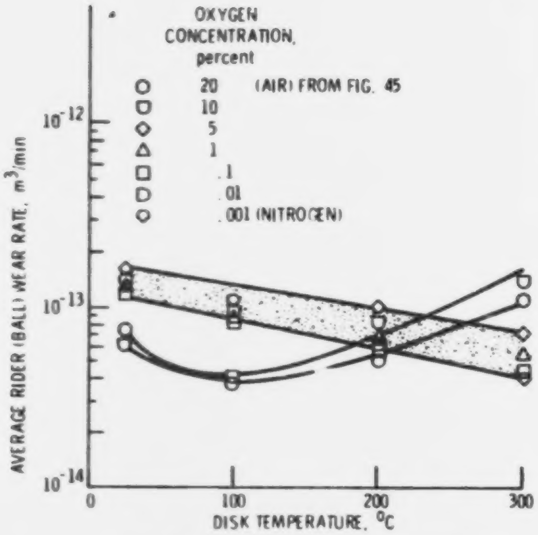

Figure 52. - Average rider (ball) wear as a function of disk temperature with a thioether base fluid in atmospheres with several oxygen concentrations. Specimen material, CVM M-50 steel; load, 1 kilogram; sliding speed, 17 meters per minute (100 rpm); test duration, 25 minutes.

Two different wear modes are observed in figure 52. At high oxygen levels (10 to 20 percent), wear decreased with increasing temperature from 25 to 100 °C and increased with further increasing temperature from 100 to 300 °C. At all other oxygen levels (0.001 to 5 percent) wear decreased with increasing temperature over the entire temperature range.

The thioether exhibited lower wear at high oxygen levels (10 to 20 percent) from 25 to 200 °C and at low oxygen levels (0.001 to 1.0 percent) from 200 to 300 °C.

Table 8 summarizes all of the thioether friction and wear results.

5P-4E wear. - The unformulated polyphenyl ether (5P-4E) was tested at two oxygen levels, 20 percent (air) and 0.001 percent (nitrogen). Figure 53 contains the wear results for this fluid in both atmospheres as a function of disk temperature.

Negligible rider wear ($<10^{-14}$ m^3/min) was observed at 25 °C with 5P-4E in both air and nitrogen. This is a fluid-film effect resulting from the high viscosity of 5P-4E at 25 °C and the good surface finish ($<10\times10^{8}$ m (<4 µin.) CLA) of the test specimens. Maximum wear occurred at approximately 75 °C. From 75 to 300 °C, rider wear decreased with increasing temperature.

Much higher wear was observed in nitrogen than in air over practically the entire temperature range. The maximum wear occurred at approximately 150 °C. A rapid decrease in wear was observed from 150 to 300 °C.

Comparison of Wear for Thioether and 5P-4E. - Wear rates for both thioether and 5P-4E at oxygen levels of 20 percent (air) and 0.001 percent (nitrogen) are presented in figure 54. The thioether yielded lower wear than the 5P-4E in dry air from 50 to 195 °C and in dry nitrogen from 50 to 265 °C.

It is evident that the structural modifications of the thioether (which primarily consists of substitution of sulfur for oxygen) have minimized the lower temperature (<200 °C) boundary lubrication problems associated with the polyphenyl ethers. It should also be

TABLE 8. - SUMMARY OF FRICTION AND WEAR RESULTS FOR THIOETHER BASE FLUID

[Test conditions: load, 1 kg; sliding speed, 17 m/min (100 rpm); duration, 25 min; material, CVM M-50 steel.]

Disk temperature °C	Concentration of oxygen in test atmosphere, percent (by volume)						
	0.001 nitrogen	0.01	0.1	1.0	5.0	10	20 (air)[a]
	Coefficient of friction						
25	0.08	0.07	0.07	0.07	0.08	0.10	0.12
100	.18	.18	.17	.14	.14	.14	.16
200	.21	.24	.23	.21	.20	.18	.18
300	.22	.22	.20	.17	.14	.14	.20
	Average rider (ball) wear rates, m^3/min						
25	14×10^{-14}	12×10^{-14}	11×10^{-14}	12×10^{-14}	16×10^{-14}	6.2×10^{-14}	7.5×10^{-14}
100	11.0	9.4	8.3	8.6	11.0	3.9	3.8
200	8.0	6.5	5.8	6.4	10.0	8.4	5.0
300	4.2	4.2	4.4	5.4	7.6	14.0	11.0

[a] Data from figure 45.

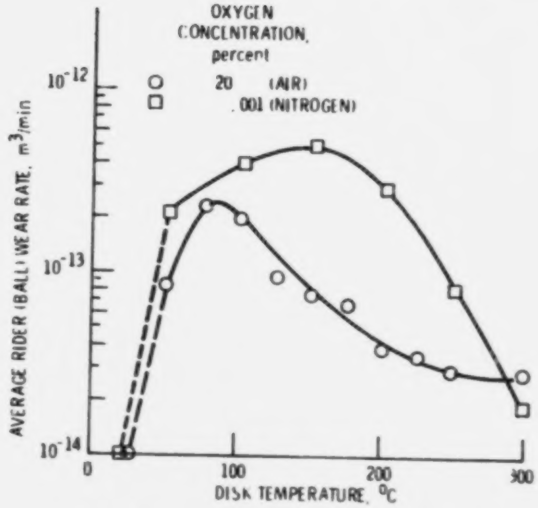

Figure 53. - Average rider (ball) wear as a function of disk temperature with a five-ring polyphenyl ether in atmospheres with two oxygen concentrations. Specimen material, CVM M-50 steel; load, 1 kilogram; sliding speed, 17 meters per minute (100 rpm); test duration, 25 minutes.

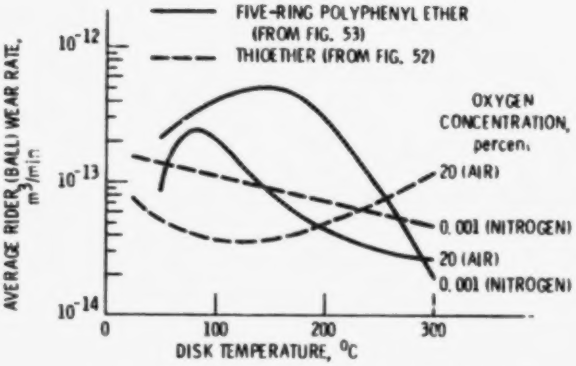

Figure 54. - Average rider (ball) wear rate as a function of disk temperature with a thioether and a five-ring polyphenyl ether in atmospheres with two oxygen concentrations. Specimen material, CVM M-50 steel; load, 1 kilogram; sliding speed, 17 meters per minute (100 rpm); test duration, 25 minutes.

noted that these modifications increase wear at the higher disk temperature in both atmospheres. However, additives to the thioether base fluid may lessen or eliminate this effect as has previously been shown.

Coefficient of friction. - The coefficient of friction as a function of disk temperature for the thioether at a number of oxygen levels is shown in figure 55 (a). The data fall into a band that has the general trend of increasing friction with increasing disk temperature to 200 °C. The coefficient of friction as a function of temperature for 5P-4E in air and in nitrogen is given in figure 55 (b). The friction-coefficient band obtained with the thioether at all oxygen levels is shown for comparison.

At an oxygen level of 20 percent (air), the 5P-4E exhibits the similar trend of increasing friction with increasing temperature over most of the temperature range. At an oxygen level of 0.001 percent (nitrogen) from 50 to 200 °C, the 5P-4E exhibited stick-slip friction, which is indicative of very poor boundary lubrication. This friction region coincides with the high-wear region in figure 53. It is evident that the thioether exhibited lower friction coefficients than the 5P-4E over the entire temperature range in nitrogen. In air, the thioether exhibited similar or lower friction coefficients than the 5P-4E.

Discussion. - Highly aromatic fluids have often been reported as poor boundary lubricants in low-oxygen environments. Appledoorn and Tao (ref. 46) showed that heavy aromatics (such as 1-methylnaphthalene) scuffed at low loads (1 kg) in dry argon in ball-on-cylinder tests. They also found that small amounts of dissolved oxygen or dissolved water prevented scuffing with aromatic materials. Fein and Kreuz (ref. 57) reported that benzed (an aromatic) yielded high wear in four ball tests at low oxygen concentrations. The lowest wear was observed when air or oxygen was used as the saturating atmosphere. Spar and Damasco (ref. 19) studied a four-ring polyphenyl ether in nitrogen with a four-ball tester. High wear was observed, and the maximum wear occurred between 135 and 204 °C. Vinogradov et al. (ref. 58) reported lower friction coefficients and higher seizure

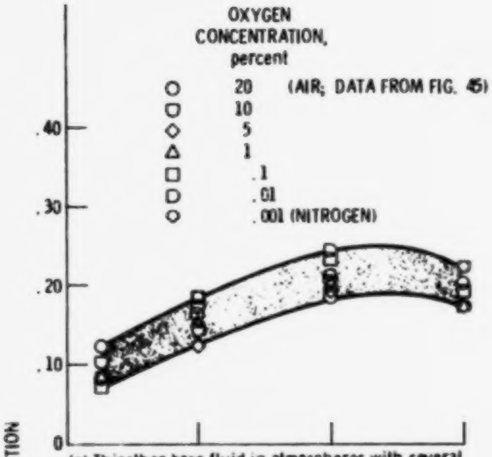

(a) Thioether base fluid in atmospheres with several oxygen concentrations.

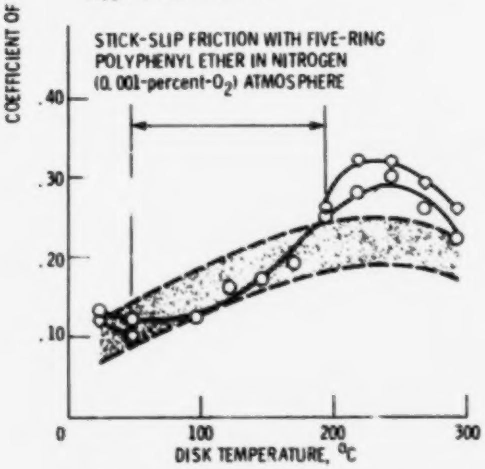

(b) Five-ring polyphenyl ether in atmospheres with two oxygen concentrations.

Figure 55. - Coefficient of friction as a function of disk temperature. Specimen material, CVM M-50 steel; load, 1 kilogram; sliding speed, 17 meters per minute (100 rpm); test duration, 25 minutes.

loads for benzene in air than in argon in four-ball tests. Similar phenomena are reported in this thesis with polyphenyl ethers in the vane-pump studies and with the ball-on-disk apparatus.

Therefore, the fact that aromatic fluids are poor boundary lubricants in the absence of oxygen and water vapor at temperatures below 200 °C is well documented. The reasons for this behavior, however, are not well understood.

A phenomenon that has been observed by many investigators in sliding-friction experiments is the formation of "friction polymer" (refs. 57, 59, and 60). This is the carbonaceous polymer-like residue found in and around wear scars in sliding experiments. It has been theorized (ref. 59) that this highly viscous product of sliding actually causes the formation of a partial elasto-hydrodynamic film. This film then greatly reduces friction and wear.

It would follow that materials that produce copious amounts of friction polymer would be good boundary lubricants. Based on the previous discussion, one could then speculate that highly aromatic fluids require high oxygen concentrations in order to produce adequate quantities of friction polymer. Hermance and Egan (ref. 28) found that in air, aromatic compounds did produce larger quantities of friction polymer than nonaromatic compounds under identical test conditions. Fein and Kreuz (ref. 57) also observed increased production of friction polymer with benzene in air.

Friction polymer was observed around most of the wear scars in this study. There were no quantitative measurements, but visual observation did not reveal any correlation between the amount of friction polymer present and the level of wear. Three typical wear scars for tests at 25 °C and at three oxygen levels are shown in figure 56(a). Three wear scars obtained under similar oxygen levels and at 300 °C are shown in figure 56(b). In figure 56(a), Schnurmann and Pedersen (ref. 61) have related these sigmoid patterns to the combined action of a magnetic field and a hydrodynamic flow field. It is theorized that the magnetic field is the result of an electrical discharge at the frictional contact.

ORIGINAL PAGE IS
OF POOR QUALITY

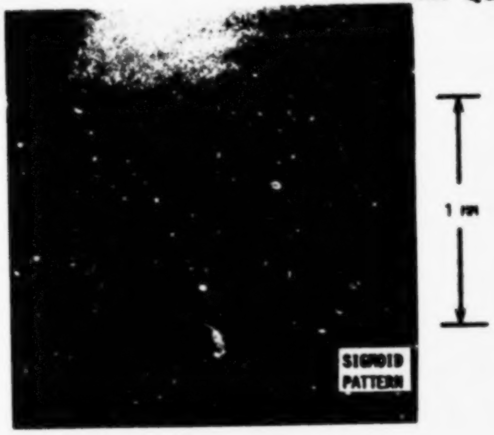

(a) Oxygen concentration, 20 percent (air).

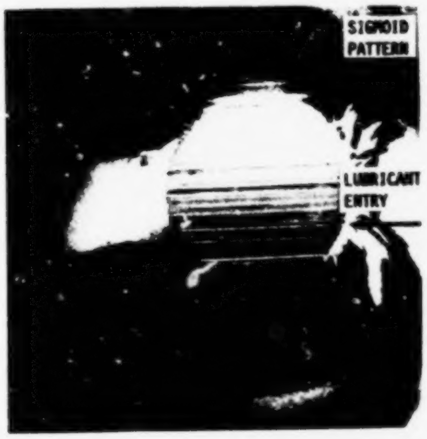

(b) Oxygen concentration, 1 percent.

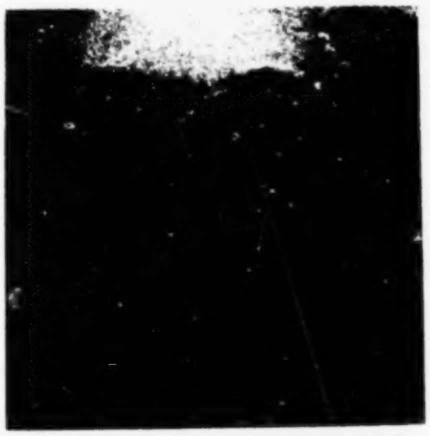

(c) Oxygen concentration, 0.001 percent (nitrogen).

Figure 56(a). - Typical rider (ball) wear scars with a thioether at a disk temperature of 25 °C in atmospheres with three oxygen concentrations. Specimen material, CVM M-50 steel; load, 1 kilogram; sliding speed, 17 meters per minute (100 rpm); test duration, 25 minutes.

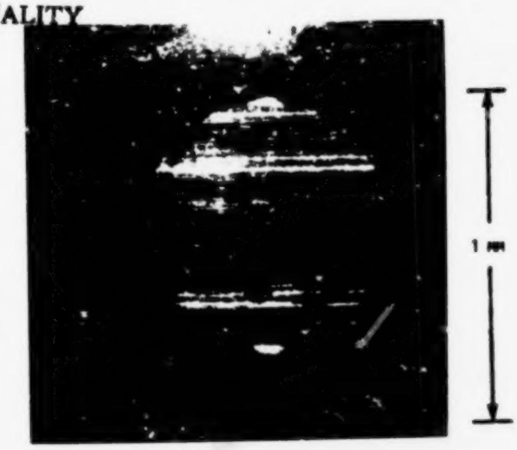

(a) Oxygen concentration, 20 percent (air).

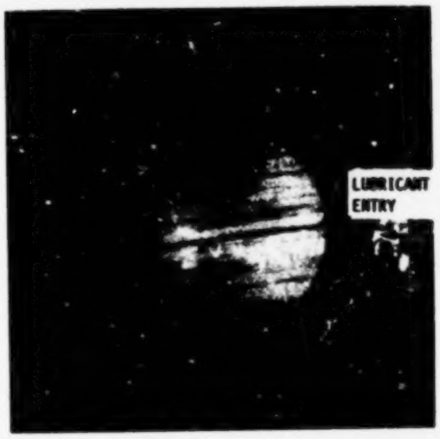

(b) Oxygen concentration, 5 percent.

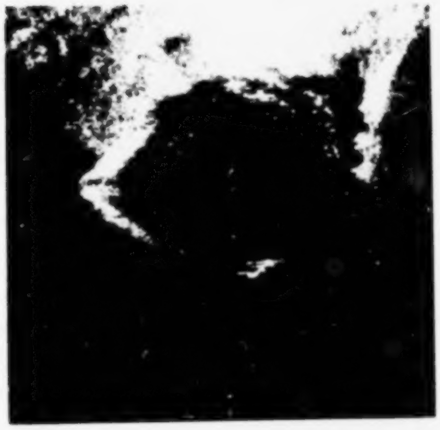

(c) Oxygen concentration, 0.001 percent (nitrogen).

Figure 56(b). - Typical rider (ball) wear scars with a thioether at a disk temperature of 300 °C in atmospheres with three oxygen concentrations. Specimen material, CVM M-50 steel; load, 1 kilogram; sliding speed, 17 meters per minute (100 rpm); test duration, 25 minutes.

In general, the friction polymer appeared to be held more tenaciously to the specimen surface at the lower temperatures. At the higher temperatures, an alcohol rinse to remove residual oil easily detached the debris around the wear scar.

A cleaned wear scar obtained with 5P-4E in dry nitrogen in the high-wear regime is shown in figure 57. Although the stick slip friction observed during this test is indicative of a scuffing type of wear, the wear scar is surprisingly smooth. This type of scuffing wear was also observed by Appeldoorn and Tao (ref. 46).

The apparent lack of any correlation between the amount of observed friction polymer and the level of wear may be the result of a number of factors. First, it is obviously somewhat difficult to visually compare amounts of friction polymer around the wear scars. Secondly, compositional changes in the friction polymer due to changes in test conditions (i.e., changes in temperature or oxygen concentration) may have a greater effect on the wear process than the variation in the quantity generated. Finally, as mentioned before, friction polymer appeared to be more easily detached from the specimen surface after tests at high temperatures. Solubilization by the bulk oil at the higher temperatures is a distinct possiblity.

Goldblatt (ref. 62) put forth a theory which may explain the anomalous behavior of aromatic compounds in friction and wear tests. His theory involves the formation of a radical anion from an adsorbed polynuclear aromatic compound. This anion could then undergo several reactions depending on the conditions. In a dry inert atmosphere (nitrogen or argon), it could react directly with the metal surface to produce a type of corrosive wear. It would react with paraffinic material (if present) to produce friction polymer (called surface resin by Goldblatt). Finally, if either water or oxygen is present, a type of quenching reaction could take place which would eventually lead to the production of friction polymer. These reactions would then explain why aromatics are poor boundary lubricants under inert conditions and are improved by the presence of water, oxygen, or paraffins. The Goldblatt model is more thoroughly discussed later.

ORIGINAL PAGE IS
OF POOR QUALITY

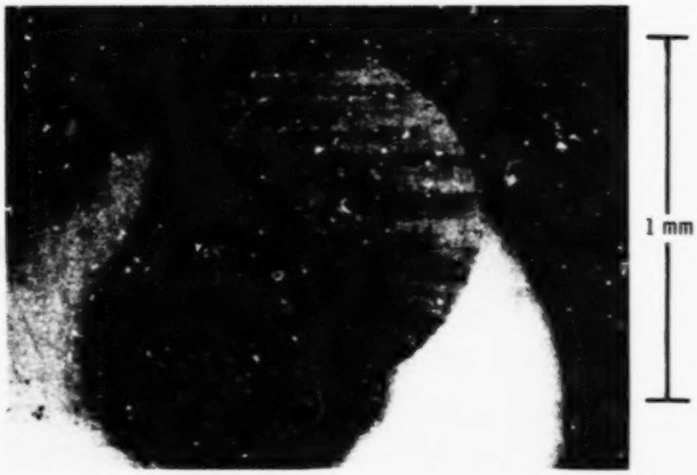

Figure 57. - Cleaned rider wear scar with 5P-4E at a disk temperature of 200 °C in an atmosphere with an oxygen concentration of 0.001 percent (nitrogen). Specimen material, CVM M-50 steel; load, 1 kilogram; sliding speed, 17 meters per minute (100 rpm); test duration, 25 minutes.

Summary of results. - The effect of various oxygen concentrations, ranging from 20 percent (air) to 0.001 percent (nitrogen), on the boundary-lubricating characteristics of an unformulated thioether was studied with the use of a ball-on-disk sliding-friction apparatus. Disk temperatures ranged from 25 to 300 °C. Other conditions included a load of 1 kg (initial Hertz stress of 10^9 N/m^2), a surface speed of 17 m/min (100 rpm), and a test duration of 25 min. Test specimens were made of CVM (consumable electrode vacuum melted) M-50 steel. The thioether friction and wear results were compared with those obtained with a five-ring polyphenyl ether. The major results were the following:

1. The thioether yielded lower wear and lower friction coefficients than a five-ring polyphenyl ether in air (20 percent O_2) and nitrogen (0.001 percent O_2) over most of the temperature range.
2. The thioether exhibited lower wear at high oxygen levels (10 to 20 percent O_2) from 25 to 200 °C and at low oxygen levels (0.001 to 1.0 percent O_2) from 200 to 300 °C.
3. Friction polymer was observed around the wear scars of most test specimens.

PIN-ON-DISK STUDIES (AROMATIC SILICON AND TIN COMPOUNDS)

Background

Another class of compounds which has elicited considerable interest as possible high-temperature lubricants or additives is the organometallics. This group includes siloxanes, ferrocenes, silanes, and stannanes (refs. 9, 63, 64, and 65).

Tetraalkyl silanes have been studied as base stocks for high temperature lubricants (ref. 63). Thermal decomposition temperatures as high as 350 °C were reported. Some of these fluids exhibited good viscosity properties to 316 °C. They also exhibited good lubricating ability to 200 °C in four-ball tests.

A number of organotin compounds have been synthesized for use as lubricant additives to improve oxidation stability (ref. 64) or antiwear behavior (ref. 65). Zimmer and co-workers (ref. 66) have synthesized a variety of sterically hindered Group IVA organometallic compounds. These compounds are characterized by decreased reactivity because of the bulky groups shielding the central tin or silicon atom.

Friction and wear properties of two selected aromatic organometallic compounds were determined. The standard procedure for the ball-on-disk apparatus was used. The two compounds appear in table 1. One is an organo-tin compound: n-butylstannyl(diphenyl) and the other, an organosilicon compound: n-butylsilyl(diphenyl).

Friction and Wear Results

The meta-n-butyl derivatives were chosen as the representative compounds from a series of derivatives for the friction and wear tests. The n-butyl derivatives were selected because of their ease of preparation and the fact that they were both viscous liquids at room temperature.

Figure 58 contains the friction and wear results for these two fluids. The temperature range studied was 25 to 225 °C. The upper temperature limit was dictated by fluid volatility. As can be seen, the tin derivative yields slightly lower wear than the silicon analog at low temperatures (25 to 75 °C) but greater wear at the higher temperatures (75 to 225 °C). The increase in wear rate at the high temperatures for both fluids may in part be due to loss of lubricant by evaporation.

The coefficient of friction for the tin derivative is essentially constant over the entire temperature range. The silicon analog exhibited a linearly increasing friction coefficient.

A comparison of the tin and silicon results with those obtained with the thioether (fig. 45) and 5P-4E (fig. 53) appears in figure 59. As can be seen, both the tin and silicon compounds yielded lower wear than 5P-4E over practically the entire overlapping temperature range.

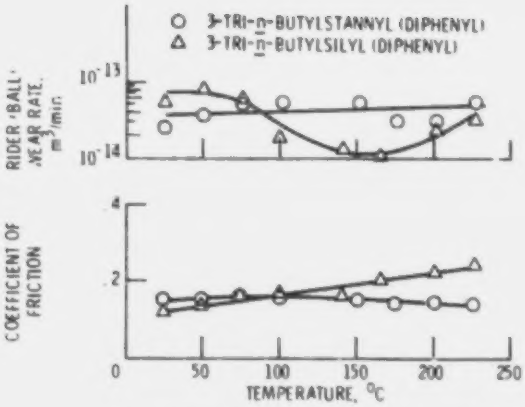

Figure 58. - Coefficient of friction and rider (ball) wear rate for 3-tri-n-butylstannyl (diphenyl) and 3-tri-n-butylsilyl (diphenyl) as function of disk temperature. Load, 1 kilogram; sliding speed, 17 meters per minute (100 rpm); test duration, 25 minutes; M-50 steel; dry-air atmosphere.

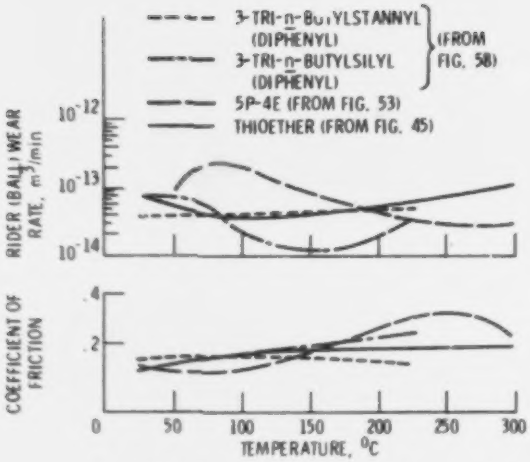

Figure 59. - Coefficient of friction and rider (ball) wear rate for 3-tri-n-butylstannyl (diphenyl), 3-tri-n-butylsilyl (diphenyl), a polyphenyl ether, and a thioether. Load, 1 kilogram; sliding speed, 17 meters per minute (100 rpm); test duration, 25 minutes; M-50 steel; dry-air atmosphere.

From 25 to 75 °C the tin and silicon compounds exhibit wear rates similar to those obtained with the thioether. From 75 to 225 °C, the tin compound yielded wear similar to that for the thioether, and the silicon compound yielded wear lower than that for the thioether. Figure 60 summarizes the wear results for the four fluids at four disk temperatures.

The coefficient of friction as a function of temperature for all four fluids appears in figure 59. In general, all fluids exhibited similar friction coefficients from 25 to 150 °C. From 150 to 225 °C, the lowest friction was observed with the tin compound and the highest with 5P-4E. Thermal stability tests on two series of organometallics, which include these two n-butyl derivatives, appear later in the section on thermal stability.

Summary of Results

In general, the 3-tri-n-butylstannyl(diphenyl) and the 3-tri-n-butylsilyl(diphenyl) compounds yielded friction and wear results either lower than or similar to to those for 5P-4E and the thioether over a temperature range of 25 to 225 °C.

FERROGRAPHY

BACKGROUND

The detection and analysis of wear debris generated in lubrication systems plays an important role in elucidating what wear mechanisms are occurring. In addition, the sudden appearance of or an increase in the rate of production of a particular type of wear particle may be related to the incipient failure of a system component.

There are a number of methods available for detecting and analyzing wear debris in lubricants. The quantity and size distribution of particles may be measured by using ordinary particle counters which are based on a variety of different principles. Atomic absorption, emission spectroscopy, and x-ray fluorescence are

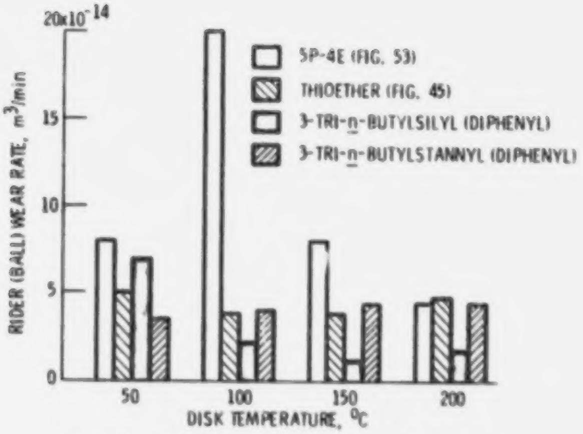

Figure 60. - Rider (ball) wear rates for four fluids at four disk temperatures in dry air. Load, 1 kilogram; sliding speed, 17 meters per minute (100 rpm); test duration, 25 minutes; M-50 steel.

also commonly used techniques for elemental analysis. Debris may be collected by filtration, examined microscopically, and subjected to other analytical procedures such as x-ray diffraction and neutron activation analysis.

However, each of these methods has certain deficiencies. Particle counters are not able to differentiate between metallic and organic debris. Nor do they provide any information concerning particle morphology. Filtration often results in a massive pileup of all particulates (including those unrelated to the wear process) on the filter. Thus, it is very difficult to study individual particles. The spectroscopic and irradiation techniques are extremely sensitive but again do not differentiate between particles of different chemical nature.

In 1972, a new instrument, the Ferrograph, was developed which is capable of precipitating magnetic particles from a lubricant onto a transparent substrate to yield a Ferrogram (ref. 67). The precipitated particles range in size from approximately 0.02 to a few micrometers and are arranged according to size on the substrate. The density of the deposit may be measured optically, and individual particles may be observed with a unique bichromatic microscope, the Ferroscope. The Ferrogram may also be examined with an electron microscope.

The objectives of this portion of this thesis were (1) to determine types of wear particles generated by a five-ring polyphenyl ether in boundary lubrication experiments by using Ferrographic analysis and (2) to relate the particle types to the wear mechanisms occurring with this fluid.

Lubricant samples were obtained from friction and wear tests previously conducted on a ball-on-disk sliding friction apparatus and reported in figure 53. Conditions included a 1-kg load (initial Hertz stress, 10^9 N/m^2), a 17-m/min (100-rpm) sliding speed, 100 to 250 °C disk temperatures, test atmospheres of air and nitrogen of varying moisture contents, and a test duration of 25 min (in most cases). Test specimens were consumable electrode vacuum melted (CVM) M-50 steel.

APPARATUS AND PROCEDURE

The apparatus and procedure for these tests are the same as previously described in the boundary lubrication section, except for the following.

Cleaning Procedure

Because of the extreme sensitivity of the Ferrographic technique, a rigorous cleaning procedure was adopted. All parts of the test apparatus that came into contact with the test lubricant were cleaned with a dilute acid solution. This acid solution was prepared by adding 10 drops of concentrated nitric acid and 10 drops of concentrated hydrochloric acid to $5\text{x}10^{-5}$ m^3 (50 ml) of distilled water. This solution dissolved any metallic debris left from the previous test. In addition, the solvents and the unused oil were subjected to Ferrographic analysis to determine if they were free of metallic debris. Essentially no metallic contamination was found in these fluids.

Analytical Ferrograph

The Analytical Ferrograph is an instrument used to magnetically precipitate wear particles from a used oil onto a specially prepared glass slide. A mixture of 3 ml of used oil and 1 ml of solvent is prepared. This mixture is then slowly pumped over the slide as shown in figure 61. A solvent wash and fixing cycle follows which removes residual oil and permanently attaches the particles to the slide. The resulting slide with its associated particles is called a Ferrogram. A sketch of a Ferrogram slide is illustrated in figure 62.

The SEM used in this study is an ISI-40/4 having a 60 Å resolution with 10 X to 600 000 X magnification range. In addition, the system is equipped with a PGT SYSTEM III energy dispersive x-ray analyzer for elemental particle analysis.

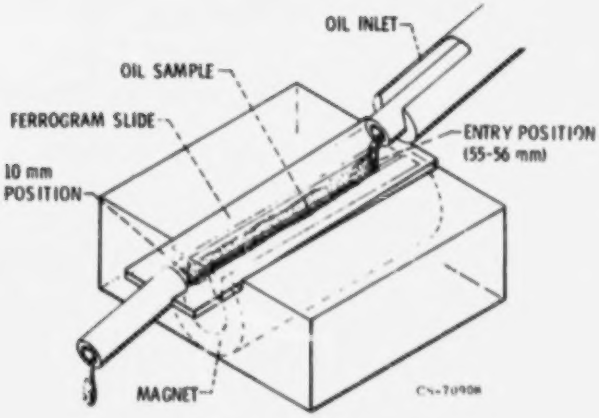

Figure 61. - Analytical ferrograph.

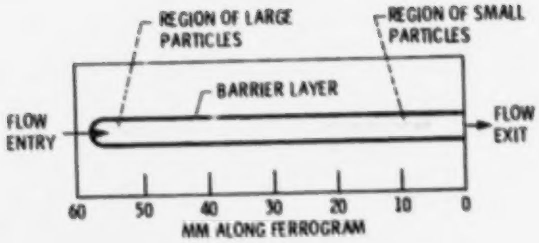

Figure 62. - Ferrogram slide.

Ferroscope

The Ferroscope used in this study is a Richert Zetopan large research microscope equipped with a bichromatic illumination system, a camera and a photodetector. The system provides for both transmitted green light and reflected red light simultaneously. This high contrast combination makes it possible to distinguish light transmitted through particles from light reflected by the surfaces of the particles. Opaque particles return the reflected light and appear red. Transparent particles reflect little light but pass the transmitted light and appear green. The microscope is also equipped with polarizers which allow examination of particles in reflected polarized light. This yields information concerning the optical activities of the particles. The photodetector is used to measure the amount of particles at various locations on a Ferrogram.

Test Atmospheres

Four test atmospheres were used in this study. They were wet and dry air and wet and dry nitrogen. Dry air and dry nitrogen contained less than 50 and 20 ppm of moisture, respectively. Both wet gases had a relative humidity of greater than 95 percent at 25 °C.

Relative humidity of the wet gases was monitored with an electronic hygrometer accurate to ±4 percent. The moisture content of the dry gases was monitored by a moisture analyzer with an accuracy of ±10 ppm. A wet gas was obtained by bubbling the dry gas through a water reservoir.

RESULTS - 5P-4E

Several different types of wear debris were observed when the oil samples from the friction and wear tests were subjected to Ferrographic analysis. Table 9 summarizes the types of wear debris observed in this study. In addition, table 9 contains information regarding the morphology, size range, and appearance in the bichromatic microscope.

TABLE 9. - DESCRIPTION OF DIFFERENT TYPES OF WEAR DEBRIS GENERATED BY A FIVE-RING POLYPHENYL ETHER (5P-4E)

Type of wear debris	Morphology(as debris appears in Ferrograms)	Size range, µm	Appearance in bichromatic microscope
Free metal			
Adhesive	Strings(actually made up of small asymmetrical flakes which have agglomerated during precipitation)	Length, <5	Bright red
Cutting	Individual particles (wire-like turnings and crescent-shaped chips)	Variable	Bright red
Spheres	Spherical particles (often found interspersed in adhesive strings)	Diameter, 1 to 10	Bright red.
Severe wear	Large irregularly shaped fragments	Diameter, 30 to 50	Bright red
Inorganic (oxides)	Translucent islands or randomly oriented strings	Diameter, <1	Yellow-green
Organic	Carbonaceous particles (containing some metallic debris)		Dark red
	Rocklike	Diameter, 5 to 20	
	Cylindrical	Diameter, 1 to 3	

Wear

Wear results for 5P-4E have previously appeared in figures 41 and 53.

Figure 53 gave rider wear for the polyphenyl ether as a function of disk temperature for atmospheres of dry air and dry nitrogen. The effect of moisture on rider wear was shown in figure 41 at three disk temperatures: 150, 250, and 350 °C. It should be noted that the wear rates in the dry atmospheres of figure 53 do not exactly correspond to the rates shown in figure 41. The discrepancies arise because these results are from two separate studies and the wear rates were based on different test durations (25 min and 1 hr). In addition, the relative humidity of the wet gases in the study of figure 41 was 50 percent compared with greater than 95 percent in the present data. Nevertheless, the figures are qualitatively consistent and do illustrate the following points: High wear occurs under dry inert conditions. The presence of either oxygen or moisture in the test atmosphere reduces wear, with moisture having the greater effect. The abnormally low wear at 25 °C in figure 53 is due to the generation of an elastohydrodynamic film.

Ferrograph

Particles in the used oil are precipitated according to size on a transparent substrate, and the result is called a Ferrogram. The largest and the greatest density of wear particles occurs at the end of the Ferrogram where the used oil first contacts the substrate. For comparison purposes all photomicrographs were taken in this region.

The bichromatic (red-green) system of the Ferroscope facilitates differentiation among the types of wear debris. Free metal appears bright red, nonmetallic translucent particles appear yellow or green, and nonmetallic opaque debris appears black or dark red.

A typical photomicrograph from a Ferrogram appears in figure 63. At least three particle types are discernible. First, the horizontal red strings of material are adhesive wear particles. Second, the green material which appears in islands or randomly oriented strings is oxides. Third, the large black rocklike particles are carbonaceous debris. It should be noted that the term carbonaceous is used in a descriptive rather than a chemical sense.

EFFECT OF TEMPERATURE

Figure 64 illustrates the effect of disk temperature on the generation of wear debris in dry nitrogen. Some adhesive and cutting debris are evident. However, the most important observation is the large amount of carbonaceous debris present. Note the large increase in this type of debris at 250 °C. There also appears to be two distinct types. Some particles are irregularly shaped and rocklike. Others appear as small cylinders which are typically 1 to 3 μm in diameter and 10 to 15 μm in length. In general, the rocklike particles decrease and the cylinders increase with increasing temperature. The cylinders also decrease in size with increasing temperature.

Effect of Oxygen and Moisture

The effect of oxygen or moisture in the test atmosphere on wear debris generation at 100 °C is illustrated in figure 65. It is immediately evident that the presence of moisture in the test atmosphere almost completely inhibits the formation of the carbonaceous debris. The presence of oxygen also decreases the production of carbonaceous debris, but to a much lesser extent than moisture. More metallic debris is noted in wet air than in wet nitrogen.

Cutting wear debris was observed in all Ferrograms but was more prevalent under moist conditions, particularly in wet air. Some examples of this type of debris appear in figure 66.

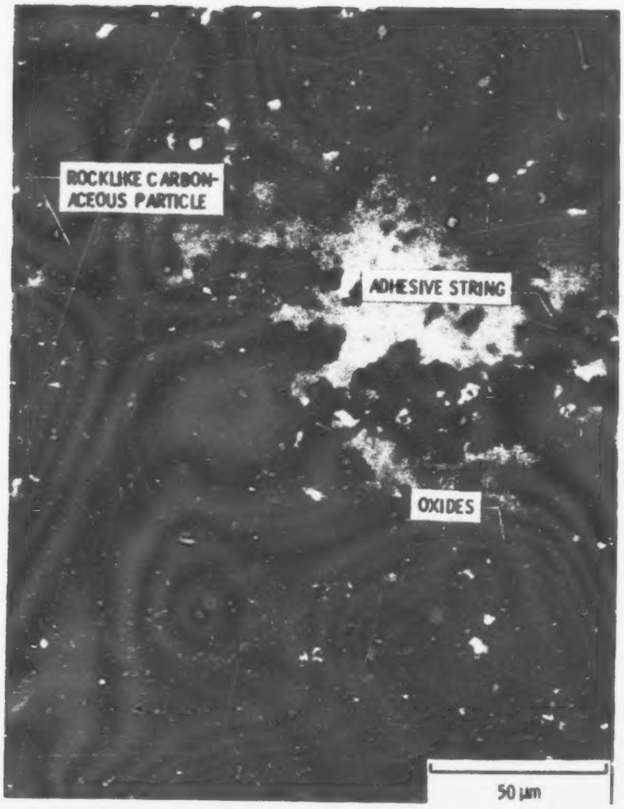

Figure 63. - Photomicrograph of wear debris generated by 5P-4E at 100 °C in dry test atmosphere of 1 percent oxygen and 99 percent nitrogen (by volume).

ORIGINAL PAGE IS
OF POOR QUALITY

ORIGINAL PAGE IS
OF POOR QUALITY

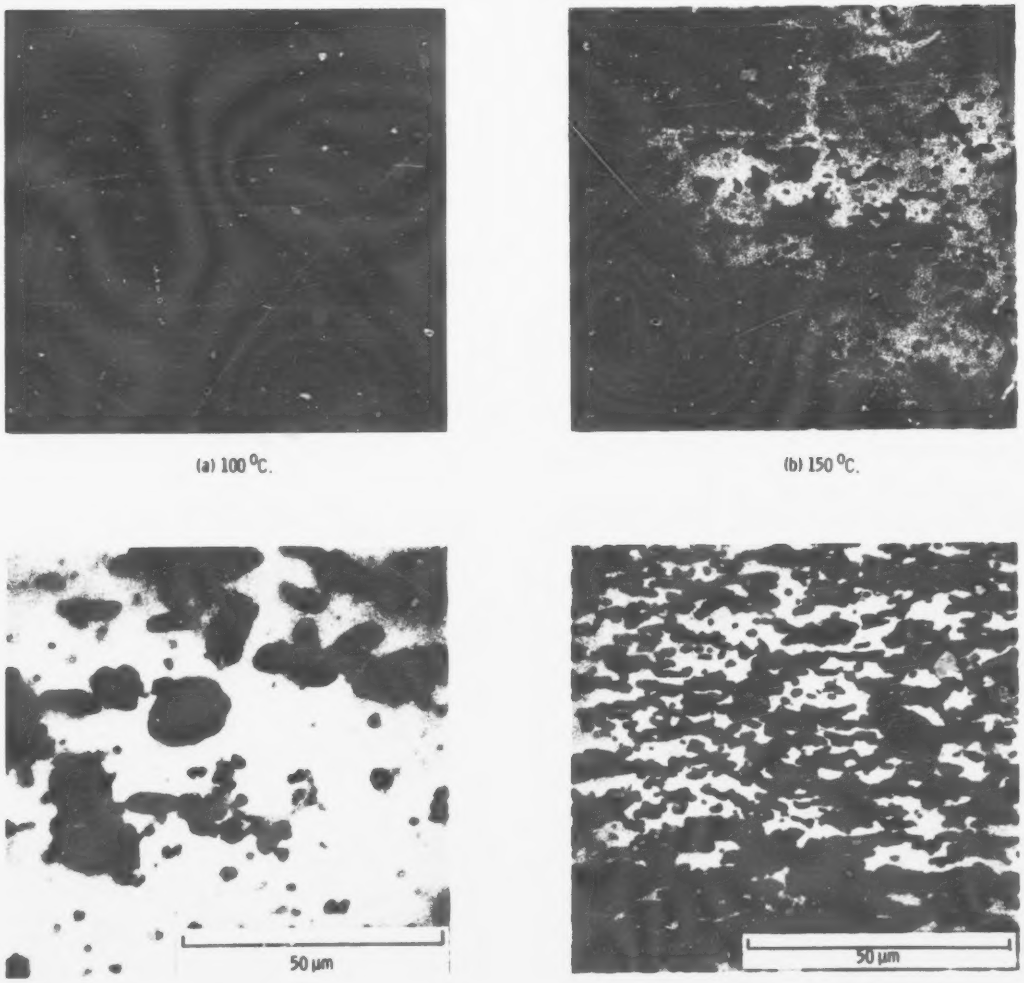

(a) 100 °C.

(b) 150 °C.

(c) 200 °C.

(d) 250 °C.

Figure 64. - Phitomicrographs of wear debris generated by 5P-4E in dry nitrogen at four test temperatures.

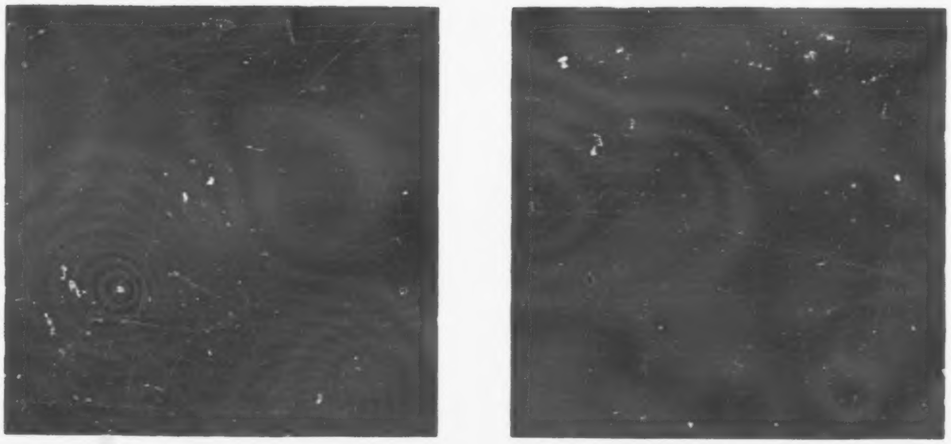

(a) Dry nitrogen.

(b) Wet nitrogen (relative humidity, >95 percent).

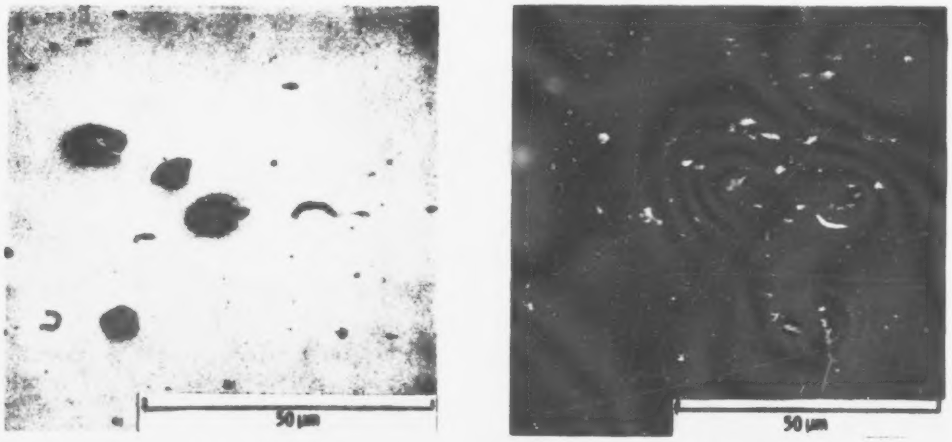

(c) Dry air.

(d) Wet air (relative humidity, >95 percent).

Figure 65. - Photomicrographs of wear debris generated by 5P-4E at 100 °C in four test atmospheres.

ORIGINAL PAGE IS
OF POOR QUALITY

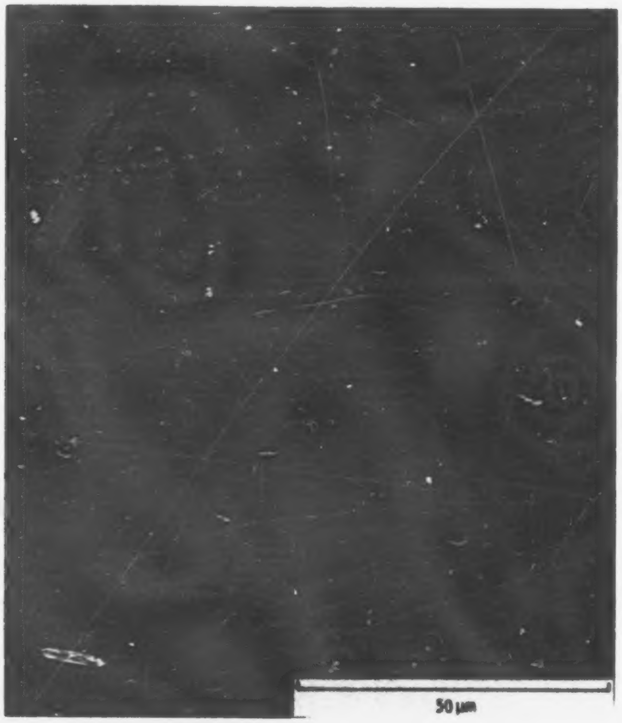

(a) Nitrogen.

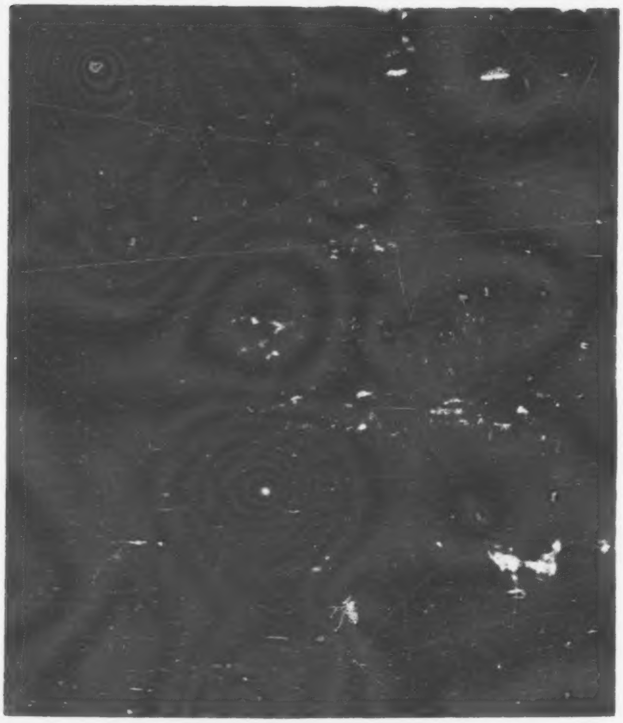

(b) Air.

Figure 66. - Photomicrographs of cutting wear debris generated by 5P-4E at 100 °C in wet test atmospheres (relative humidity, >95 percent).

ORIGINAL PAGE IS
OF POOR QUALITY

Another moisture effect manifests itself in the generation of spherical debris such as that illustrated in figure 67. Spheres were rarely observed in dry atmospheres but always under moist conditions.

Finally, a number of Ferrograms contained some severe (large) wear particles, such as the large wear fragment shown in figure 68. Again, these particles appeared more frequently in moist atmospheres.

Carbonaceous Debris

Many investigators have observed the generation of carbonaceous debris in boundary lubrication experiments with polyphenyl ethers. Apparently, a wearing situation must exist for its production, since this type of debris is not normally observed in static thermal stability tests. Spar and Damasco (ref. 19) found large quantities of metallic debris in the carbonaceous product from their experiments. Analysis of the organic portion of their debris yielded a higher molecular weight structure similar to the base fluid. Analysis of the carbonaceous debris in the study of reference 68 yielded similar results. Therefore, this debris is not just a cokelike deposit caused by high-temperature degradation of the lubricant.

As previously mentioned, Goldblatt (ref. 62) proposed the following model to explain the lubricating behavior of aromatics: he theorized that aromatic radical anions are generated at the wearing surfaces. These highly reactive molecules can then react with the metal surfaces and produce a form of corrosive wear. The radical anions can also be "quenched" by reacting with either oxygen or water and are thus prevented from corrosively attacking the surface.

One may speculate that a similar phenomenon occurs with the polyphenyl ethers. In dry nitrogen, radical anions formed from the polyphenyl ether molecules attack the metal surface and produce an organometallic friction polymer (called surface resin by Goldblatt). This product is removed from the surface during the sliding process and accumulates around the wear scar and in the fluid. The fact that

ORIGINAL PAGE IS
OF POOR QUALITY

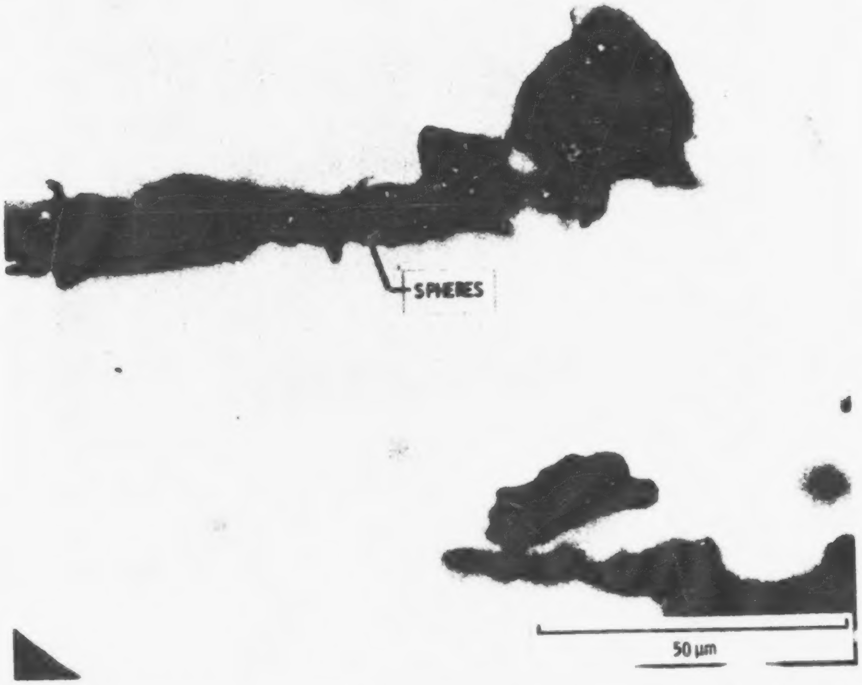

Figure 67. - Photomicrograph of wear debris containing metallic spheres generated by 5P-4E at 100 °C in air (relative humidity, >95 percent).

ORIGINAL PAGE IS
OF POOR QUALITY

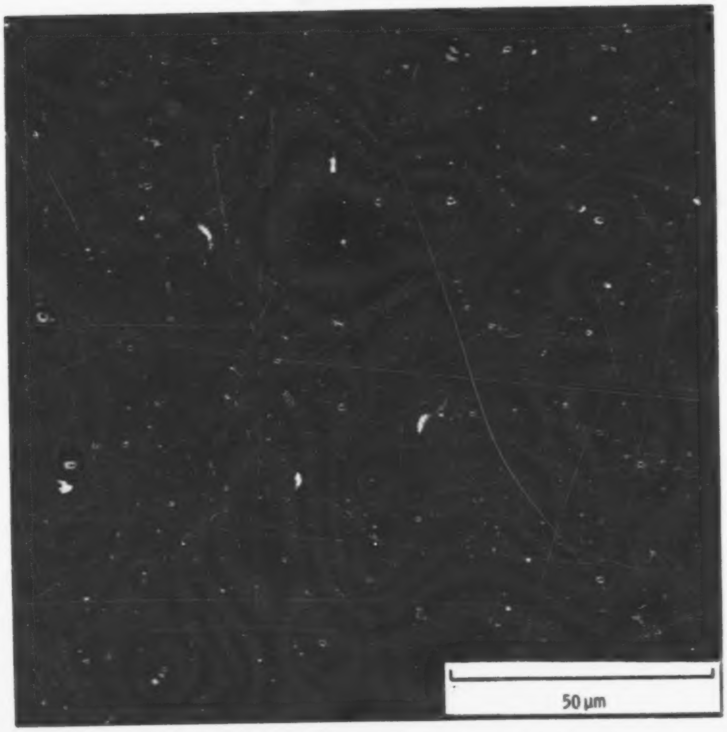

Figure 68. - Photomicrograph of large wear fragment generated by 5P-4E at 100 °C in air (relative humidity, >95 percent).

much of the observed carbonaceous debris is in the form of small cylinders tends to support this idea. Other investigators, such as Antler (ref. 69), have reported the production of roller-shaped debris in sliding experiments.

Another interesting observation is that, even though the wear (determined by the wear scar) is high in dry nitrogen, very little free metallic debris is evident in the Ferrograms. If a corrosive mechanism is operative, one would expect much of the worn metal to be contained in the carbonaceous debris in the form of an organometallaic reaction product. Of course, it would also be possible for free metallic particles to become embedded in the carbonaceous debris while it is being stripped off the surface. At any rate, when a Ferrogram containing carbonaceous debris is placed on a hotplate at 480 °C, the debris becomes translucent and retains its original morphology. It also exhibits the orange-red color of iron oxide. The fact that large quantities of this carbonaceous debris are precipitated by the magnetic field of the Ferrograph further indicates the presence of iron. An electron micrograph of some of the carbonaceous particles appears in figure 69(a). An iron x-ray map of the same area appears in figure 69(b) and confirms the presence of iron in both types of particle.

The large decrease of wear rate at temperatures above 200 °C (in dry nitrogen) may be a consequence of the increased reactivity of the radical anions at high temperature. If the rate of production of surface resin were greater than its effective removal rate during the sliding process, a reduction in wear could be effected. This would be a result of a quasi-hydrodynamic film formation or a microelastohydrodynamic effect such as proposed by Fein and Kreuz (ref. 57).

The decrease in carbonaceous debris in the presence of water or oxygen follows the Goldblatt model. Either water or oxygen "quenches" or ties up radical anions before they can react with the surface. The apparent greater effectiveness of water compared with oxygen in quenching the anions may be a concentration effect. The high solubility parameter of polyphenyl ethers indicates a high solubility

ORIGINAL PAGE IS
OF POOR QUALITY

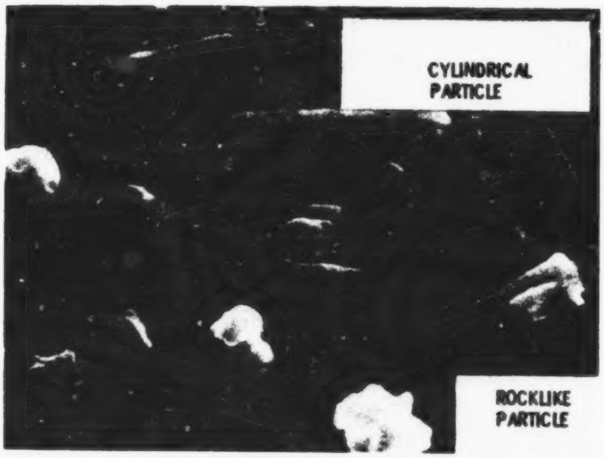

(a) Electron micrograph of carbonaceous wear debris.

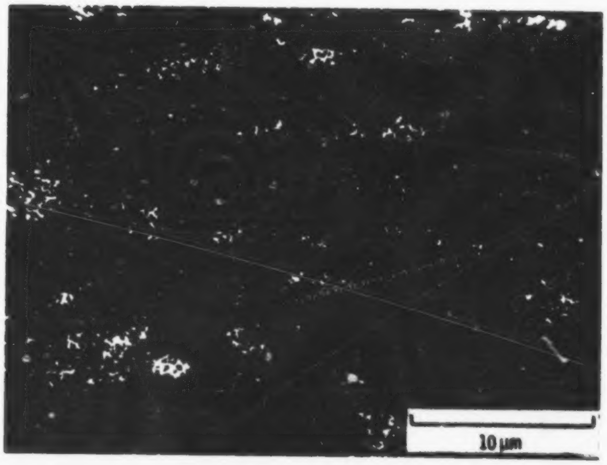

(b) Iron X-ray map.

Figure 69. - Electron micrograph of carbonaceous wear debris and iron X-ray map of same area.

for water but a low solubility for the fixed gases, such as oxygen (ref. 70). The Goldblatt model is more thoroughly discussed in the Models section.

Adhesive Wear Debris

The generation of wear particles by an adhesion mechanism has been proposed by many investigators (refs. 31 and 71). This mechanism is operative when the boundary film fails and metal-to-metal junctions are formed. Relative motion then causes the welded junction to shear. Material is transferred from one surface to another and is subsequently removed during the sliding process.

Suh (ref. 72) has proposed a wear mechanism based on dislocation theory. It involves the formation of subsurface voids, crack propagation between the voids, and the subsequent shearing of this material to form a sheetlike wear particle. This sheetlike particle may then be broken into smaller particles or may be rolled into a larger particle during the sliding process. Many of the particles observed in this study which have been referred to as adhesive wear do appear as sheets.

Figure 70 is a photomicrograph of a portion of a wear scar from one of the experiments in this study. It was taken with the Ferroscope by utilizing an interference contrast technique. It appears that a thin layer of material was generated on the surface. This layer may have been related to the often mentioned but little understood white or nonetching wear transformation layer (ref 73) and may have been the source of so-called adhesive wear particles. In fact, there is an area in the center of the photograph where some of this layer was stripped off. The vertical resolution in this photograph is about 5×10^{-8} m (500 Å).

Cutting Wear Debris

Another common wear mode is cutting. This type of wear results when a hard particle or surface plows out a softer surface. It is

ORIGINAL PAGE IS
OF POOR QUALITY

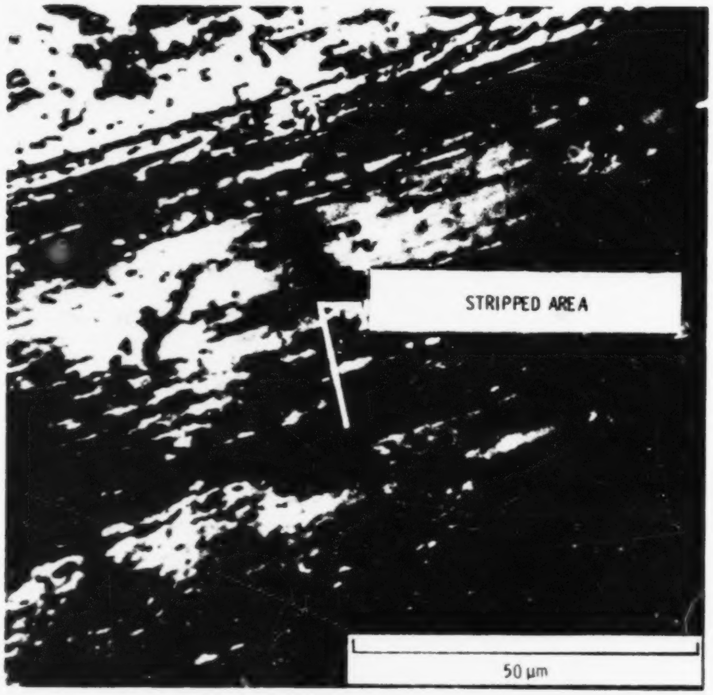

Figure 70. - Photomicrograph of wear scar obtained from interference contrast system. Lubricant, 5P-4E, specimen material, M-50 steel; temperature, 100 °C; test atmosphere, nitrogen (relative humidity, 50 percent).

also often referred to as abrasive wear. Loose work-hardened wear particles are no doubt present in the fluid during the test. However, Scott, Seifert, and Westcott (ref. 74) were unable to reproduce cutting wear particles by adding abrasive particles (sand) to lubricants. A possible explanation for this type of debris could be a micromachining process caused by work-hardened particles adhering to the rider prow. Another possibility may be hard inclusions in the metal itself, such as carbides. The increased generation of cutting wear particles in wet atmospheres may have been caused by the formation of abrasive oxides under these conditions.

Spherical Debris

Many investigators have noted the occurrence of spherical particles in bearing and friction and wear tests. Scott and Mills (ref. 75) observed metallic spheres during microscopic examination of bearing fatigue surfaces. They felt that the spheres are formed by a deformation process within propagating fatigue cracks.

The spheres observed in this study appeared as free metal in the bichromatic system (i.e., they appeared red). Energy-dispersive x-ray analysis confirmed their metallic content. These spheres may have been generated by a fatigue related process. Certainly, fatigue under sliding conditions has been demonstrated by a number of investigators. However, the number of stress cycles generated in the wear tests of this study was very low (generally less than 2500). And it is probable that the disk surface was worn away before crack propagation could occur. Nevertheless, spheres were always observed under moist test conditions and rarely in dry atmospheres. An electron micrograph of some typical spheres appears in figure 71.

Occasionally some severe (large) wear particles (diam >30 μm) were observed in the Ferrograms. These particles may have been the result of processes such as surface fatigue or surface fracture. However, they were only rarely encountered and did not appear to be a major component in the wear processes of this study.

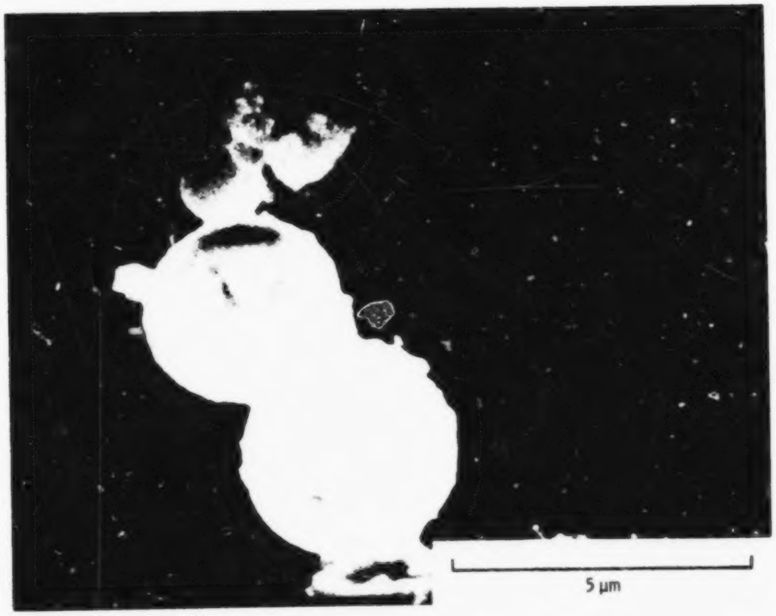

Figure 71. - Spherical particles.

ORIGINAL PAGE IS
OF POOR QUALITY

Summary of Ferrography Results

The major results of the Ferrographic analysis of the wear debris generated by a five-ring polypheryl ether in boundary lubrication experiments may be summarized as follows:

1. In dry nitrogen (where high wear occurred) large quantities of carbonaceous organometallic wear debris were observed; this debris consisted of either cylindrical or rocklike particles. The amount of the debris increased with increasing test temperature.

2. In dry air (where lower wear occurred) smaller amounts of the carbonaceous debris were observed.

3. In wet atmospheres (air and nitrogen, where the lowest wear occurred) very little carbonaceous debris was generated. However, under these conditions, some spherical and a few severe (large) wear particles were observed.

4. Adhesive and cutting wear debris were observed under all conditions. However, the cutting debris appeared to be more prevalent in wet atmospheres (particularly wet air).

5. Therefore, it appears that a corrosive wear mechanism is operative with the polyphenyl ether under dry inert conditions. The presence of moisture (and to a lesser extent oxygen) inhibits this corrosive action. These observations are in accord with the radical anion wear model proposed by Goldblatt for polynuclear aromatics.

THIOETHER RESULTS

Ferrographic analysis of thioether lubricant samples from the boundary lubrication tests yielded similar results as 5P-4E. Some of these results are illustrated in figures 72 (a) and (b).

Under dry nitrogen conditions (fig. 72(a)), a large amount of friction polymer debris is evident. Some in the form of rocklike chunks, some as cylindrical rolling pins, and some as translucent patches. In contrast, under dry air conditions (fig. 72) very little friction polymer is observed. Most of the debris is in the form of normal rubbing wear particles.

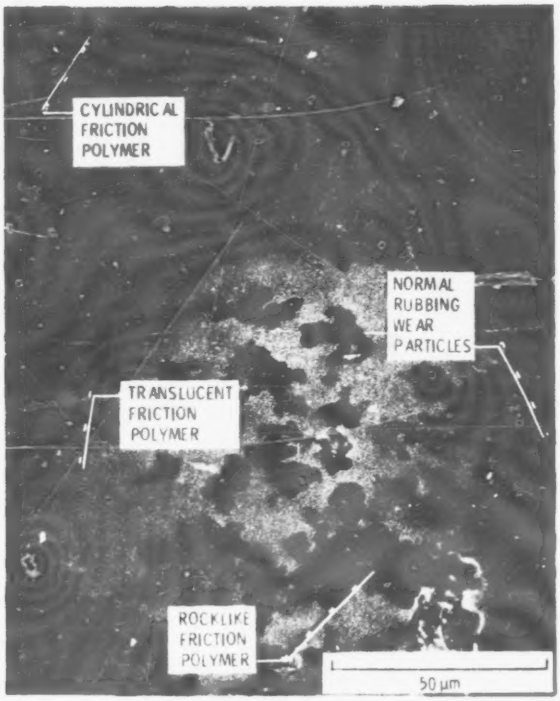
CYLINDRICAL FRICTION POLYMER
NORMAL RUBBING WEAR PARTICLES
TRANSLUCENT FRICTION POLYMER
ROCKLIKE FRICTION POLYMER
50 µm

(a) Dry nitrogen (ferrogram position, 53.4 mm).

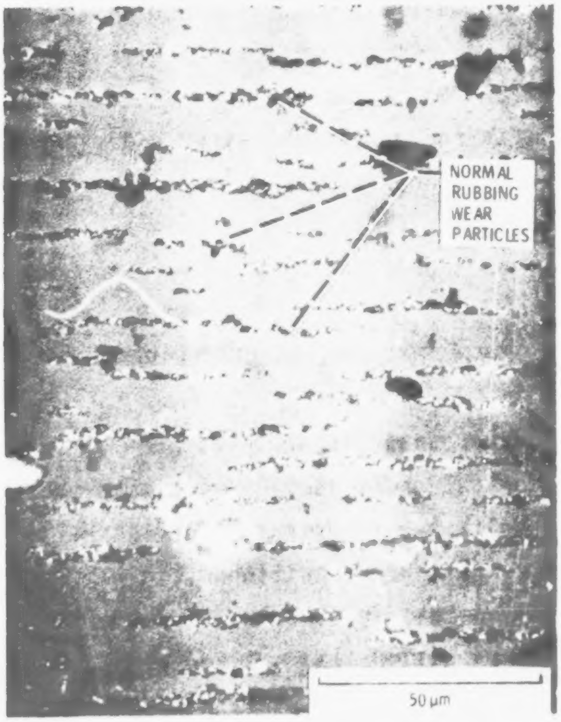

(b) Dry air (ferrogram position, 55 mm).

Figure 72. - Photomicrograph of wear debris generated by a thioether at 100 $^{\circ}$C.

INAL PAGE IS
F POOR QUALITY

THERMAL STABILITY

BACKGROUND

It is unfortunate that the literature is often not explicit concerning the term "thermal stability." It is sometimes used interchangeably with thermal-oxidative stability. However, the proper definition is reserved for processes occurring in the absence of oxygen.

Mechanism

In the case of hydrocarbons and most other fluid classes, thermal decomposition or pyrolysis proceeds through a free-radical chain reaction process yielding many products. Free radicals are organic fragments containing an unpaired electron. These radicals are produced by homolysis (breaking) of C-C bonds. These radicals can be generated by radiation, mechanical processes, and thermal energy (ref. 76).

The production of free radicals from a hydrocarbon by a thermal process is illustrated in equation (6)

$$R\text{-}CH_2\text{-}CH_3 \rightarrow R\cdot + R\text{-}CH_2\text{-}\dot{C}H_2 + R\text{-}\dot{C}H\text{-}CH_3 \qquad (6)$$

These radicals are highly reactive and start reaction chains by abstracting hydrogen atoms (H) from the parent hydrocarbon. The chainlike reaction arises from a simple mathematical principle - the sum of an even plus an odd number is always an odd number. When a radical (odd number of electrons) attacks a nonradical (even number of electrons) one of the resulting species must have an odd number of electrons. Therefore, it is a radical itself and also capable of attacking a nonradical. Attack by this second radical (possibly different than the initial radical) will produce a third radical. Abstraction reactions are illustrated in equation (7).

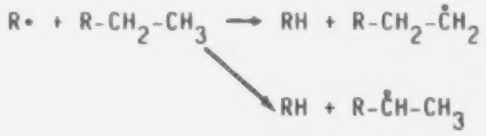

$$R\cdot + R\text{-}CH_2\text{-}CH_3 \rightarrow RH + R\text{-}CH_2\text{-}\dot{C}H_2$$
$$\searrow RH + R\text{-}\dot{C}H\text{-}CH_3 \qquad (7)$$

This chain sequence will continue until the radicals are destroyed or all of the reactants are consumed. Hence, a single radical can bring about changes in thousands of molecules. Radicals may be destroyed by recombination (eq. (8))

$$R\cdot + R\cdot \rightarrow R\text{-}R \qquad (8)$$

or through disproportionation reactions (transfer of an atom from one radical to another) as in equation (9).

$$R\cdot + H\text{-}CH_2\text{-}\dot{C}H_2 \rightarrow RH + CH_2 = CH_2 \qquad (9)$$

Radical themselves may also fragment producing new radicals and unsaturated species (eq. 10)).

$$R\text{-}CH_2\text{-}\dot{C}H_2 \rightarrow R\cdot + CH_2 = CH_2 \qquad (10)$$

These reactions occur in industrial "cracking."

Although higher molecular weight products may be produced in this series of reactions, the most general change in properties of the lubricant is an increase in the vapor pressure of the system. This is brought about by cleavage of large molecules into smaller, more volatile, gaseous fragments. This gaseous evolution can be utilized to quantitate the thermal stability of organic compounds.

Arrhenius Rate Law

The rate of thermal decomposition usually varies with temperature according to the empirical Arrhenius rate law (ref. 77) as shown in the following equation:

$$k = Ae^{-E/RT} \qquad (11)$$

where k is the rate constant, A is the frequency factor or preexponential factor, E is the activation energy, R the gas constant, and T the absolute temperature. According to this equation, a straight line should be obtained when log k is plotted as a function of the reciprocal of the absolute temperature. It has been shown (ref. 77) that for most organic compounds log dp/dt versus $1/T$ is also a straight line. Then, by analogy,

$$\frac{dp}{dt} = A'e^{-E'/RT} \tag{12}$$

Using this equation, one can define the rate constant for thermal decomposition by measuring the isothermal rate of vapor pressure rise at several temperatures. However, it is more convenient to have a single parameter for thermal decomposition rather than to tabulate values of A' and E' which actually define the rate constant.

Therefore, an arbitrary thermal decomposition temperature (T_D) is defined as the temperature at which the isothermal rate of vapor pressure rise is 1.85 Pa/sec (50 torr/hr). Then, the decomposition points for a series of organic compounds are the temperatures at which all have identical isothermal rates of vapor pressure rise. This is the technique used in the standard test method (ASTM D2879) (ref. 78) for measuring the initial decomposition temperature of liquids. This test uses a constant volume device (the isoteniscope) which can also be used to measure vapor pressure as a function of temperature.

Tensimeter

An automated device (the tensimeter), based on the same principle, also yields thermal decomposition temperatures and vapor pressure data. A schematic representation of the tensimeter appears in figure 73.

The sample cell assembly is shown in figure 74. The sample cell is made of ordinary borosilicate glass and has a volume of about 5 ml (5×10^{-6} m^3). Three to 4 ml (3×10^{-6} to 4×10^{-6} m^3) of test fluid are

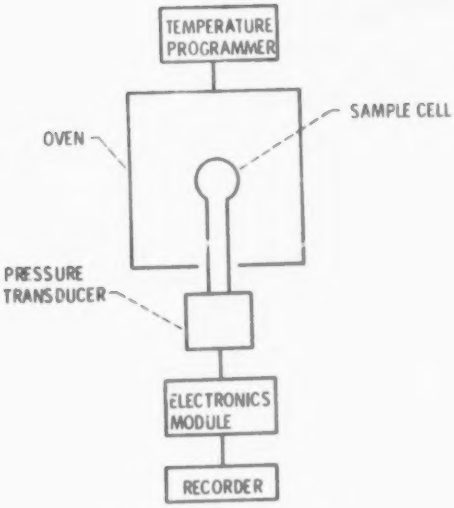

Figure 73. - Recording tensimeter.

ORIGINAL PAGE IS
OF POOR QUALITY

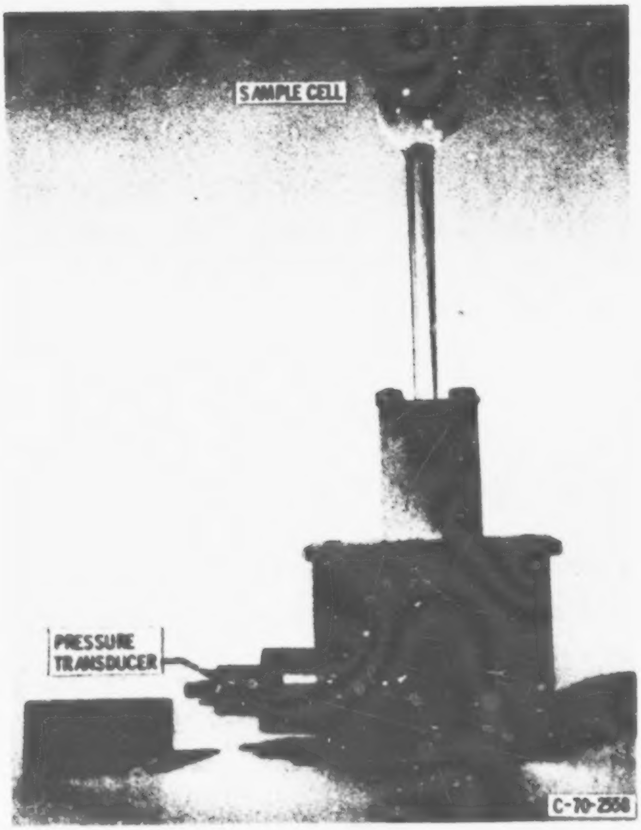

Figure 74. - Sample cell assembly.

placed in the sample cell. The sample is then degassed and refluxed under a vacuum. The cell is placed in a temperature-programmed oven and heated to an initial temperature about 50 °C below the suspected decomposition temperature. After a 5-min stabilization period, the increase in vapor pressure, if any, is recorded as a vertical bar during a fixed time interval. Then the programmer automatically raises the temperature by a preset amount (usually 5 °C) and the same process is repeated. A typical thermal decomposition curve for a synthetic hydrocarbon is shown in figure 75.

This is a plot of the logarithm of the isothermal rate of vapor pressure increase as a function of reciprocal absolute temperature. A straight line is drawn connecting the tops of the recorded bars. The intersection of this line with the temperature axis is the T_D. In addition, the activation energy for decomposition (E') can be calculated from the slope of this line.

Useful Lives

From a knowledge of the T_D and E', a useful life of a lubricant (in the absence of oxygen) can be calculated from the following equation (ref. 77)

$$t = \frac{0.0285\ T_D}{MW} \log\left(\frac{100-x}{100}\right) \text{antilog}\left[5 - 219\ E'\left(\frac{1}{T_D} - \frac{1}{T}\right)\right] \qquad (13)$$

where t is time, MW is molecular weight, and x is the percent decomposition at temperature T. The useful life is typically defined as the time in hours required for 10 percent decomposition. A plot of useful lives for several lubricants appears in figure 76.

Generalizations

Blake at al. (ref. 77) reported on the thermal decomposition of a variety of different chemical structures. From their data and

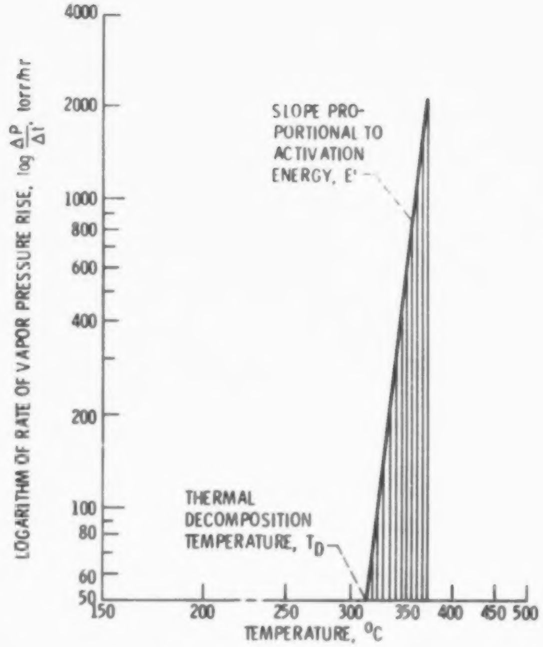

Figure 75. - Typical thermal decomposition curve, logarithm of rate of vapor pressure rise as function of reciprocal of absolute temperature. Heating interval, 5 °C lubricant; synthetic hydrocarbon.

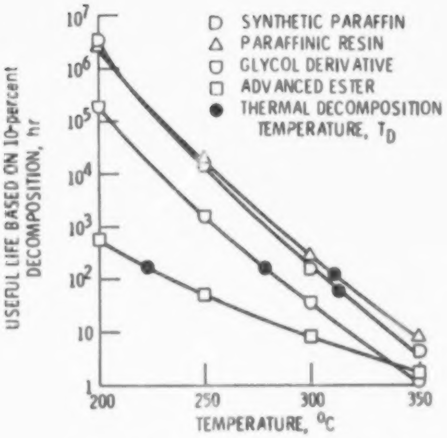

Figure 76. - Useful life (based on 10-percent decomposition) of four lubricants in nitrogen as function of temperature.

that of others (refs. 9 and 70) one can make the following generalizations:

(1) The maximum thermal stability of a straight chain hydrocarbon or other compounds containing such groups is about 350 °C.

(2) Branched chain hydrocarbons are less stable than straight chain hydrocarbons due to steric effects and the fact that free radicals of greater stability are formed.

(3) Aromatic bonds (C-H and C-C) have higher dissociation energies due to resonance and therefore these compounds are much more stable than their aliphatic analogs. Maximum stabilities of this class approach 450 °C.

(4) Esters of alcohols having β-hydrogens decompose through a low energy transition state with maximum T_D's near 280 °C.

(5) Esters not containing β-hydrogens have the low energy reaction path blocked and therefore exhibit stabilities approaching hydrocarbons (320 to 340 °C).

(6) Substitutions on an aromatic ring decrease its stability. Increasing the number of substituents continually decreases stability. Increasing the chain length also decreases stability until it approaches that of aliphatic hydrocarbons.

(7) Saturated ring compounds are more stable than their straight chain analogs.

(8) Completely replacing hydrogen with fluorine sometimes increases the thermal stability of an organic compound (some exceptions are aromatics and esters).

Bond Dissociation Energy

These generalizations arise from the fact that thermal decomposition occurs at the weakest link in the compound. Therefore, thermal decomposition should be a function of the weakest bond dissociation energy (E_{DIS}) in that compound. Table 10 tabulates T_D and E_{DIS} values for a variety of compounds. The thermal decomposition temperature is then plotted as a function of the bond dissociation energy in figure 77. Here the general trend of increasing T_D with

TABLE 10. - THERMAL DECOMPOSITION TEMPERATURES AND BOND DISSOCIATION ENERGIES FOR VARIOUS COMPOUNDS

Compound	Bonds	E_{DIS},[a] kJ/mole	T_D, °C
Octacosane	C-C	337	350
11-ethyl-11-methyl pentacosane	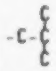 $-C-\underset{\underset{\displaystyle C}{\vert}}{\overset{\overset{\displaystyle C}{\vert}}{C}}$	314	331
p-quartaerphenyl	φ-φ	432	454
Polyphenyl ether (5P-4E)	φ-Oφ	423	443
p-bis(*p*-chlorophenoxy) benzene	φ-Cl	419	409
p-bis(p-bromophenoxy) benzene	φ-Br	335	387
Fluorinated polyether	CF_3-CF_3	406	390
Synthetic paraffin	C-C	337	314
Alkylated benzene	φ-C-CH	335	340

[a] From ref. 79

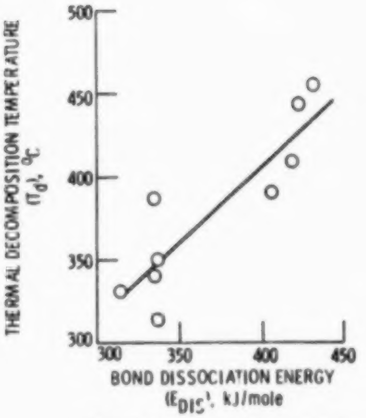

Figure 77. - Thermal decomposition temperature (T_d) as a function of bond dissociation energy (E_{DIS}).

increasing t_{DIS} is apparent. Since bond length is inversely related to bond strength, it can also be correlated with thermal decomposition temperature. Figure 78 contains a plot of T_D versus the reciprocal of bond length for a series of aromatic compounds of the type $(C_6H_5)_nM$ where M is a Group V element. Here the correlation is much better than in figure 77 since the compounds are structurally very similar except for the central atom.

A compilation of a number of T_D's for various chemical classes are tabulated in table 11.

AROMATIC TIN AND SILICON COMPOUNDS

As previously discussed in the Boundary Lubrication section another class of potential high temperature fluids are the organometallics. Two fluids from this class, a diphenyl tin and a diphenyl silicon compound yielded friction and wear results comparable to 5P-4E and the thioether.

In this section, the thermal stabilities of a series of diphenyl tin and silicon compounds with varying substituents will be addressed. The tensimeter, previously described, was used for these studies.

Results and Discussion

Table 12 lists the thermal decomposition results for both the organotin and organosilicon series of compounds. Both meta- and para-linked compounds have been included, and their general chemical structures are illustrated in figure 1(e).

Emphasis was placed on the meta-linked compounds for two reasons. First, from theoretical considerations, the meta-linked compounds should be more thermally stable than their para-analogs. Thermal decomposition usually proceeds by means of free radicals. If the potential free radical cannot by stabilized by resonance, it will be more difficult to form than one which is stabilized. This stabilization is not possible with meta-linkages. Second,

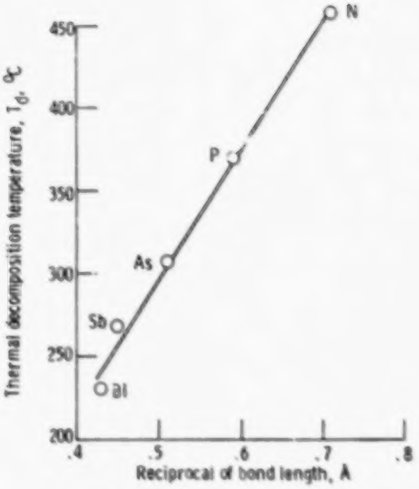

Figure 78. - Thermal decomposition temperature (T_d) as a function of the reciprocal bond length for a series of group V aromatic compounds of the type $(C_6H_5)_nM$ (ref. 77).

TABLE 11. - THERMAL DECOMPOSITION TEMPERATURES FOR VARIOUS CLASSES OF LIQUID LUBRICANTS

Chemical class	T_D, °C
Dibasic acid esters	
Di-2-ethylhexyl sebacate	283
Polyol esters	
Trimethyolpropane triheptanoate	315
Synthetic alkyl hydrocarbons	315
Superrefined mineral oils	330
Synthetic alkyl aromatics	340
Fluorinated polyether (HFPO)	354
Thioether	390
Polyphenyl ether (3P-2E)	407
(4P-3E)	446
(5P-4E)	466
(6P-5E)	457
(7P-6E)	449

TABLE 12. - THERMAL DECOMPOSITION TEMPERATURES (FROM ISOTENISCOPE) FOR VARIOUS ORGANOTIN AND ORGANOSILICON COMPOUNDS

Type of compound	Substituent[a]								
	Methyl	Ethyl	n-propyl	n-butyl	hexyl	n-octyl	2-Ethyl hexyl	Phenyl	Neopentyl
	Thermal decomposition temperature (from isoteniscope) T_D, °C								
Meta-trialkylstannyl	[b]230	--	[b,c]236	236	[b]236	--	[b]260	--	[b]283
Para-trialkylstannyl	---	- -	[b]240	[b]240	--	---	---	[b]297	---
Meta-trialkylsilyl	278	[b]296	276	295	[b]300	358	---	---	---
Para-trialkylsilyl	[b]311	---	--	[b]320	--	---	--	---	---

[a] Substituents given in order of increasing steric hindrance.

[b] Value corrected for dilution effects (compound was mixed with 4P-3E to produce a 20 to 50 vol % concentration).

[c] Value for 3,3,' disubstituted derivative was 214 °C

meta linkages produce a more asymmetrical molecule, which should reduce the melting points and thus produce a greater liquid range.

A minimum quantity of 3 to 5 cm^3 of fluid is required for each thermal decomposition test. If a compound was a solid at room temperature or was available only in small quantities, a mixing procedure had to be utilized. The compound was mixed with 4P-3E to produce a concentration of 20 to 50 vol %. 4P-3E had a thermal decomposition temperature (T_D) of about 450 °C. Therefore, any decomposition taking place below this temperature must be attributed to the tin or silicon compound. However, there is a dilution effect which causes a small error (approximately 7 percent) in the T_D measurement. The amount of the error was determined by checking the T_D of a standard fluid mixed with the polyphenyl ether. The fluids tested as mixtures are noted in table 12 and their corrected T_D values are given. In general, the reproducibility of T_D values for pure compounds is better than ±5 °C. However, the T_D values for the mixtures may vary by ±10 °C.

The substituents in table 12 are listed in order of increasing steric hindrance. As can be seen, the thermal stability generally increases with increasing steric hindrance (i.e., increasing size of the substituent groups). This is somewhat surprising, since steric crowding usually causes a decrease in thermal stability (ref. 77). A possible explanation could be that if vibrational energies are evenly distributed over the entire molecule, a higher energy (i.e., higher temperature) would be required to rupture the same bond in a larger molecule than in a smaller one.

It is apparent that the steric factor does not influence the T_D in a linear fashion. Much greater changes in T_D occur in the latter part of the series (n-hexyl to neopentyl) than in the initial part (methyl to n-hexyl). An example from the literature may serve to illustrate this nonlinear effect on reaction rates. Dostrovsky and Hughes (ref. 80) have shown that the rate of basic ethanolysis of alkyl bromides decreases enormously with the increasing bulk of groups attached to the carbon atom under attack. The reaction is

$$C_2H_5OH + RBr \rightarrow Br + \text{product} \qquad (14)$$

Table 13 shows the relative reaction rates as the size of the R group increases. Again the greatest effect occurs with the bulky neopentyl group.

A second interesting observation from table 12 is that the para-compounds do not appear to be less stable than their meta-analogs. Within experimental error their thermal stabilities appear to be essentially the same. Apparently resonance stabilization of decomposition products is not an important factor with the compounds studied here.

The highest thermal stability attained in the tin series was 297 °C with the para-phenyl derivative. In the silicon series, the meta n-octyl derivative yielded the highest T_D (358 °C). One disubstituted compound (3,3'bis(tri-n-propyl-tin)biphenyl) was synthesized and found to be less thermally stable (T_D = 214 °C) than the monosubstituted derivative (T_D = 236 °C).

SUMMARY OF RESULTS

Thermal decomposition temperatures were determined for a number of organotin and organosilicon compounds.

(1) The maximum thermal decomposition temperatures obtained in the silicon and tin series were 358 °C and 297 °C, respectively.

(2) Increasing the steric hindrance (i.e., increasing the size of the substituent groups) around the silicon or tin atoms increased the thermal stability in both series.

OXIDATION STABILITY

BACKGROUND

The oxidation of an organic compound with molecular oxygen is usually referred to as autoxidation. As was the case with thermal decomposition, oxidation usually proceeds through a free radical chain mechanism (ref. 81). However, with the additional participant

TABLE 13. - RELATIVE REACTION RATES FOR BASIC ETHANOLYSIS OF ALKYL BROMIDES (R-Br) AS FUNCTION OF SIZE OF ALKYL GROUP (R)

[Data from ref. 80.]

Alkyl group	Reaction rate relative to that of methyl group
Methyl	1.0
Ethyl	5.7×10^{-2}
n-propyl	1.6×10^{-2}
Isobutyl	1.7×10^{-3}
Neopentyl	2.4×10^{-7}

(oxygen) the reactions can become exceeding complex. The importance of hydroperoxides in the oxidation process was shown by Criegee (ref. 82).

Mechanism

The liquid-phase oxidation of organic compounds and liquid lubricants has been studied by many investigators. In general, the basic mechanism is thought to proceed as follows (ref. 83).

$$In_2 \xrightarrow{R_1} 2\ In\cdot \qquad \text{Initiation} \qquad (15)$$

$$In\cdot + RH \rightarrow InH + R\cdot \qquad (16)$$

Here an initiator (In) produces free radicals (In•) at reaction rate (R_1) which abstracts a proton from the hydrocarbon and produces an alkyl free radical (R•). This highly reactive species reacts with oxygen in the propagation step of the chain reaction:

$$R\cdot + O_2 \rightarrow RO_2\cdot \qquad \text{Propagation} \qquad (17)$$

This propagation step produces a peroxy radical ($RO_2\cdot$) which, in turn, reacts with the parent hydrocarbon (RH) to produce a hydroperoxide (RO_2H).

$$RO_2\cdot + RH \xrightarrow{k_p} RO_2H + R\cdot \qquad (18)$$

This reaction regenerates an alkyl free radical (R•) which propagates the chain.

The chain reaction can be terminated by radical coupling of two peroxy radicals ($RO_2\cdot$)

$$2RO_2\cdot \xrightarrow{2k_t} RO_4R \qquad \text{nonradical products} \qquad (19)$$

or by cross termination of an alkyl radical (R•) and a peroxy radical ($RO_2\bullet$).

$$R\bullet + RO_2\bullet \rightarrow RO_2R \tag{20}$$

The third possibility is the termination reaction of two alkyl radicals (R•).

$$2R\bullet \rightarrow R - R \tag{21}$$

Rate Equations

For normal oxygen concentrations where $[RO_2\bullet] >> R\bullet$, reactions (20) and (21) can be neglected. Therefore, the rate of oxidation of hydrocarbon R-H can be expressed as

$$\frac{-d[R-H]}{dt} = k_p[R-H]\left(\frac{R_1}{2k_t}\right)^{1/2} \tag{22}$$

The rate of oxidation is then directly proportional to the hydrocarbon concentration and the square root of the rate of chain initiation. This relationship is illustrated in figure 79. This shows the rate of oxidation of ethyl linoleate (initiated by benzoyl peroxide) as a function of its concentration. For other types of chain termination, different rate of consumption equations will be obtained.

Oxidizability

The ratio $k_p/(2k_t)^{1/2}$ which appears in equation (22) is referred to as the oxidizability. For a specific rate of initiation, the autoxidation of a hydrocarbon (R-H) is then determined by the values of k_p and k_t. The rate of chain propagation (k_p) can be estimated if the bond energy for the weakest C-H bond is known. The termination rate constant k_t can also be estimated. Thus, in

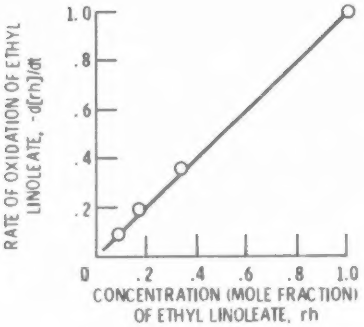

Figure 79. - Oxidation rate as a function of concentration for ethyl linoleate (ref. 81).

theory, the oxidizability should be predictable for any pure hydrocarbon. Table 14 (ref. 83) contains a list of oxidizabilities for various hydrocarbons. This list illustrates the wide range of oxidation rates for different hydrocarbon structures.

However, this simple relationship (eq. (22)) breaks down at high conversions (>20 percent). Complications are caused by the accumulation and reaction of secondary products such as aldehydes and ketones.

Chain Initiation

As mentioned earlier, chain initiation can be effected by the deliberate addition of an initiator. Typical initiators are azo compounds and peroxides. This circumvents the long and sometimes irreproducible induction periods (time before oxygen absorption begins).

Initiation can also take place by direct reaction with oxygen:

$$RH + O_2 \rightarrow R\cdot + HO_2\cdot \tag{23}$$

However, this reaction is thermodynamically and kinetically unfavorable. Initiation in the absence of added initiators is probably due to peroxidic impurities.

However, a common source of free radicals is the thermal decomposition of the alkyl hydroperoxides, producing an alkoxy and a hydroxy radical:

$$RO_2H \rightarrow RO\cdot + \cdot OH \tag{24}$$

These radicals can then react with the parent hydrocarbon (RH)

$$RO\cdot + RH \rightarrow ROH + R\cdot \tag{25}$$

$$\cdot OH + RH \rightarrow HOH + R\cdot \tag{26}$$

TABLE 14. - OXIDIZABILITY OF VARIOUS ORGANIC COMPOUNDS

[From ref. 83.]

Substrate	$k_p/(2k_t)^{1/2} \times 10^3 (M^{-1/2} sec^{-1/2})$
2,3-Dimethyl-2-butene	3.2
Cyclohexene	2.3
1-Octene	.06
Cumene	1.5
Ethylbenzene	.21
Toluene	.01
p-Xylene	.05
Benzaldehyde	290
Benzyl alcohol	.85
2,4,6-Trimethylheptane	.09

producing water, alcohols, and alkyl radicals. These reactions are referred to as chain branching.

Chain Propagation

As indicated, the reaction of an alkyl radical (R•) and O_2 (in itself a biradical) proceeds very rapidly. The rate controlling step is then hydrogen abstraction by the alkylperoxy radical in equation (18).

The alkylperoxy radicals (RO_2•) are more stable than the alkyl radicals (R•). They are quite persistent and selective. They preferentially abstract only the most labile hydrogen atom (weakest C-H bond). A group of H-bond energies appears in Table 15 (ref. 83).

It is obvious that phenols, thiols, aromatic amines, and phosphines have the most labile hydrogen atoms. It is also clear that the relative attack for primary, secondary, and tertiary bonds should be in the order: tertiary (90 kcal) > secondary (94 kcal) > primary (103 kcal). Indeed, this has been shown to be the case for 2-methylpentane where the order is 300:30:1, for tertiary, secondary, and primary bonds, respectively.

The propagation rate is also dependent on the type of hydrogen abstracting alkylperoxy radical. In order to correlate rates with C-H bond energies, rate constants for a series of hydrocarbons (R-H) should be compared for the same alkylperoxy radical.

Table 16 (ref. 83) shows rate constants for a series of hydrocarbons against their own peroxy radicals (k_p) and against t-butylperoxy radicals (k'_p).

Obviously, reactivities are very structurally dependent. For example, the benzoylperoxy radical is 40 000 times more reactive than the t-butylperoxy radical toward benzaldehyde. Comparing only C-H bond energies (table 15) would lead one to conclude that aldehydes and alkylaromatic compounds would oxidize at similar rates. However, aldehydes oxidize at appreciably greater rates than the alkylaromatics due to the strong electron withdrawing effect of the carbonyl group.

TABLE 15. - X-H BOND

ENERGIES

[From ref. 83.]

Compound	Energy kcal/mol
CH_3-H	103
n-C_3H_7-H	99
i-C_3H_7-H	94
t-C_4H_9-H	90
CH_2=CH-H	105
C_6H_5-H	103
CH_2=CH-CH_2-H	85
PhCH_2-H	85
RCO-H	86
CH_3S-H	88
CH_3PH-H	85
PhO-H	88
PhNH-H	80
ROO-H	90

TABLE 16. - RATE CONSTANTS PER LABILE HYDROGEN FOR REACTION OF SUBSTRATES WITH THEIR OWN PEROXY RADICALS (k_p) AND WITH tert- BUTYLPEROXY RADICALS (k_p') AT 30 °C

[From ref. 83.]

Substrate	k_p ($M^{-1}sec^{-1}$)	k_p' ($M^{-1}sec^{-1}$)	k_p/k_p'
1-Octene	0.5	0.084	6.0
Cyclohexene	1.5	.80	1.9
Cyclopentene	1.7	.85	2.0
2,3-Dimethyl-2-butene	1.14	.14	1.0
Toluene	.08	.012	6.7
Ethylbenzene	.65	.10	6.5
Cumene	.18	.22	.9
Tetralin	1.6	.5	3.2
Benzyl ether	7.5	.3	25.0
Benzyl alcohol	2.4	.065	37.0
Benzyl acetate	2.3	.0075	307
Benzyl chloride	1.50	.008	190
Benzyl bromide	.6	.006	100
Benyl cyanide	1.56	.01	156
Benzaldehyde	33 000	.85	40 000

Chain Termination

As previously mentioned, the normal termination reaction is

$$2RO_2\cdot \rightarrow RO_4R \qquad (19)$$

which is a tetroxide.

The decomposition of tetroxides is also highly dependent on the nature of the R-group. For example, secondary and primary alkylperoxy radicals undergo disproportionation to an alcohol and a ketone.

$$RO_4R \rightarrow R_2CO + R_2CHOH + O_2 \qquad (27)$$

Tert-alkylperoxy radicals yield a different mechanism resulting in the formation of dialkyl peroxides and O_2. The dialkyl peroxides undergo further decomposition. Therefore, primary and secondary alkylperoxy radicals yield much higher termination rates than tert-alkylperoxy radicals.

The oxidation rate of a hydrocarbon is determined by both the propagation rate (k_p) and the termination rate (k_t) as indicated in equation (22). This illustrates why a reactive hydrocarbon such as toluene (C_6H_5-CH_2H), which has a C-H dissociation energy of only 85 kcal/mole, has a rather low autoxidation rate. This is due to the high termination rate of its primary alkylperoxy radicals.

Inhibition of Autoxidation

Autoxidations can be inhibited by the addition of scavengers which break the chain reaction by forming stable free radicals:

$$RO_2\cdot + XH \rightarrow RO_2H + X\cdot \qquad (28)$$

An example is in the use of substituted phenols (2,6-di-t-butyl-4-methylphenol) that would yield stable phenoxyl radicals (ArO•) which are far less reactive than the $RO_2\cdot$ radical or the R• normally formed by hydrogen abstraction from the parent hydrocarbon.

A second type of inhibitor causes the destruction of hydroperoxides (RO_2H). Here the inhibitor (X) reacts with the hydroperoxide (RO_2H) yielding nonradical products.

$$RO_2H + X \rightarrow ROH + XO \qquad (29)$$

An example of this type of inhibitor is phenothiazine (PTZ).

Metal coaters (such as tricresylphosphate) can sometimes be considered as a third type of inhibitor. Here their action is to prevent catalytic effects by coating metal surfaces.

The effectiveness of a chain breaking inhibitor is dependent on two factors: (1) the reactivity or stability of the radical (X) formed from the inhibitor (X) and (2) the reaction rate of the peroxy radicals ($RO_2\cdot$) with the inhibitor (X). The reactivity of X is determined by the ratio of k_p/k_{30} of the following:

$$RO_2\cdot + RH \xrightarrow{k_p} RO_2H + R\cdot \qquad (18)$$

$$RH + X\cdot \xrightarrow{k_{30}} XH + R\cdot \qquad (30)$$

The lower this ratio, the greater the inhibition of the additive. If X• are completely inactive, k_p/k_{30} is very small and X is an excellent inhibitor. If X• is still capable of chain propagation, the chain reaction proceeds but at a lower rate.

The inhibitor's effectiveness is also a function of its rate of reaction with peroxy radicals (k_{28})

$$RO_2\cdot + XH \xrightarrow{k_{28}} RO_2H + X\cdot \qquad (28)$$

The higher this rate (k_{28}) the lower the concentration of inhibitor required to decrease the rate of oxidation by a certain factor. The effectiveness may be defined as k_{28}/k_s where k_s is the reaction rate for some inhibitor in reaction 28 taken as a standard.

Metal Catalysis in Oxidation

Metal catalyzed oxidations are either homolytic (one electron processes) or heterolytic (two electron processes). Homolytic catalysis usually involves soluble transition metal salts (homogeneous) such as napthenates of Co, Mn, Fe, and Cu, or the metal oxides (heterogeneous). Homolytic catalysis requires recycling of the metal species between several oxidation states by one electron change. In addition, free radicals are produced during this mechanism. An example of this type of catalysis is illustrated in the following equations.

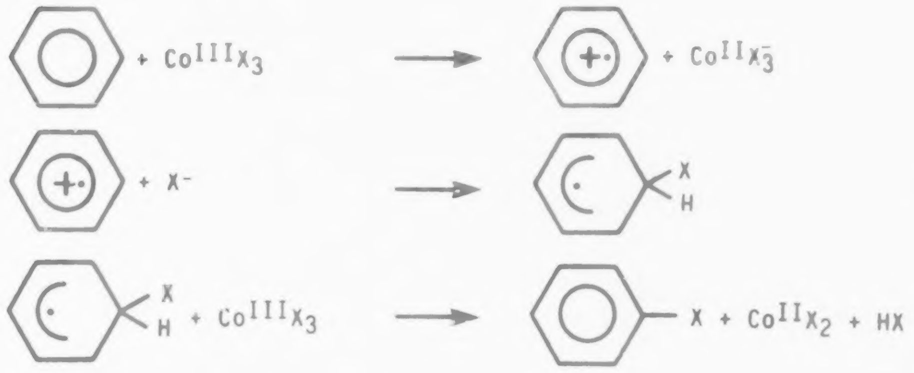

(31)

Although this is an oxidative substitution it does illustrate the homolytic process (i.e., the formation of free radicals and one electron transfer).

In contrast, heterolytic catalysis involves reactions of compounds coordinated to transition metals. The metal complex acts as a Lewis acid and undergoes two-equivalent changes. Free radicals are not involved. An example of this mechanism is shown here for another oxidative substitution.

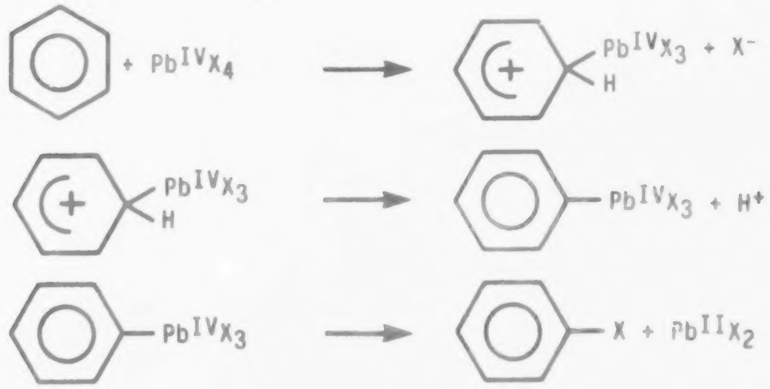

(32)

Catalysis of liquid phase autoxidations often proceed by homolytic decomposition of alkyl hydroperoxides. The rapid decomposition of these hydroperoxides in solutions containing iron, manganese, cobalt, and copper compounds is well known. The two basic reactions are:

$$RO_2H + M^{(n-1)+} \rightarrow RO\cdot + M^{n+} + HO^- \qquad (33)$$

$$RO_2H + M^{n+} \rightarrow RO_2\cdot + M^{(n-1)+} + H^+ \qquad (34)$$

Therefore, metal complexes catalyze autoxidations by generating chain initiating radicals (eqs. (33) and (34)). In addition, alkyl radicals ($R\cdot$) may be produced directly from the parent hydrocarbon.

$$RH + M^{n+} \rightarrow R\cdot + H^+ + M^{(n+1)+} \qquad (35)$$

$$M^{n+} + O_2 \rightarrow M^{(n+1)} + O_2^-\cdot \qquad (36)$$

Homogeneous and Heterogeneous Catalysis

The fundamental chemical processes occurring during oxidation are the same whether the process takes place in the coordination sphere of a soluble metal complex (homogeneous) or at an adsorbate-metal interface. The same mechanistic pathways are available to both kinds of catalysis. The local chemical structure of the active site is more important than the macroscopic features of a system, such as its physical state.

Chain Branching

From the introductory material it might appear that, at least for pure component systems, predictions of reaction rates and product distributions should be relatively easy to make. At sufficiently low temperatures (<100 °C) and low conversions (<10 percent) this is probably true for many simple hydrocarbon systems.

Above 100 °C there is an increasing tendency for the primary oxidation products (alkylhydroperoxides) (RO_2H) to decompose homolytically into alkoxy and hydroxy radicals as previously shown:

$$RO_2H \rightarrow RO\cdot + \cdot OH \tag{24}$$

These reactive species can further react with the parent hydrocarbon RH to produce more alkyl radicals.

$$RO\cdot + RH \rightarrow ROH + R\cdot \tag{25}$$

$$\cdot OH + RH \rightarrow HOH + R\cdot \tag{26}$$

These branching reactions can greatly accelerate the oxidation (autocatalysis) and complicate the reaction picture. Another complication is that the increased reaction rate may drive the system out of the kinetic region (i.e., into a region where oxygen diffusion becomes a limitation). Therefore, this must be taken into account in high-temperature oxidation.

EXPERIMENTAL METHODS

Reaction kinetics of liquid-phase oxidation processes must be studied in the kinetic region. That is, the reaction must not be oxygen diffusion limited. Most standard oxidation-corrosion tests developed in the past have been bulk tests. Air or oxygen is passed over a static fluid, bubbled through the fluid or over a constantly agitated fluid. An example of a macro-oxidation cell is shown in figure 80.

Oxygen Diffusion

Oxygen transport into the liquid-phase involves three processes.

(1) Diffusion of oxygen in the gas phase to the liquid-gas interface.

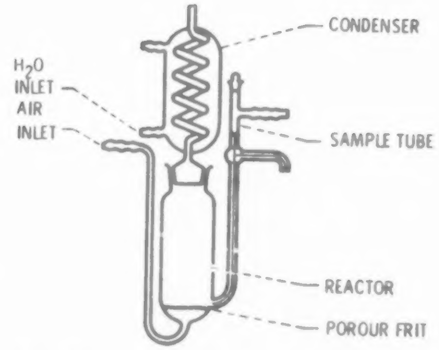

Figure 80. - Typical macro-oxidation cell (ref. 81).

(2) Dissolution of oxygen into the liquid at the gas-liquid interface.

(3) Diffusion of the dissolved oxygen into the liquid phase. Process (1) is very rapid and not a limiting factor. Process (2) is related to the partial pressure of oxygen and Henry's law constant. Process (3) depends on the interfacial surface area, rate of agitation, and the oxygen concentration gradient. Basically, to determine if oxygen diffusion is a problem, the amount of fluid or oxygen can be varied and agitation rates can be changed. If the rate of oxidation is altered, then the reaction is not taking place in the kinetic region.

Microtests

Because of diffusion problems, many investigators have designed new experiments involving small quantities of fluid. A number of thin film tests have been developed. One of the most successful is that developed by Klaus and his coworkers (ref 84).

This test is illustrated in figure 81.

Basically, a very small quantity of lubricant (40 to 100 μl) is injected onto the surface of a catalyst after the entire apparatus has been equilibrated at test temperature. A constant flow of air is maintained through the air entry tube. Volatile oxidation products can be trapped for analysis. At the conclusion, which could be a few minutes or a few hours, depending on test temperature, the apparatus is removed from the oven or bath and quenched to room temperature.

Then, the degraded lubricant remaining on the catalyst surface is dissolved in an appropriate solvent. This solution can then be analyzed by a variety of techniques. From this analysis, a rate of oxidation can be determined.

This apparatus has a number of advantages. It is simple, requires little test sample, has good reproducibility, and test durations are not long. Surface area is also constant and does not vary during the test. An infinite variety of catalysts can be studied and each can be recycled. However, there are some drawbacks.

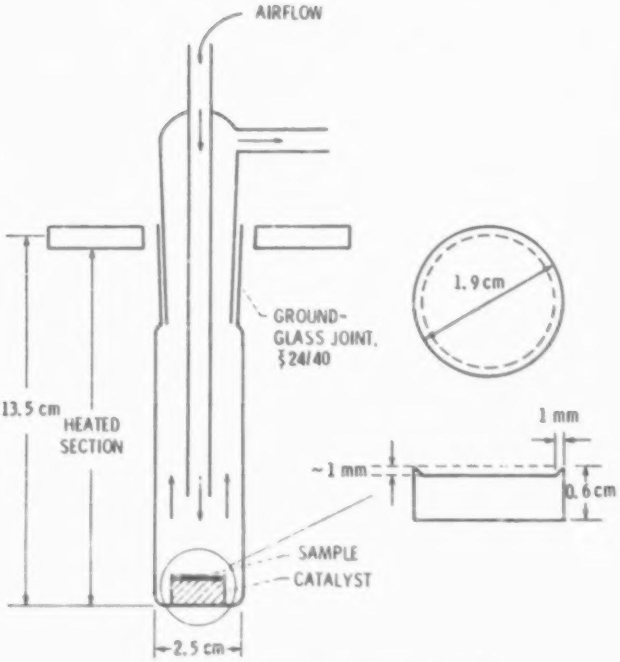

Figure 81. - Micro-oxidation apparatus (ref. 84).

The thin film test is a batch process and is subject to evaporation as well as oxidation. This usually can be taken into account by running identical tests in nitrogen. However, some highly stable materials require higher temperatures for reasonable reaction rates to take place. Sometimes the original charge disappears well before test conclusion. Of course, this can be alleviated by running tests above atmospheric pressure as has been done by others (ref. 81).

Another problem caused by the thin films is rapid loss of additives from formulated fluids. Even with thin film tests, diffusion limitations can occur, especially at high temperatures, where local oxygen consumption is great. In addition, these tests are usually run to high conversion (up to 50 percent). At high conversion the chain branching reactions which take place can greatly complicate the reaction picture. Here many products are formed and chemical analysis and kinetic treatment of the data become difficult if not impossible. Nevertheless this technique has been successful in reproducing high-temperature oxidation degradation from bearing tests (ref. 85), and gas turbine engine tests (ref. 86), and it has contributed to the fundamental understanding of the degradation of esters and hydrocarbons.

Stirred Flow Reactor

The thin film test just described is an example of a batch process. A single charge of material is used. In a continuous process, a constant flow of material to be oxidized is fed to the reactor. It has been shown that the instantaneous reaction rate can be determined by balancing the rate of reaction with this flow. This essentially maintains steady-state conditions. The stirred flow reactor is an example (ref. 87).

The material to be oxidized is fed into the reactor of constant volume in which there is thorough agitation producing a homogeneous mixture. This mixture is then removed at the same flow rate as the input of oxidizable material. Eventually, steady-state conditions will prevail and all reactants, intermediates, and final products have constant concentrations. The rate of consumption or formation of any product, intermediate, or reactant can then be calculated from the following equation.

$$\frac{d(X)}{dt} = \frac{(X)_\tau - (X)_0}{\tau} \qquad (37)$$

where $d(X)/dt$ is the rate of consumption of formation of substance X, $(X)_\tau$ is the concentration of X in the effluent at steady state at residence time τ, and $(X)_0$ the concentration of X in the entering fluid.

This equation is valid for any species, regardless of the complexity of the reaction. This is obviously a plus for kinetic studies. An empirical rate law can then be determined by finding a relationship that describes the rate of formation of a species as a function of its concentration in the reactor.

An example of a stirred flow microreactor is shown in figure 82. It consists of two pyrex spheres A and B. The inside sphere (B) is perforated. The hydrocarbon (RH) enters at the top and is mixed with a stream of oxygen. This mixture passes through the perforated sphere into sphere A. Theoretically, ideal mixing of the reactants, oxygen, and products occurs. The outlet is on the upper right.

This technique also has some drawbacks. Since a continuous flow of reactants is necessary, a much greater quantity of test material is required than in the thin film test. In addition, reactant purity must be stringently controlled. Nor is it clear how a catalytic surface could be incorporated. Although soluble metal catalysts could be incorporated in the reactant.

This type of apparatus has been successfully used in kinetic and mechanistic studies of n-hexadecane (ref 87).

Microoxidation Corrosion Apparatus

Another microapparatus for batch operations is shown in figure 83. It consists of a pyrex decomposition tube and rod assembly. Metal catalysts may be positioned on the rod assembly. In

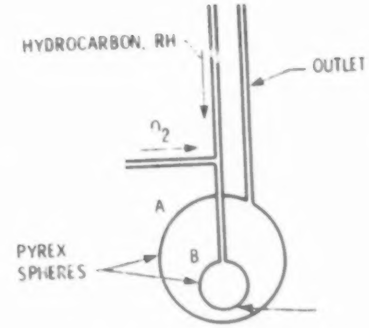

Figure 82. - Stirred flow microreactor (ref. 87)

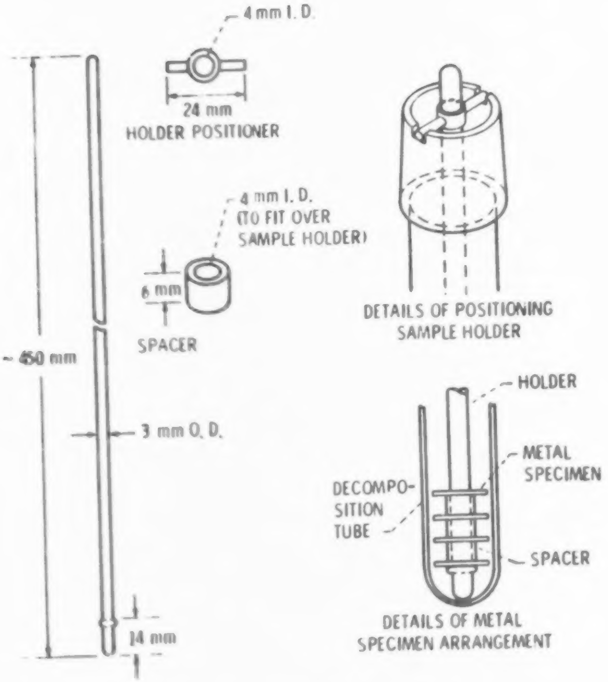

Figure 33. - Thermal oxidative decomposition tube.

a typical experiment, fluid is introduced into the decomposition tube. The system is evacuated and backfilled with oxygen to a known pressure. The tube is then placed in a preheated furnace for the specified test time. At test conclusion, the system is cooled and connected to a vacuum system. The liquid nitrogen noncondensibles are collected quantitatively, measured, and analyzed by various chemical means. The liquid nitrogen condensibles as well as the fluid residue are also analyzed. The rate of degradation is calculated from the amount of liquid nitrogen condensibles and is usually reported as milligrams of condensible product per gram of original fluid per hour of test.

This type of device has been used in a variety of studies on linear (ref. 88) and branched fluorinated polyethers (ref. 89). Again this apparatus suffers from the same disadvantages as other batch reactors. Conditions must be chosen so as to eliminate oxygen depletion or diffusion problems.

Chemiluminescence

Chemiluminescence (CL) is simply light emitted from a chemical reaction. It was first observed in biological sources such as the firefly. If a reaction is to produce light, several criteria must be met: (1) sufficient energy for excitation, (2) a species capable of forming an excited state, (3) an emitter to give off excitation energy, (4) a rapid chemical reaction, and (5) a reaction-coordinate system favoring production of an excited state over direct ground state formation.

It has been observed for many years that CL is associated with many oxidation processes (ref. 90). Referring back to the sequence of reactions in the autoxidation of hydrocarbons, it is believed that equation (19) is responsible for the observed CL:

$$\begin{tikzcd} 2RO_2\cdot \arrow[r] \arrow[dr] & ROH + R_2C = O + O_2 \\ & (R_2C = O)^* \end{tikzcd} \tag{19}$$

This disproportionation reaction produces a small amount of excited states $(R_2C = O)^*$. For most hydrocarbons, only one photon is emitted for each 10^8 to 10^{10} termination reactions. This inefficiency is caused, in part, by quenching reactions between the excited ketone and oxygen and other species.

$$(R_2C = O)^* + Q \rightarrow R_2C = O + Q \tag{38}$$

$$(R_2C = O)^* \rightarrow R_2C = O + h\nu \tag{39}$$

The intensity of the emitted radiation $(h\nu)$ is directly proportional to the square of the concentration of peroxy radicals $[RO_2\cdot]^2$. This dependence is the basis for determining the concentration of peroxy radicals and thus the kinetics of hydrocarbon oxidation. The advantages of CL are: (1) it is extremely sensitive, (2) it is noninvasive, (3) it provides a continuous monitor of peroxy radicals, and (4) only small samples are required.

Emission as Function of Time

An idealized curve of light emission as a function of time for an oxidation reaction is shown in figure 84. The emission of light gradually increases as oxidation proceeds, and the concentration of peroxy radicals increases until steady state is reached. At this point the light intensity reaches a maximum I_{max}. The time to reach this maximum t_{max} is a measure of the induction period. More commonly, the time to reach one half of maximum intensity $t_{1/2}$ is used.

If the oxygen flow is shut off while the oxidation reaction is proceeding, there is sometimes an immediate increase in light emission. This occurs because O_2 molecules are effective quenchers for the excited state species. The time between oxygen cutoff and the eventual drop in light emission is called the oxygen drop time t_F.

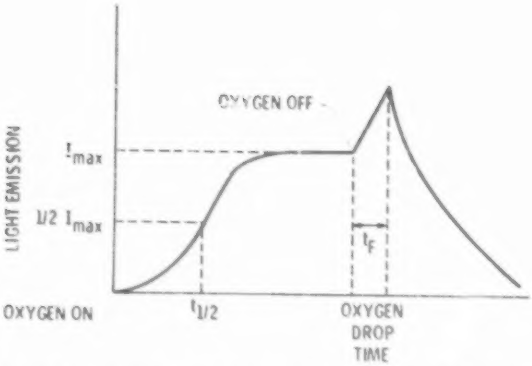

Figure 84. - Idealized curve of light omission as function of time for oxidation reaction.

The oxygen drop time is a direct measure of oxygen consumption and, therefore, a direct measure of the reaction rate. The oxygen concentration in the oil film at the oxygen cutoff point must be known so that oxygen consumption can be calculated.

Apparatus

Micro-oxidation apparatus. - Figure 85 illustrates the micro-oxidation apparatus used in this study. It is a modification of the oxidation apparatus previously described (fig. 81). It consists of two heat-resistant glass sections connected by a ground glass joint. The catalyst specimen is held in place by an annular glass ring on the base of the outer, or lower, section. The material to be oxidized is placed on the catalyst surface. The fiber-optic probe used to sense the light emission from the catalyst surface is held in the inner, or upper, section. This assembly consists of two vertical, concentric tubes forming an annular space for reduction of heat transfer to the probe, which contains a heat-sensitive epoxy. The bottom of each of these tubes is sealed with a quartz window to prevent absorption of the emitted light before it can be detected. The upper section also contains a gas inlet tube for oxygen or argon flow. The distance from the end of the fiber-optic probe to the top of the lubricant film is approximately 1.5 cm.

Chemiluminescence apparatus. - A schematic diagram of the CL apparatus is shown in figure 86. The system consists of the fiber-optic probe, a photomultiplier tube (PMT) and housing, an amplifier/discriminator, a high-voltage power supply, a rate meter, and a recorder.

The fiber-optic probe is a bundle of quartz fibers (50 cm long) covered with a flexible stainless steel sheath (~7 mm o.d.). One end of the probe is inserted into the micro-oxidation apparatus; the other end is attached to a flange on the PMT housing. The flange contains a manually operated shutter. The PMT has a dark current of 4 nA and a spectral response range of 150 to 850 nm. The housing

C-3

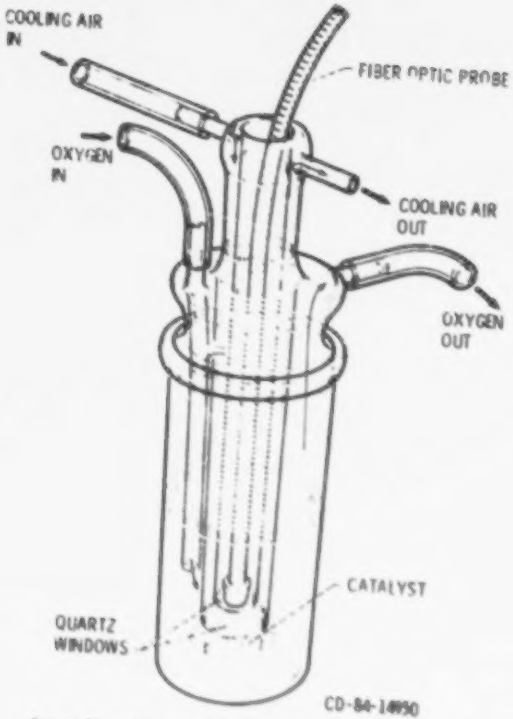

Figure 85. - Micro-oxidation apparatus.

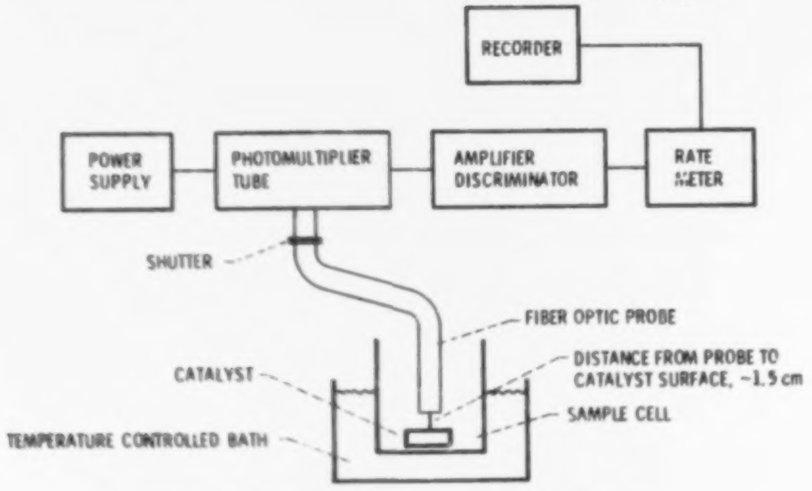

Figure 86. - Schematic of chemiluminescence apparatus.

also contains a thermoelectric refrigerated chamber in order to cool the PMT cathode to approximately 40 °C below ambient.

The input pulse from the PMT is fed into an amplifier/discriminator mounted inside the PMT housing. The output from the amplifier/discriminator is connected to a rate meter, which measures the rate of input pulses. (A 30-sec time constant was used in these studies.) The count rate is displayed on a panel meter. There is also an analog voltage output to power a strip-chart recorder.

Bath and Light-tight Enclosure. - A high-temperature (250 °C), constant-temperature bath was used in these studies. A high-viscosity fluid served as the heat transfer medium. Bath specifications indicated temperature control to ±0.1 °C. A cylindrical aluminum sleeve is mounted in the bath opening (10 cm long, 5 cm i.d., and 6.5 cm o.d.) with approximately 7 cm submerged in the bath fluid. A platinum resistance thermocouple is mounted vertically in the side of the sleeve to a depth of 9 cm. This couple is connected to a digital readout (accurate to ±0.1 °C), which has a minimum/maximum recall mode to determine the temperature range during an experiment.

The bath and PMT housing are located inside a lighttight metal box located in the corner of a fume hood. A handle on the top of the box is used to operate the PMT shutter remotely.

Procedure

At least 2 hr before a test, the PMT system was turned on and allowed to stabilize. The thermoelectric cooling system was maintained continuously. The supply voltage to the PMT was kept constant at a setting of 1000 V.

The micro-oxidation apparatus was thoroughly cleaned with trichlorotrifluoroethane and allowed to air-dry. The catalyst was cleaned with trichlorotrifluoroethane, scrubbed with a paste of submicron alumina, and rinsed with tap water and then distilled water. After air-drying, the catalyst was weighed and placed with forceps into the bottom of the lower section of the micro-oxidation apparatus. Next the catalyst and the lower section of the apparatus were weighed together. Then six drops of lubricant were placed on the catalyst surface by pipette, and the section was reweighed to determine the exact amount of added lubricant.

The upper apparatus section was inserted into the lower section, and the device was purged with argon for 5 min at room temperature (flow rate >75 ml/min). Next the assembled apparatus was placed in a steel holder on a hot plate previously heated to 130 °C and purged with argon at this temperature for 20 to 25 min to remove dissolved oxygen and water from the lubricant.

At this point the apparatus was placed in the aluminum block in the bath, which had previously been heated to test temperature. The fiber-optic probe was inserted in the upper section of the apparatus, and a high flow rate of air was directed into the annular region around the fiber-optic probe for cooling. The top of the apparatus was covered with aluminum foil to block any stray light, and the front cover of the enclosure was put in place.

While the apparatus was being purged initially, a baseline count rate with the PMT shutter closed was determined. After the lighttight box was closed, the PMT shutter was opened, and a new baseline was measured during temperature equilibration. After 20 to 30 min the argon flow was turned off, and simultaneously the oxygen flow was begun. The intensity of emitted light was recorded continuously on a strip-chart recorder. After the light intensity reached a maximum, the test was continued for another 5 to 15 min, and then the oxygen and argon flows were exchanged.

The box was opened, and the apparatus still under an argon purge was removed and allowed to cool. The two sections were separated, and the lower part was weighed to determine the lubricant weight loss. Then 4 ml of chloroform was added to the lower section to dissolve the remaining lubricant. This sample was retained for high-pressure liquid chromatographic analysis (HPLC). The catalyst was thoroughly rinsed with trichlorotrifluoroethane, allowed to air-dry, and weighed to determine whether deposits remained on the catalyst.

The catalyst material used was aluminum alloy 2024, which has the following nominal composition: 3.8 to 4.9 percent copper, 0.3 to 0.9 percent manganese, 1.2 to 1.8 percent magnesium, balance aluminum. This alloy was chosen because it is the aluminum alloy used in the standard oxidation-corrosion test developed by the Air Force (ref. 91). The dimensions of the catalyst are illustrated in figure 87.

Results

Results from chemiluminescence studies for the three aromatic basestocks (1) 5P-4E, (2) 4P-3E, and (3) thioether appear in table 17. Each basestock contained diphenylanthracene (DPA) as an intensifier at a concentration of 10^{-3} M. Because of the high viscosity of these fluids, it was impossible to place identical amounts of each fluid on the catalyst surface. Therefore, each test was normalized to an arbitrary sample size of 0.05 g. All following plots have been scaled based on this normalization.

Figure 88(a) to (c) contains normalized light emission I^* as a function of time for 5P-4E, 4P-3E, and the thioether, respectively. All curves have been smoothed. The four plots represent actual tests at bath settings of 180, 190, 200, and 210 °C. The actual sample temperature was approximately 2 °C lower than the bath temperature.

The typical features of these curves are similar to those obtained previously with a pure ester (TMPTH) with an identical concentration of intensifier (10^{-3} M DPA). These features include an approximately 30 to 45 sec delay or induction period before light emission begins after oxygen flow is turned on. Each curve reaches a maximum at about 2 or 3 min into the test and then drops off to a relatively steady value after a few minutes. This drop off has been shown (ref. 91) to be caused by oxidative degradation of the

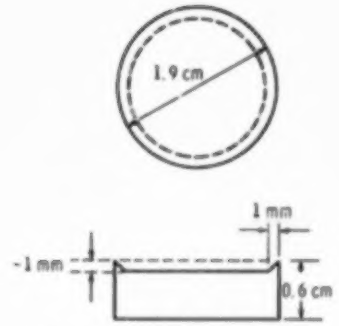

Figure 87. - Catalyst dimensions.

TABLE 17. - SUMMARY OF CHEMILUMINESCENCE DATA

Catalyst: Aluminum Alloy 2024,

Atmosphere, Oxygen; Intensifier,

9,10-diphenylanthracene, (10^{-3}M)

Test fluid	Normalized maximum light emission, I^{*}_{max}	Average temperature, °C
4P-3E	0.30	173.45
	0.37	173.15
	0.32	178.40
	0.39	178.35
	0.41	183.55
	0.42	183.30
	0.46	188.30
	0.48	188.40
	0.50	193.15
	0.49	193.05
	0.54	198.00
	0.80	203.45
	1.05	208.55
Thioether	0.29	173.25
	0.18	173.30
	0.22	178.45
	0.19	178.25
	0.20	183.60
	0.14	183.20
	0.27	188.35
	0.40	198.35
	0.57	203.30
	0.45	208.75
	0.33	208.55
5P-4E	0.11	173.30
	0.25	173.30
	0.10	178.35
	0.23	178.30
	0.18	183.40
	0.28	183.35
	0.29	188.40
	0.29	188.35
	0.32	192.90
	0.26	198.15
	0.37	198.40
	0.34	203.40
	0.41	208.75

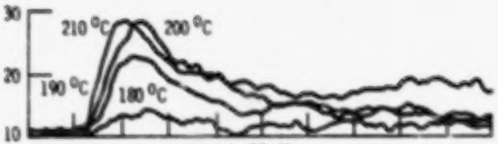

(a) 5P-4E.

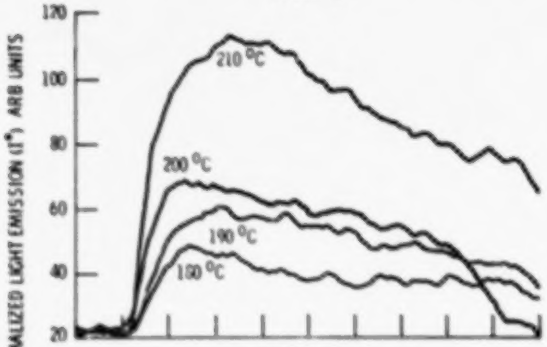

(b) 4P-3E.

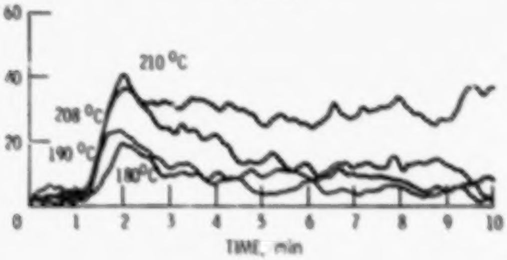

(c) Thioether.

Figure 88. - Normalized light emission (I^*) as a function of time for three fluids at bath temperatures of 180, 190, 200, and 210 °C. (Al 2024 catalyst, 10^{-3} M DPA, oxygen.)

intensifier DPA. It is assumed for these tests that the depletion of DPA is the same at similar test temperatures. This allows one to compare different fluids at the same test condition. For example, figure 89 contains a set of smoothed curves of normalized light emission I^* as a function of time for 5P-4E, 4P-3E, and the thioether at a bath temperature of 210 °C.

In general, at any particular temperature, the order of the maximum normalized light emission I^*_{max} was: 4P-3E >thioether >5P-4E. Then this order would also represent the order of increasing oxidation stabilities if I^*_{max} can be taken as a measure of fluid oxidation. However, it has previously been pointed out that the light emission occurs in equation (19) which is really a side reaction. Therefore one one must be careful in comparing I^*_{max} from completely different chemical classes. However, the three aromatic fluids are structurally so similar that this may not be a problem. One comparison can be made with a totally different chemical class, an ester, trimethylolpropane triheptanoate (TMPTH) which was run under identical conditions. This is a fluid which is known to oxidize at a much greater rate than these aromatic fluids. The ratio of I^*_{max} for the ester to that of the aromatic fluids ranged from 10 to 17 times at 175 °C to 35 to 58 times at 205 °C.

Another method of treating CL data is by plotting the log of the normalized maximum light emission I^*_{max} as a function of the reciprocal of the absolute temperature. If only one mechanism of oxidation is occurring, this plot should yield a straight line. The slope of this line is then related to the activation energy of the propagation reaction (eq. (18)). When oxygen diffusion into the oil film is rate limiting, $E_{I_{max}} = 2E_{propagation}$, where E is the activation energy. Plots of log I^*_{max} versus 1/T appear in figure 90 for 5P-4E, 4P-3E, and the thioether. $E_{propagation}$ calculated from these plots are approximately 5.9, 6.2, and 5.2 kcal/mole for 5P-4E, 4P-3E, and the thioether, respectively. These can be compared with a value of 11 kcal/mole previously obtained for an ester, (TMPTH) in identical experiments.

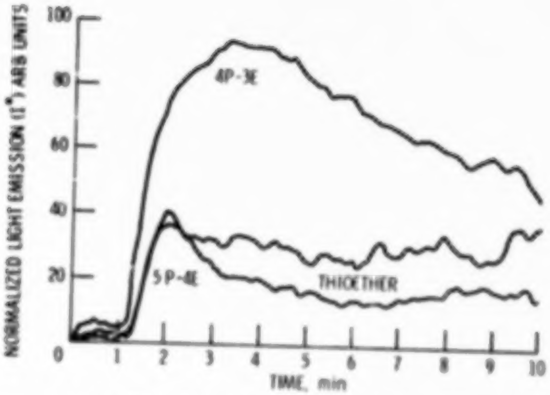

Figure 89. - Normalized light emission (I^*) as a function of time for 5P-4E, 4P-3E and a thioether at a bath temperature of 210 °C. (Al 2024 catalyst, 10^{-3} M DPA, oxygen.)

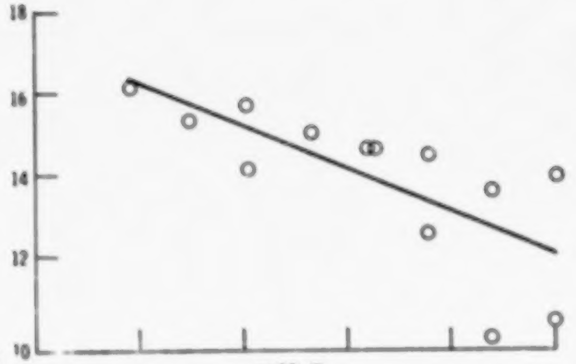

(a) 5P-4E.

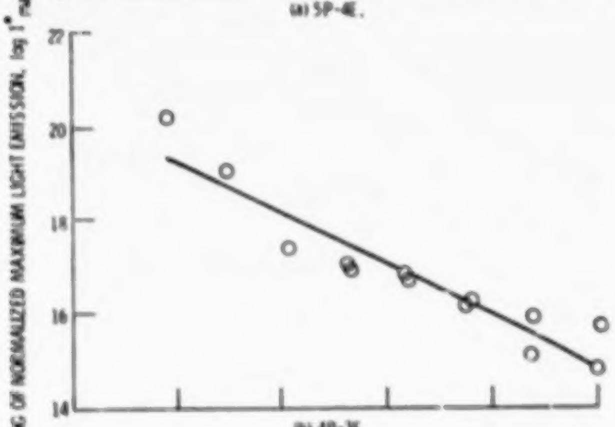

(b) 4P-3E.

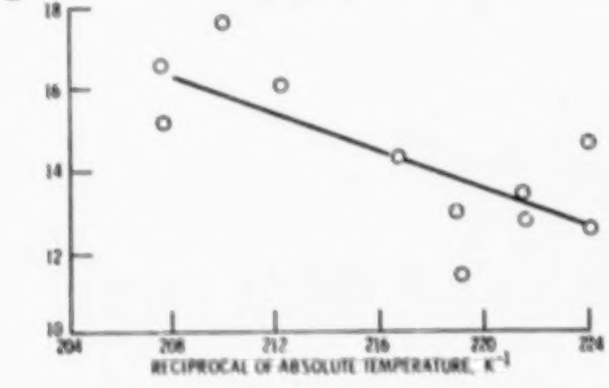

(c) Thioether.

Figure 90. - Log of normalized maximum light emission as a function of reciprocal of absolute temperature. DPA (10^{-3} M), aluminum 2024 catalyst, oxygen atmosphere.

Comparison With Microoxidation Corrosion Data

A microoxidation corrosion apparatus was described in the Experimental Methods Section under Oxidation Stability. This device is illustrated in figure 83. The identical fluids described in the CL section (4P-3E, 5P-4E, and the thioether) were also studied in this apparatus. Test conditions included: sample size approximately 3 g; tube volume 93-100 cc; sealed with air at approximately 700 mm Hg at room temperature; test duration, 24 hours; test temperature 316 °C; catalyst, aluminum 2024 alloy.

Experimentally, the fluid was introduced into the decomposition tube which was then evacuated and filled to 700 mm Hg at a known temperature with air. Since the apparatus was calibrated and the fluid volume measured accurately, the quantity of gas introduced was exactly known. The decomposition tube was then inserted into a preheated box furnace for 24 hours; during this exposure the temperature was continuously recorded. After removal from the furnace, the tube was allowed to cool to room temperature, attached to a vacuum line, and opened. The liquid nitrogen condensibles, which were volatile at room temperature, were weighted. The fluid residue itself was weighed and subjected to infrared spectral analysis.

The degradation rate is calculated from the amount of liquid nitrogen condensibles formed and is reported as milligrams of volatiles per gram of original fluid. A summary of test results appear in table 18.

As can be seen, the order of increasing oxidation stabilities (based on volatile formation and oxygen consumption) is as follows: 4P-3E < 5P-4E < thioether. This is not the same order obtained from the CL data. The ranking of 4P-3E as the most easily oxidized fluid is the same in both studies. The other two fluids are reversed. In reviewing the CL data for 5P-4E and thioether indicates that their I^{*}_{max} values were quite similar. It was also mentioned in the CL section that the incorporation of sulfur into the thioether structure may have altered its CL emission characteristics enough to make

TABLE 18. - SUMMARY OF MICROOXIDATION CORROSION RESULTS[a]

Sample	Amt g	Volatiles		O_2		O_2 in air		CO		Catalyst[b] wt change, mg
		mg	mg/g	Consumption		Initial conc, %	Final conc, %	Production		
				mg	mg/g			mg	mg/g	
Thioether	3.53	8.1	2.3	10.5	3.0	17.6	9.1	0.9	0.2	-0.2
Five-ring polyphenyl Ether (5P-4E)	2.67	11.0	4.1	14.5	5.4	17.6	6.4	1.5	.6	.0
Four-ring polyphenyl Ether (4P-3E)	3.14	19.8	6.3	20.1	6.4	17.6	.7	2.4	.8	-.3

[a] Air approximately 700 mm Hg at room temperature; tube volume 93-100 cc; 316 °C for 24 hr in the presence of aluminum catalyst.

[b] Aluminum 2024 alloy.

comparisons difficult. At any rate, the correlation of the CL data for the two chemically similar structures (4P-3E and 5P-4E) with the bulk oxidation tests is good.

MECHANISM OF OXIDATION

The general free radical mechanism of hydrocarbons has been previously discussed in the section Oxidation Stability, Background, Mechanism.

Initiation

In the autoxidation of hydrocarbons the classical mechanism calls for attack of molecular oxygen at the C-H bonds. Theoretically, one can show by various resonance structures that there are higher electron densities on ring positions that are ortho or para to the ether linkage. Therefore, one would predict that electrophilic attack by molecular oxygen would occur at these positions. An example (shown for m,m-4P-3E) follows.

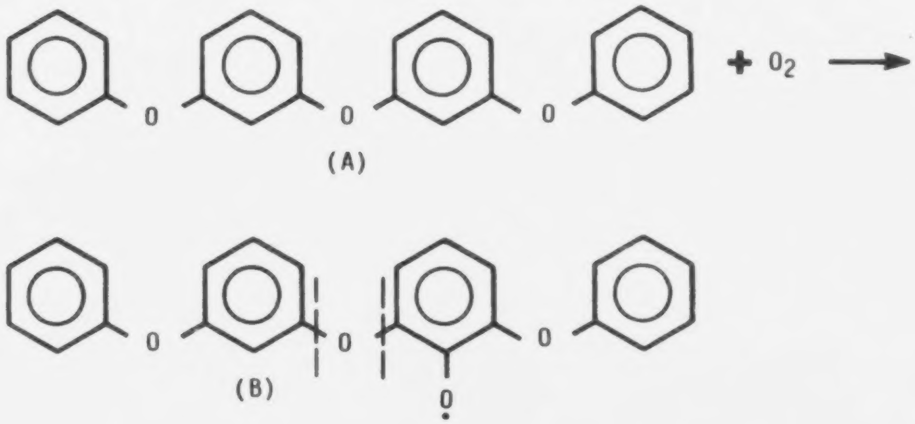

(40)

Oxidative cleavage of B (shown by dotted lines) would yield either products C and D or E and F.

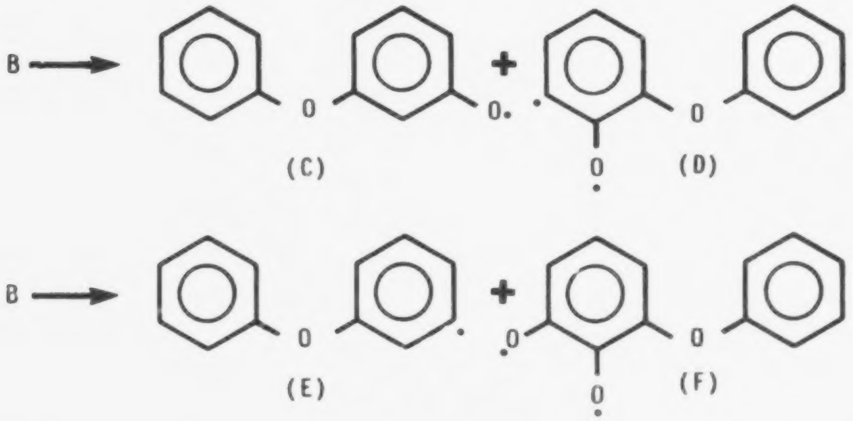

(C) (D)

(E) (F)

These are products for symmetrical cleavage. Similar reactions could be written for unsymmetrical cleavage. This type of initiation sequence has been proposed by Archer and Bozer (ref. 92). However, as pointed out by Wilson et al. (ref. 93), the phenyl type radicals proposed in this scheme are rather high energy radicals compared to phenoxyl radicals that can be stabilized by resonance.

Therefore, perhaps a more likely initiation scheme would involve attack of molecular oxygen at the ether carbons (C-O-C) rather than the C-H bonds. Oxidative cleavage would then result in the formation of low energy, resonance stabilized phenoxyl and substituted phenoxyl radicals. This is illustrated for 4P-3E in the following equation (symmetrical cleavage only):

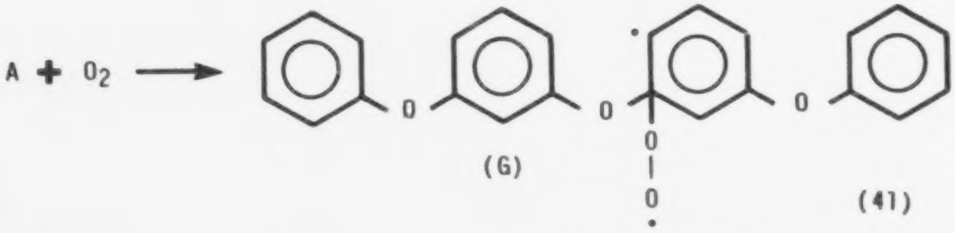

(G)

(41)

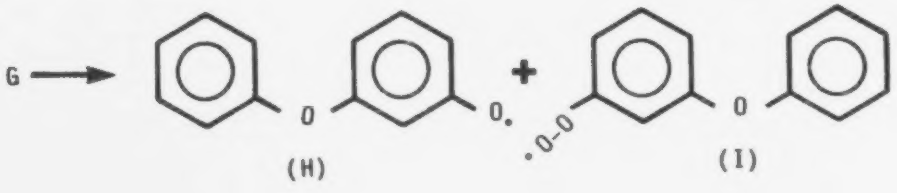

(H) (I)

(42)

Propagation

The free radical intermediates such as (H) and (I) can attack the parent molecule (A) resulting in additional radicals:

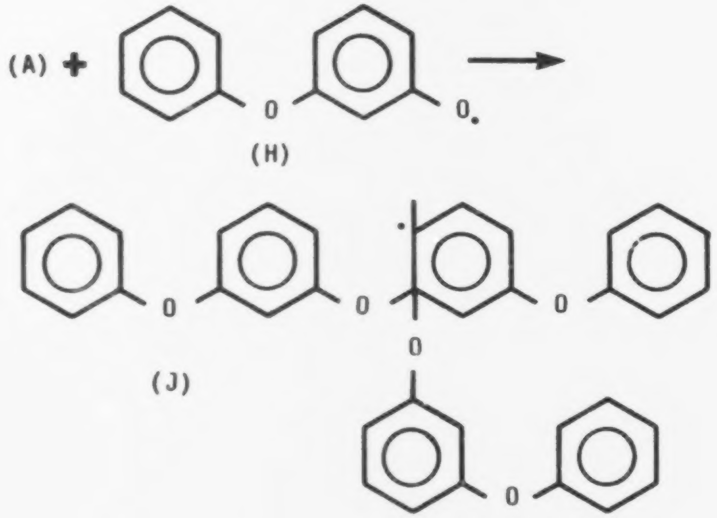

(43)

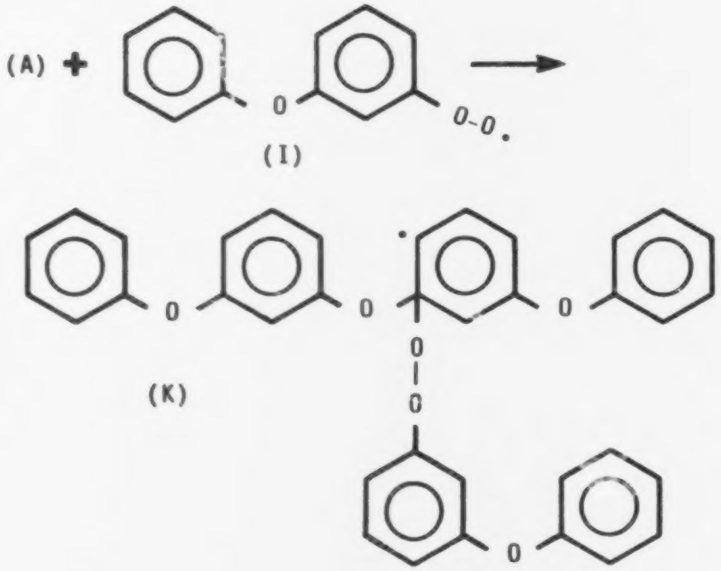

(44)

Further cleavage results in the following products:

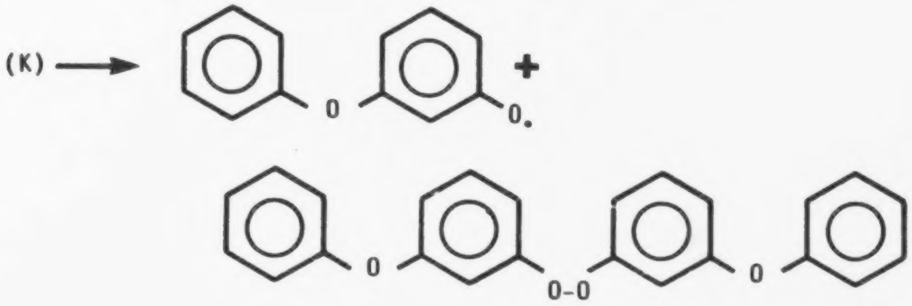

(L)

(45)

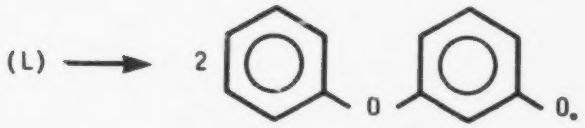

(H)

(46)

Therefore, the net result of the initiation and propagation steps is that 2 molecules of 4P-3E react with oxygen to produce four substituted phenoxyl radicals.

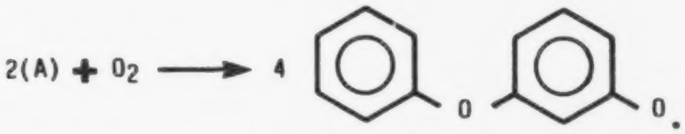

(H)

(47)

Combinations of symmetrical and unsymmetrical cleavages yield mixtures of the following

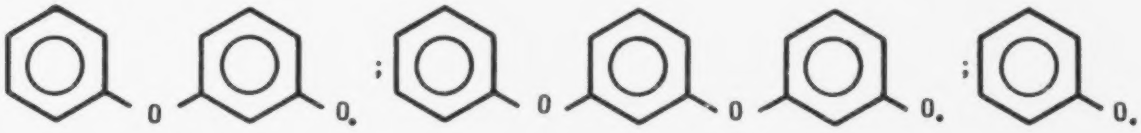

These radicals can undergo many other reactions such as coupling and dehydrogenation with O_2 which produces water which has been shown to be a product of the oxidation of polyphenyl ether (ref. 92).

Termination

The coupling of the free radical intermediates probably constitutes the termination sequence. This could produce oxygenated bridge compounds. This is illustrated in the following set of equations:

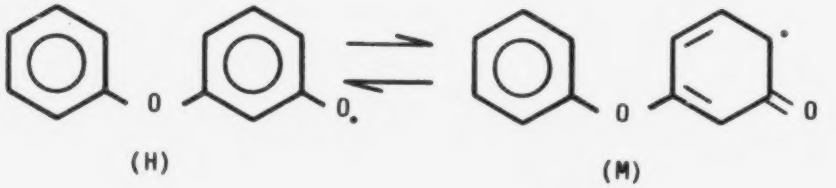

(48)

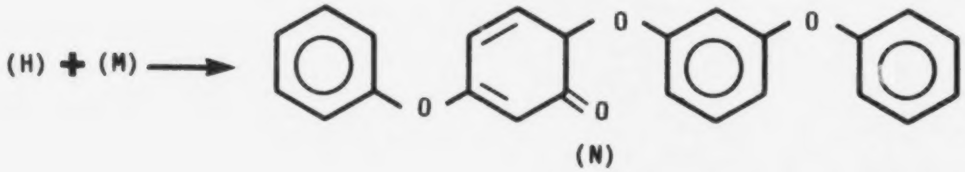

(49)

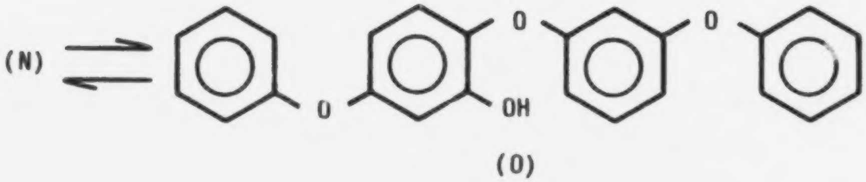

(50)

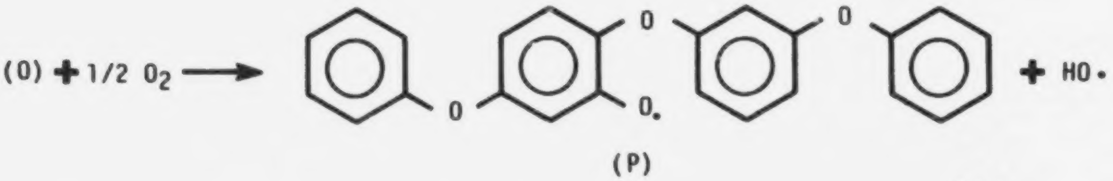

(51)

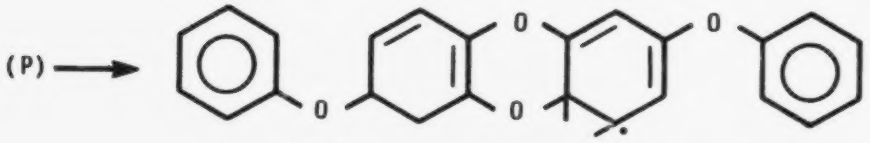

(Q)

(52)

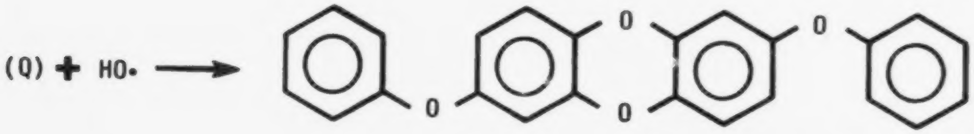

(R)

+ H_2O

(53)

It should be obvious that even from a single molecular structure, such as the meta-linked 4P-3E molecule, which was used for the previous example, a very complex mixture of compounds will result from oxidation. Molecular weight of the products will continually increase with increasing oxygen consumption. The final products will be highly fused ring compounds consisting of C-O-C and C-C bridges. The overall reaction of 5 molecules of 4P-3E can be summarized as follows:

$$\begin{aligned} 5C_{24}H_{18}O_3 + 4O_2 \longrightarrow\ & 9C_6H_4O_{0.9}\ \text{(Solubles)} \\ & + \\ & 11C_6H_4O_{0.9}\ \text{(Insoluble)} \\ & + \\ & 5H_2O \end{aligned} \qquad (54)$$

OXIDATION INHIBITORS

Because of the inherent stability of these fluids, conventional antioxidants (such as amines and phenols) are not useful. This is related to the volatility or thermal instability of these additives. However, some additives are effective above 260 °C. These include aromatic tin compounds such as tetraphenyl tin (ref. 94) and certain other organometallic compounds (ref. 92). Cuprous and cupric oxides (refs. 95 and 96)) were also effective.

A continuation of this work (ref. 97) showed that soluble alkali or alkaline earth metal phenoxides are also effective inhibitors to 370 °C. Oxides, hydroxides, and carbonates of alkali metals and barium are very effective inhibitors (to approximately 370 °C). A proposed mechanism is the destruction of peroxy radicals by a superoxide formation (ref. 96)

In fact, oxidation/corrosion tests (ref. 98) showed that the presence of a variety of metal coupons reduced the oxidation of a polyphenyl ether (measured by viscosity increase). Lead and copper seemed to be the most effective.

FORMATION OF HIGH MOLECULAR WEIGHT PRODUCTS

The formation of higher molecular weight products from 5P-4E and the thioether have been previously discussed in the Boundary Lubrication and Ferrography sections. The possible oxidative mechanism has also been previously discussed. Another study on thioether formulations has also been reported (ref. 99).

In this study, gel permeation chromatography was used to analyze various thioether formulations from high temperature bearing tests and from micro-oxidation tests (see section Oxidation Stability, Experimental Methods, Microtests). The micro-oxidation tests yielded degradation results similar to those observed from the bearing tests. An example of a gel permeation chromatogram appears in figure 91.

Here a number of peaks are evident in the chromatogram sensed by the UV detector. They roughly correspond to species having molecular weights of 290, 390, 450, 600, 700, 800, and 2400. It must be remembered that the chromatography calibration points are based on individual aromatic compound standards. In addition, the mechanism of separation is based on molecular size in solution and not molecular weight. Nevertheless, it is compelling to resort to the

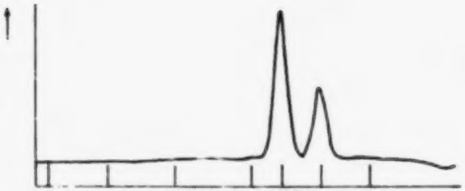

(a) RI detector (16X).

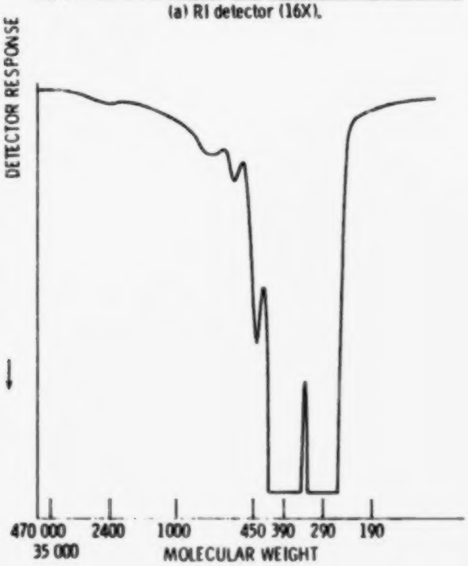

(b) UV detector (1.0 AUFS).

Figure 91. - Gel-permeation chromatogram of thioether formulation from micro-oxidation test - catalyst, M-50 steel; test atmosphere, dry air, test temperature, 353 °C, test time, 60 minutes.

oxidative cleavage and coupling reactions previously described. The peaks at 290 and 390 are from the thioether basestock. Addition of a series of phenyl sulfur moieties to a four-ring thioether component would produce compounds having approximate molecular weights of 500, 600, 700, and 800, which compares well with observed results.

MODELS

GOLDBLATT RADICAL ANION MODEL

It was pointed out in the Boundary Lubrication and Ferrography sections that a model proposed by Goldblatt (ref. 62) seemed to explain most of the anomalous boundary lubricating behavior of the polyphenyl ethers. The main point of this model is that negatively charged free radicals (radical anions) are generated at the rubbing surface. The primary processes of this model are summarized below:

$$\text{METALLIC SURFACE} \xrightarrow{\text{SLIDING}} \text{VIRGIN METAL SURFACE (VM)}$$

VM + polynuclear aromatic (ArO) → M; Aro
(Adsorbed aromatic on metal M) (55)

M; Aro → $\mathrm{M^+}$; $\mathrm{Aro\cdot^-}$ (Adsorbed radical anion) (56)

$\mathrm{M^+}$; $\mathrm{Aro\cdot^-} \rightarrow \mathrm{H^+} + \mathrm{Aro\cdot^-}$ (Desorbed radical anion) (57)

$\mathrm{Aro\cdot^-}$ + Metal or metal oxide →
Reduced metal oxides or abrasives (58)

Abrasives + metal → abrasive wear (59)

$\mathrm{Aro\cdot^-} + \mathrm{H_2O} \rightarrow \mathrm{AroH} + \mathrm{OH^-}$ → Dihydronaphthalene (60)

$\mathrm{Aro\cdot^-} + \mathrm{O_2} \rightarrow \mathrm{Aro} + \mathrm{O_2\cdot^-}$ → Peroxides →
Acids or resins (61)

$$\text{Aro}\cdot^{-} + \text{Aliphatic} \xrightarrow{\Delta} \text{Adduct (higher molecular weight products} \qquad (62)$$

$$\text{Aro}\cdot^{-} + \text{Aliphatic} + O_2 \xrightarrow{\Delta} \begin{array}{l}\text{Peroxides (of aliphatics)}\\ \text{Acids (of aliphatics)}\end{array} \qquad (63)$$

What this model then predicts is that reactions initiated by radical anions of polynuclear aromatics cause (a) accelerated wear under inert atmospheres, (b) reduced wear in oxygenated or moist atmospheres and (c) synergism with aliphatics.

Phenomena (a) and (b) have been observed with the polyphenyl ethers and thioethers and have been previously discussed. Of course, the above model was developed for polynuclear aromatics, such as napthalene or anthracene. These are species containing multiple fused benzene rings. The polyphenyl ethers contain multiple benzene rings but they are separated by ether linkages. However, the main question is, "Do the polyphenyl ethers also produce radical anions?"

Morales (ref. 100), has shown that radical anions can be generated from a thioether using an electrochemical cell. It was also shown that biphenyl and polyphenyl ethers also yield radical anions. Therefore, it is not surprising that the Goldblatt model predicts the boundary lubricating behavior of these aromatic fluids quite well.

However, the above model does not explain how other hydrocarbons act such as monoaromatics, napthenes, and paraffins. Nor does the Goldblatt model explain how the radical anions actually form. It is also not clear what is meant by the metal cation-radical anion complex $M^{+};\text{Aro}\cdot^{-}$.

KAJDAS NEGATIVE-ION CONCEPT

Another model, the negative-ion concept, has been proposed by Kajdas (ref. 101) which complements the above model. Essentially, this model is based on the formation of negative ions from hydrocarbons and their subsequent chemisorption onto positively charged spots on rubbing metal surfaces.

Exoelectron emission from surfaces is well known (ref. 102). Kajdas believes that these electrons interact with hydrocarbons to produce negatively charged ions. The following mechanisms could produce these ions:

$$AB + e^- \rightarrow AB^{\bullet -} \qquad \text{(Resonance capture)} \qquad (64)$$

$$AB + e^- \rightarrow A^- + B^{\bullet} \qquad (65)$$

or (Dissociative resonance capture)

$$AB + e^- \rightarrow B^- + A^{\bullet} \qquad (66)$$

$$AB + C^- \rightarrow ABC^- \qquad \text{(Ion attachment)} \qquad (67)$$

where AB is a molecule and C^- a negative ion. An aromatic hydrocarbon Ar could yield two types of negative ions.

$$Ar + e^- \rightarrow Ar^{\bullet -} \qquad (68)$$

or by attachment of O^-:

$$Ar + O^- \rightarrow (Ar-1)O^{\bullet -} + H^{\bullet} \qquad (69)$$

The species $Ar^{\bullet -}$ formed in equation 68 could attack the surface (as in the Goldblatt model) to produce a form of corrosive wear. In the presence of water or oxygen, ions would be formed as in equation (69). These ions could react with the surface to control wear. And finally, if the shear strength of the rubbing interface is high, the bonds of the chemisorbed ions may be broken to produce free radicals. These species could then form resins or friction polymers around wear scars.

CONCLUDING REMARKS

What finally emerges from this plethora of data is that the promises of this once exciting class of organic materials have yet to be fulfilled. Although some of these fluids have found a niche for some special applications, in general, this fluid class has been largely bypassed. Whether or not structural improvements or new additive technology will come into play remains to be seen. At any rate, the results compiled in this thesis can be summarized as follows:

(1) Most of the aromatic fluids are autophobic and will therefore exhibit poor wettability except at high temperatures.

(2) The use of wettability additives with these fluids has not been successful.

(3) These fluids are inherently poor boundary lubricants under dry inert conditions and only marginal in a moist air atmosphere.

(4) Boundary lubricating additives can improve their performance but have not been as successful as with other chemical classes.

(5) The thioethers are inherently better boundary lubricants than the polyphenyl ether analogs.

(6) Aromatic silicon and tin compounds do not possess the thermal-oxidative stability to be considered as base fluids. They may be useful as additives, particularly the tin compounds.

(7) The aromatic class of fluids produce a great deal of friction polymer or surface resin under boundary lubricating conditions. Their behavior can be adequately explained by the Goldblatt radical anion theory and the Kajdas negative ion concept.

(8) This aromatic fluid class yields some of the most thermally stable organic compounds known to man. In general, the order of stability is 5P-4E > 4P-3E > thioether > aromatic silicon compounds > aromatic tin compounds.

(9) All three basic aromatic fluids chemiluminesce in the temperature range 175 to 210 °C in the presence of an intensifier. Based on this data, the order of increasing oxidation stability is: 4P-3E < thioether < 5P-4E.

(10) Bulk oxidation tests with a microoxidation corrosion apparatus yielded a different order of increasing oxidation stabilities: 4P-3E < 5P-4E < thioether.

(11) The mechanism of oxidative degradation is free radical in nature and most likely occurs by attack of molecular oxygen at the ether carbons with the resulting symmetrical and unsymmetrical cleavage forming phenoxyl and peroxy radicals.

(12) The termination step in the oxidative degradation involves a coupling reaction which yields higher molecular weight aromatic compounds containing C-O-C and C-C bridges. These compounds generally separate as an insoluble sludge.

(13) Conventional antioxidants are not normally useful in these fluids. However, organometallic compounds of tin, cuprous and cupric oxides, alkali or alkaline earth metal phenoxides, oxides, hydroxides, and carbonates of alkali metals are effective oxidation inhibitors.

REFERENCES

1. Streitwieser, A.; and Heathcock, C.H.: Introduction to Organic Chemistry, acmillan Publ. Co., New York, 1976.
2. Ullman, F.; and Sponagel, P.: Ann. 350, 1906, p. 83.
3. Staudinger, H.; and Staiger, F., Ann. 517, 1935. p. 67.
4. Akchurin, Z.S.: C.A., 40, 1946, p. 557.
5. Kotera, A.: J. Chem. Soc. Japan 70, 1949, p. 213.
6. Mahoney, C.L.; Barnum, E.R.; Kerlin, W.W.; and Sax, K.J.: Meta-Linked Polyphenyl Ethers as High-Temperature Radiation-Resistant Lubricants. ASLE Trans., vol. 3, no. 1, Apr. 1960, pp. 83-92.
7. McHugh, K.L.; and Stark, L.R.: Properties of a New Class of Polyaromatics for Use as High-Temperature Lubricants and Functional Fluids. ASLE Trans., vol. 9, no. 1, Jan. 1966, pp. 13-23.
8. Zimmer, H.; Barcelon, M.A.; and Jones, W.R., Jr.: Sterically Hindered Group IV_B Organometallics. X. Preparation and Some Properties of Biphenylsilicon and Tin Compounds, J. Organometallic Chem., 63, 1973, pp. 133-138.
9. Gunderson, R.C.; and Hart, A.W.; eds: Synthetic Lubricants. Reinhold Publ. Corp., 1962.
10. Hirano, F.: Effect of Molecular Weight Distribution on Lubrication of Machine Elements and Proc., Shell Industrial Lubricants Technical Symposium, Tokyo, Japan, Oct. 22, 1980.
11. Bikerman, J.J.: Surface Chemistry. Second ed., Academic Press, Inc., 1958, pp.. 1-128.
12. Sugden, S.: Determination of Surface Tension from Maximum Pressure in Bubbles. J. Chem. Soc., vol. 121, pt. I, 1922, pp. 858-866.
13. Sugden, Samuel: Determination of Surface Tension from the Maximum Pressure in Bubbles. Part II. J. Chem. Soc., vol. 125, pt. I, 1924, pp. 27-31.

14. Kreith, F.: Principles of Heat Transfer. International Textbook Co., 1958.
15. Fox, H.W.; Hare, E.F.; and Zisman, W.A.: Wetting Properties of Organic Liquids on High-Energy Surfaces. Rep. NRL-4569, Naval Research Laboratory, July 29, 1955.
16. Freeman, A.P.; Allen, S.; and Singer, H.B.: Ball Bearing Surface Chemistry. Paper E-2288 presented at Bearings Conference at Dartmouth College, Hanover, N. H., Sept. 4, 1968.
17. Wedeven, L.D.; Evans, D.; and Cameron, A.: Optical Analysis of Ball Bearing Starvation. Trans. ASME, J. Lub. Tech., series F, vol. 93, no. 3, July 1971.
18. Zisman, W.A.: Relation of the Equilibrium Contact Angle to Liquid and Solid Constitution. Contact Angle, Wettability, and Adhesion. Advances in Chemistry Series No. 43. Am. Chem. Soc., 1964, pp. 1-51.
19. Spar, C.; and Damasco, F.: High-Temperature Fluid Lubrication. ASLE Trans., vol. 7, no. 2, Apr. 1964, pp. 211-217.
20. Shim, J.; and Leonardi, S.J.: Microfog Lubricant Application System for Advanced Turbine Engine Components - Phase II. Mobil Research and Development Corp. (NASA CR-72743), May 1970.
21. McBain, M.E.L.; and Perry, L.H.: J. Am. Chem. Soc. 62, 1940, p. 989.
22. Banks, W.H.: Nature 174, 1954, p. 365.
23. Stribeck, R.: "Characteristics of Plain and Roller Bearings," Ziet. V. D. I., vol. 46 (1902).
24. Hersey, M.D.: "The Laws of Lubrication of Horizontal Journal Bearings," J. Wash. Acad. Sci., 4 1914, pp. 542-552.
25. Beerbower, A., "Boundary Lubrication," Scientific and Technical Applications Forecasts, Department of the Army, DAHC-19-69-C-0033, 1972.
26. Adamson, A.W., Physical Chemistry of Surfaces, John Wiley and Sons, 2nd. ed., 1967.
27. Godfrey, D., "Boundary Lubrication," in Interdisciplinary Approach to Friction and Wear, NASA SP-181, ed. by P.M. Ku, 1968, pp. 335-384.

28. Hermance, H.W.; and Egan, T.F.: Organic Deposits on Precious Metal Contacts," *Bell Syst. Tech. J.*, 37, 1958, pp. 739-776.
29. Russell, J.A.; Campbell, W.E.; Burton, R.A.; and Ku, P.M.: "Boundary Lubrication Behavior of Organic Films at Low Temperatures," *ASLE Trans.*, 8(1), 48, 1965.
30. Bowden, F.P.; and Tabor, D.: *The Friction and Lubrication of Solids, Part 1*, Oxford University Press, 1971, p. 182.
31. Akhmatov, A.S.: *Molecular Physics of Boundary Friction*, Israel Program for Scientific Translations 1966, p. 248.
32. Kragelski, I.V.: *Friction and Wear*, Butterworths, 1965, pp. 158-163.
33. Rowe, C.N., "Wear-Corrosion and Erosion," *Interdisciplinary Approach to Liquid Lubricant Technology*, NASA SP-318, ed. by P.M. Ku, 1973, pp. 527-568.
34. Hirano, F.; and Sakai, T.: Further Evidences of Chain Matching Effect, Proc. 9th Int. Conf. Fluid Sealing, HBRA, 1981, p. 429.
35. Whitehead, J.R., "Surface Deformation and Friction of Metals at Light Loads," *Proc. R. Soc. London Ser. A*, 201 (1064), 1950, pp. 109-124.
36. Ling, F.F., Klaus, E.E., and Fein, R.S.: *Boundary Lubrication, an Appraisal of the World Literature*. American Society of Mechanical Engineers, 1969.
37. Clayton, D.: An Introduction to Boundary and Extreme Pressure Lubrication. Physics of Lubrication, *Br. J. Appl. Phys. 2*, Suppl. 1, 1951, p. 25.
38. Forrester, P.G., "The Influence of Sliding Velocity and Other Variables on Kinetic Friction in or Near the Boundary Region," *Proc. R. Soc.* London, Ser. A, 187 (1011), 1946, pp. 439-463.
39. Faut, O.D.; and Wheeler, D.: On the Mechanism of Lubrication by TricresylPhosphate (TCP). I. The Coefficient of Friction as a Function of Temperature for TCP on M-50 Steel, NASA TP-2053 (1983).
40. Loomis, W.R.; and Jones, W.R., Jr.: "Steady-State Wear and Friction in Boundary Lubrication Studies," NASA TP-1658 (1980).

41. Goldblatt, I.L.; and Appeldoorn, J.K.: "The Antiwer Behavior of TCP in Different Atmospheres and Different Base Stocks," ASLE Trans. 13, (3), 1970, pp. 203-214.
42. Yamamoto, Y.: Effect of Running-In Condition of Scuffing Resistance of Carbon Steel in Rolling and Sliding Contact, Proc./JSLE International Tribology Conference, Tokyo, Japan, July 1985.
43. Czichos, H., "Tribology, a Systems Approach to the Science and Technology of Friction," Lubrication and Wear, Elsevier, 1978.
44. Hopkins, Vern; and Wilson, D.R.: Evaluation of Potential 700 °F Hydraulic Fluids in a Pump Loop. Ind. Eng. Chem. Prod. Res. Dev., vol. 3, no. 1, Mar. 1964, pp. 38-43.
45. Damasco, F.: Evaluation of Hydraulic Fluids for Use in Advanced Supersonic Aircraft. Rep. FHR 2701-5, Fairchild Hiller (NASA CR-72372), Nov. 14, 1967.
46. Appeldoorn, J.K.; and Tao, F.F.: The Lubricity Characteristics of Heavy Aromatics. Wear, vol. 12, no. 2, Aug. 1968, pp. 117-130.
47. Buckley, D.H.; Johnson, R.L.; and Brainard, W.A.: Influence of Entrained Gases and a Halogen Additive on Boundary Lubrication of Four Oils at Temperatures to 1000 °F. NASA TN D-2686, 1965.
48. Bigelow, W.C.; Pickett, D.L.; and Zisman, W.A.: Oleophobic Monolayers. II. Temperature Effects and Energy of Adsorption. J. Colloid Sci., vol. 2, no. 6, Dec. 1946, pp. 563-591.
49. Loomis, W.R., Townsend, D.P., and Johnson, R.L., "Lubricants for Inerted Lubrication Systems in Engines for Advanced Aircraft," NASA TN D-5420 (1969).
50. Peacock, L.A.; and Rhoads, W.L.: "High Temperature Lubricant Screening Tests," Rep. AL69T069, SKF Industries, Inc. NASA CR-72615, 1969.
51. Barcroft, F.T.: "A Technique for Investigating Reactions between EP Additives and Metal Surfaces at High Temperatures," Wear, 3, 440, 1960.

52. Sakurai, T.; and Sato, K.: "Study of Corrosivity and Correlation between Chemical Reactivity and Load-Carrying Capacity of Oils Containing Extreme Pressure Agents," ASLE Trans., 9, 77, 1966.

53. Klaus, E.E.; and Bieber, H.E.: Effects of P^{32} Impurities on the Behavior of Tricresyl Phosphate-32 as an Antiwear Additive," ASLE Trans., 8, 12, 1965.

54. Davy, W.: J. Ind. Eng. Chem., 42, 41, 1950.

55. Sakurai, T.; and Sato, K., "Chemical Reactivity and Load Carrying Capacity of Lubricating Oils Containing Organic Phosphorus Compounds," ASLE Trans., 13, 252, 1970.

56. Tingle, E.D.: "The Importance of Surface Oxide Films in the Friction and Lubrication of Metals. Part 2 - The Formation of Lubrication Films on Metal Surfaces," Trans. Far. Soc., 326, 97, 1950.

57. Fein, R.S.; and Kreuz, K.L.: Chemistry of Boundary Lubrication of Steel by Hydrocarbons. ASLE Trans., vol. 8, no. 1, Jan. 1965, pp. 29-38.

58. Vinogradov, G.; Korepova, I.V.; Podolsky, Y.Y.; and Pavlovskaya, N.T.: Effect of Oxidation on Boundary Friction of Steel in Hydrocarbon Media and Critical Friction Duties Under Which Cold and Hot Seizure (or Welding) Develop. Basic Eng., vol. 87, no. 3, Sept. 1965, pp. 741-746.

59. Fein, R.S.; and Kreuz, K.L.: Cyclohexane Vapor Lubrication of Steel. Am. Chem. Soc. Div. Petrol Chem. Prepr., vol. 13, no. 2, 1968, pp. B27-B38.

60. Chaikin, S.W.: On Frictional Polymer. Wear, vol. 10, 1967, pp. 49-60.

61. Schnurmann, R.; and Pedersen, O.: Field of Force Patterns at Frictional Contacts. Wear, vol. 18, no. 4, Oct. 1971, pp. 341-355.

62. Goldblatt, I.L.: Model for Lubrication Behavior of Polynuclear Aromatics. Ind. Eng. Chem. Prod. Res. Dev., vol. 10, no. 3, Sept. 1971, pp. 270-278.

63. Harris, E.E.; Milnes, F.J.; Ravner, R.J; and Dombchewsky, R.: Research and Development on the Synthesis of Tetraalkyl Silanes. Olin Mathieson Chem. Corp. (WADC TR 57-181, AD-151-74), Mar. 1958

64. Stemniski, J.R.; Wilson, G.R.; Smith, J.O.; and McHugh, K.L.: Antioxidants for High-Temperature Lubricants. ASLE Trans., vol. 7, no. 1, Jan. 1964, pp. 43-54.

65. Smith, J.O.; Wilson, G.R.; and McElhill, E.A.: Research on High-Temperature Additives for Lubricants. Monsanto Chem. Co. (ASD-TR-59-191, Part V, AD-400950), Nov. 1962.

66. Zimmer, H.: Hechenbleikner, I.; Homberg, O.A.; and Danzik, M.: Sterically Hindered Group IVA Organometallics. Preparation and Properties of Certain Neopentyltins. J. Org. Chem., vol. 29, no. 9, Sept. 1964, pp. 2632-2636.

67. Seifert, W.W.; and Westcott, V.C.: "A Method for the Study of Wear Particles in Lubricating Oil," Wear, 21, 1972, pp. 27-42.

68. Loomis, W.R.: Evaluation of Five Bearing-Separator Materials and Polyphenyl Ether Lubricants for Use in Space Power Generation Systems. NASA TN-D2663, 1965.

69. Antler, M.: Wear, Friction, and Electrical Noise Phenomena in Severe Sliding Systems. ASLE Trans., vol. 5, no. 2, Nov. 1962, pp. 297-307.

70. Beerbower, A.: Environmental Capability of Liquid Lubricants. Interdisciplinary Approach to Liquid Lubricant Technology. NASA SP-318, 1972.

71. Finkin, E.F.: Speculations on the Theory of Adhesive Wear. Wear, vol. 21, 1972, pp. 103-114.

72. Suh, N.P.: The Delamination Theory of Wear. Wear, vol. 25, 1973, pp. 111-124.

73. Eyre, T.S.; and Baxter, A.: The Formation of White Layers at Rubbing Surfaces. Tribology, vol. 5, no. 6, Dec. 1972, pp. 256-261.

74. Scott, D.; Seifert, W.W.; and Westcott, V.C.: The Particles of Wear. Sci. Am., vol. 230, no. 5, May 1974, pp. 88-97.

75. Scott, D.; and Mills, G.H.: Spherical Debris - Its Occurrence, Formation, and Significance in Rolling Contact Fatigue, Wear, vol. 24, 1973, pp. 235-242.
76. Kochi, J.K., ed.: Free Radicals. Vol. I, Wiley, 1973.
77. Blake, E.S.; et al.: Thermal Stability as a Function of Chemical Structure. J. Chem. Eng. Data, vol. 6, no. 1, Jan. 1961, pp. 87-98.
78. Vapor Pressure-Temperature Relationship and Initial Decomposition Temperature of Liquids by Isoteniscope. Am. Soc. Test. Mater. Stand. D-2879-75, Part No. 24, 1980.
79. Van Krevelen, D.W.: Properties of Polymers, Their Estimation and Correlation with Chemical Structure. Second ed., Elsevier Scientific Publ. Co., Amsterdam, 1976.
80. Dostrovsky, I.; and Hughes, E.D.: Mechanism of Substitution at a Saturated Carbon Atom. Part XXVI. The Role of Steric Hindrance. Sec. A. Introductory Remarks, and a Kinetic Study of the Reactions of Methyl, Ethyl, n-Propyl, Isobutyl, and Neopentyl Bromides with Sodium Ethoxide in Dry Ethyl Alcohol. J. Chem. Soc., 1946, pp. 157-161.
81. Emanuel, N.M.; Denisov, E.T.; and Maizus, Z.K.; {(B.J. Hazzard, Transl.)}: Liquid Phase Oxidation of Hydrocarbons. Plenum, 1967.
82. Criegee, R.; Pilz, H.; and Flygare, H.: Olefin Peroxides. Chem. Ber., vol. 72B, 1939, pp. 1799-1804.
83. Sheldon, R.A.; and Kochi, J.K.: Metal-Catalyzed Oxidations of Organic Compounds. Academic Press, 1981.
84. Cvitkovic, E.; Klaus, E.E.; and Lockwood, F.: A Thin-Film Test for Measurement of the Oxidation and Evaporation of Ester-Type Lubricants. ASLE Trans., vol. 22, no. 4, 1979, pp. 395-401.
85. Jones, W.R., Jr.; and Morales, W.: Thermal and Oxidative Degradation Studies of Formulated C-Ethers by Gel-Permeation Chromatography. NASA TP-1994, Mar. 1982.
86. Jones, W.R., Jr.; and Morales, W.: Analysis of a MIL-L-27502 Lubricant From a Gas-Turbine Engine Test by Size-Exclusion Chromatography. NASA TP-2063, Jan. 1983.

87. Jensen, R.K.; et al.: Liquid-Phase Autoxidation of Organic Compounds at Elevated Temperatures. 1. The Stirred Flow Reactor Technique and Analysis of Primary Products from n-Hexadecane Autoxidation at 120 to 180 °C. J. Am. Chem. Soc., vol. 101, no. 25, Dec. 1979, pp. 7574-7584.

88. Jones, W.R., Jr., et al.: Thermal Oxidative Degradation Reactions of Linear Perfluoroalkyl Ethers, I and EC Product Res. and Dev., vol. 22, June 1983, pp. 166-170.

89. Jones, W.R., Jr., et al.: The Effects of Metals and Inhibitors on Thermal Oxidative Degradation Reactions of Unbranched Perfluoroalkyl Ethers, I and EC Product Res. and Dev., vol. 24, Sept. 1985, pp. 417-420.

90. Vassil'ev, R.F.: Chemiluminescence in Liquid-Phase Reactions. Progress in Reaction Kinetics, vol. 4, G. Porter, ed., Pergamon Press, 1967, pp. 305-352.

91. Jones, W.R., Jr.; Meador, M.A.; and Morales, W.: Ester Oxidation on an Aluminum Surface Using Chemiluminescence, NASA TP-2611, July 1986.

92. Archer, W.L.; and Bozer, K.B.: Oxidative Degradation of the Polyphenyl Ethers, I and EC Prod. Res. and Dev., vol. 5, no. 2, June 1966, pp. 145-149.

93 Wilson, G.R.; Smith, J.O.; and Stemniski, J.R.: Mechanism of Oxidation of Polyphenyl Ethers. ML TDR-64-98, Wright Patterson AFB, Dec. 1964 (Available as AD-457120.).

94. Smith, J.O.; et al.: Research on High Temperature Additives for Lubricants. WADC-TR-59-191, Part IV, Feb. 1962. (Available as AD 281831.).

95. Ravner, H.; Russ, E.R.; and Timmons, C.O.: Antioxidant Action of Metals and Metal-Organic Salts on Fluoresters and Polyphenyl Ethers. J. Chem. Eng. Data, vol. 8, no. 4, Oct. 1963, pp. 591-596.

96. Ravner, H.; Moniz, W.B.; and Blachly, C.H.: High Temperature Stabilization of Polyphenyl Ethers by Inorganic Salts. ASLE Trans., vol. 15, no. 1, 1972, pp. 45-53.

97. Ravner, H.; and Kaufman, S.: High-Temperature Stabilization of Polyphenyl Ethers by Soluble Metal-Organic Salts. ASLE Trans., vol. 18, no. 1, 1975, pp. 1-4.

98. Stemniski, J.R.; et al.: Antioxidants for High-Temperature Lubricants. ASLE Trans., vol. 7, 1964, pp. 43-54.

99. Jones, W. R., Jr.; and Morales, W.: Thermal and Oxidative Degradation Studies of Formulated C-ethers by Gel Permeation Chromatography, NASA TP-1994, March 1982.

100. Morales, W.: Simulation of Lubricating Behavior of a Thioether Liquid Lubricant by an Electrochemical Method, ASLE Trans., vol. 29, no. 1, Jan. 1986, pp. 67-74.

101. Kajdas, C.: About a Negative-ion Concept of the Antiwear and Antiseizure Action of Hydrocarbons During Friction, Wear 101, 1985, pp. 1-12.

102. Grunberg, L.: A Survey of Exoelectron Emission Phenomena, Br. J. Appl. Phys. 9, 1958, pp. 85-93.

NASA
National Aeronautics and
Space Administration

Report Documentation Page

1. Report No. NASA TM-100166	2. Government Accession No.	3. Recipient's Catalog No.

4. Title and Subtitle
The Tribological Behavior of Polyphenyl Ether and Polyphenyl Thioether Aromatic Lubricants

5. Report Date
July 1987

6. Performing Organization Code
505-33-62

7. Author(s)
William R. Jones, Jr.

8. Performing Organization Report No.
E-3424

10. Work Unit No.

9. Performing Organization Name and Address
National Aeronautics and Space Administration
Lewis Research Center
Cleveland, Ohio 44135

11. Contract or Grant No.

13. Type of Report and Period Covered
Technical Memorandum

12. Sponsoring Agency Name and Address
National Aeronautics and Space Administration
Washington, D.C. 20546

14. Sponsoring Agency Code

15. Supplementary Notes
This report was a dissertation in partial fulfillment of the requirements for the degree of Doctor of Philosophy in Mechanical Engineering to Kyushu University, Fukuoka, Japan in 1987.

16. Abstract

The tribological behavior of several polyphenyl ethers and polyphenyl thioethers is reported. Tribological areas covered include: surface tension and wettability measurements, boundary lubrication, ferrography, thermal and oxidative stability and chemiluminescence.

17. Key Words (Suggested by Author(s))
Bounday lubrication; Polyphenyl ethers; High temperature liquid lubricants; Wettability; Chemiluminescence

18. Distribution Statement
Unclassified - unlimited
STAR Category 27

19. Security Classif. (of this report) Unclassified	20. Security Classif. (of this page) Unclassified	21. No of pages	22. Price*

NASA FORM 1626 OCT 86

*For sale by the National Technical Information Service, Springfield, Virginia 22161